Elastic Scattering of Charged Gauge Bosons in the Standard Model of the Electroweak Interaction

Dissertation zur Erlangung
des naturwissenschaftlichen Doktorgrades
der Bayerischen Julius-Maximilians-Universität Würzburg

vorgelegt von

Thomas Hahn

aus Würzburg

Würzburg 1997

Eingereicht am
bei der Fakultät für Physik und Astronomie

Erster Gutachter: Prof. Dr. M. Böhm
Zweiter Gutachter: PD Dr. Ansgar Denner
der Dissertation

Erster Prüfer: Prof. Dr. M. Böhm
Zweiter Prüfer: Prof. Dr. M. Scheer
der mündlichen Prüfung

Tag der mündlichen Prüfung:

Doktorurkunde ausgehändigt am:

Contents

1 Introduction **5**

1.1 Why gauge-boson scattering? 5

1.2 Experimental considerations 7

2 The Standard Model **9**

2.1 Gauge principle 9

2.2 The Standard Model Lagrangian 11

2.2.1 Yang-Mills sector 11

2.2.2 Fermion sector 11

2.2.3 Higgs sector 12

2.3 The S matrix 15

2.4 Perturbative evaluation 16

3 Lowest-Order Cross-Section **19**

3.1 Kinematics and notation 19

3.2 Analytical Born formulae 21

3.3 t-channel singularity 22

3.4 Differential cross-section 26

3.5 Total cross-section 26

4 Higgs Physics **31**

4.1 Unitarity bound 31

4.2 Unitarity in longitudinal W–W scattering at tree level 32

4.3 Possibility of a strongly interacting Higgs sector 35

4.4 The equivalence theorem 37

4.5 Treatment of the Higgs resonance 39

5 One-loop Corrections **43**
5.1 Quantization and Gauge Fixing 43
5.1.1 't Hooft-Feynman gauge 45
5.2 Background field method 46
5.3 Renormalization 48
5.3.1 Ultraviolet divergences 48
5.3.2 Infrared divergences 52
5.4 Structure of the one-loop amplitudes 55
5.4.1 Scalar and tensor one-loop integrals 55
5.4.2 Reduction of the tensor integrals 56

6 Numerical Results **61**
6.1 One-loop diagram gallery 61
6.2 Differential cross-section 67
6.3 Total cross-sections 68
6.4 Accuracy of the equivalence-theorem predictions 68
6.5 Evaluation with the computer 75
6.5.1 Generating the diagrams with *FeynArts* 75
6.5.2 Algebraic simplification with *FormCalc* 78
6.5.3 Final numerical evaluation in Fortran 80
6.6 Parameters and Calculational Details 82
6.7 Difficulties beyond $\mathcal{O}(\alpha^3)$ accuracy 83

7 Conclusions **87**

8 Zusammenfassung **95**

Chapter 1

Introduction

1.1 Why gauge-boson scattering?

The current understanding of electroweak high-energy physics is based almost solely on the electroweak Standard Model (SM) which combines the electromagnetic and weak forces into a single, spontaneously broken gauge theory. Its successes in explaining experimental data are beyond doubt. However, the SM was constructed largely from phenomenological evidence, so it is not surprising that it is not entirely satisfactory from the theoretical point of view. For instance, there is the as yet undetected Higgs boson, with the related question of naturalness; there is the mass hierarchy which the SM leaves unexplained; also, there is a heap of open problems regarding unification.

The prevailing situation is thus that nobody expects the SM to be the final answer, but remarkably, there is an almost total absence of any hint at new physics beyond the SM in the experiments. In fact, expectations run so high that even minuscule fluctuations in experimental data have regularly sparked off a wave of scientific papers in the past years.

The search for new physics expands in two main directions. One direction is to try out new candidate models and see if they can be made to conform with the experimental data. The other is to test the SM more and more precisely to find out if and where there are unexplainable discrepancies. This calls for the high precision measurements and calculations which are the means of thoroughly testing an already successful theory. There remain essentially two areas where the SM has so far evaded stringent tests: the non-abelian sector as one of the pillars of the SM and the scalar sector which drives spontaneous

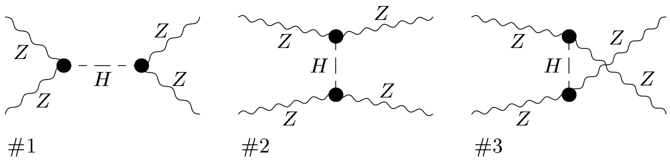

Figure 1.1: The lowest-order diagrams for ZZ $\to$ ZZ. This process unfortunately has a very small cross-section, otherwise it would be the prime candidate for testing the Higgs sector.

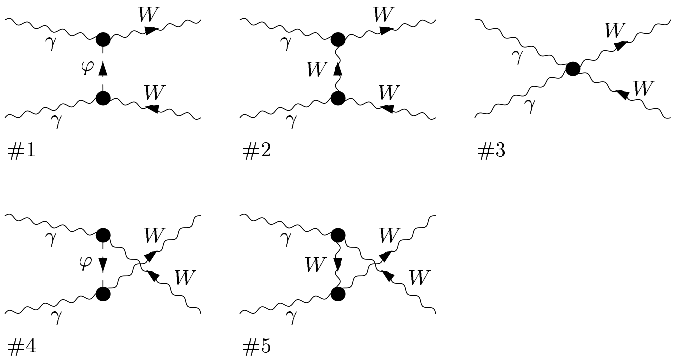

Figure 1.2: The lowest-order diagrams for $\gamma\gamma \to$ W$^+$W$^-$. Unfortunately, there is no Higgs exchange at Born level and therefore the possibilities of testing the scalar sector with this process are reduced. On the other hand, experimental accessability is likely to favour this process.

symmetry breaking.

Of all thinkable reactions, gauge-boson scattering is perhaps the cleanest window into the heart of the theory. Since to lowest order all gauge-boson scattering amplitudes involve only interactions between gauge and scalar bosons (see Figs. 1.1, 1.2, and 3.1 for examples), the corresponding cross-sections depend very sensitively on the non-abelian and scalar sector of the underlying theory. This sensitivity is even enhanced for high-energetic, longitudinally polarized massive gauge bosons, owing to the presence of gauge cancellations. For these reasons, gauge-boson scattering has found continuous interest in the literature [DiM73, LeQT77, Pa85, DaW89, MaVW89, DuJM91, GuJR93, Bo90] from the very first years of spontaneously broken gauge theories.

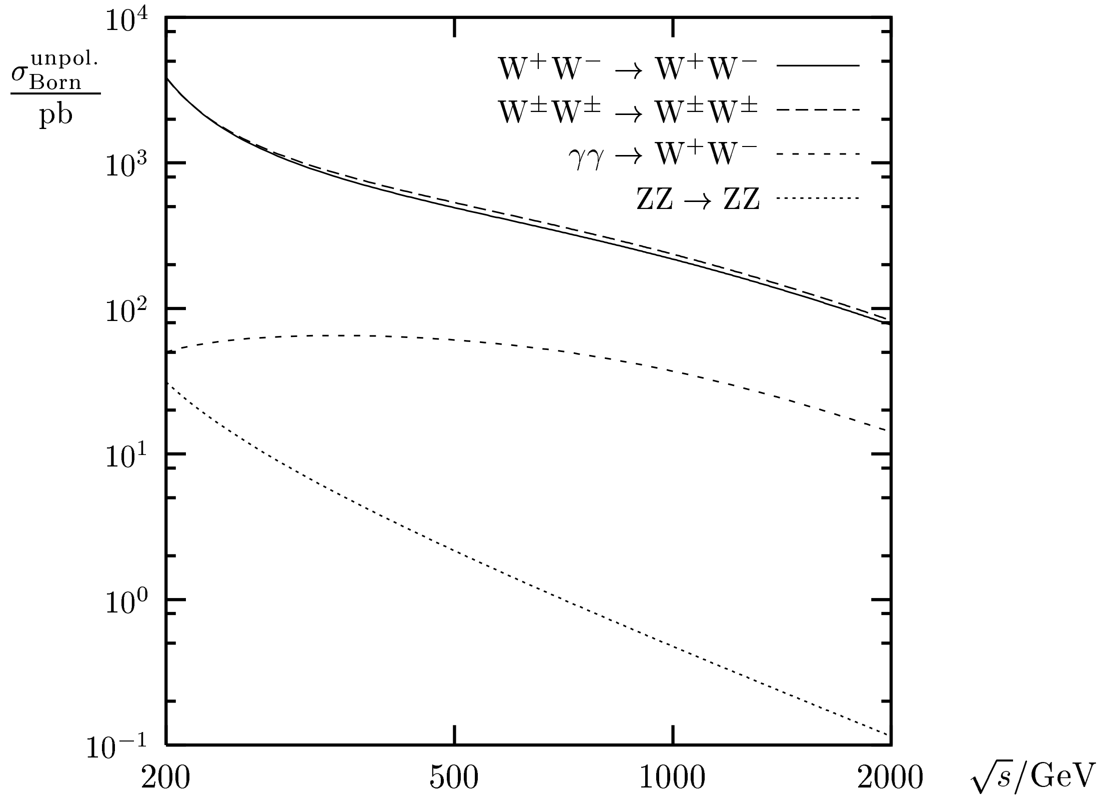

Figure 1.3: Comparison of the cross-sections of some gauge-boson scattering processes. All curves are from lowest-order (Born-level) calculations [DeDS95, DeDH97] for unpolarized bosons.

1.2 Experimental considerations

Gauge-boson scattering can be studied in principle at all high-energy colliders, for example pp colliders like LHC, e^+e^- colliders like the proposed NLC, or $\mu^+\mu^-$ colliders, where these reactions naturally appear as subprocesses.

From Fig. 1.3 it can be seen that particularly in the low-energetic regime the cross-section for elastic W scattering is nearly two orders of magnitude above those of other gauge-boson scattering processes, thus making it a preferable candidate for investigation. Equally charged W bosons will have a possible experimental advantage over oppositely charged ones due to their signature and/or background (see [Ch93], Sect. 5 for a discussion).

For a hadron collider, gauge-boson scattering can be thought of as a final-state interaction in a hadronic process, like proton–proton scattering at the

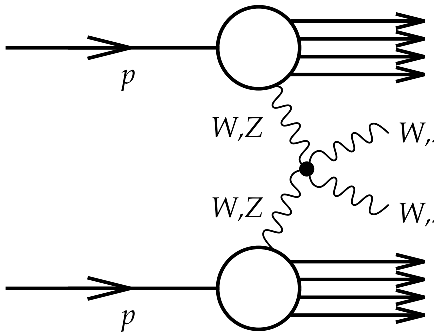

Figure 1.4: Schematical picture of massive gauge-boson scattering at a hadron collider.

LHC. This is shown schematically in Fig. 1.4. Unfortunately, there are two factors which greatly diminish the experimental prospects for gauge-boson scattering at hadron colliders. One is that even though the proton beam at LHC will have an energy of $\sim$ 7 TeV ($\gg M_{\rm W}, M_{\rm Z}$), the gauge bosons, which come into the game as sea partons, will carry only a fraction of this energy. Secondly, to arrive at the experimentally observable cross-section, the theoretical prediction must be convoluted with the parton distribution of the W inside the proton. Apart from the fact that knowledge of this distribution is at best sketchy, the convolution can take away orders of magnitude so that the actual scattering may be hard to distinguish from the background. For detailed calculations of the expectable luminosities, the reader is referred to [KuS96]. See also [Ch93] and [Yu93] for further investigation into experimental questions regarding gauge-boson scattering at a hadron collider.

Lepton colliders offer a way out of this dilemma, but as for the currently available facilities, LEP2 will reach the production threshold for $\rm W^+W^-$ but not have a sufficient signal-to-background ratio to study $\rm W^+W^-$ scattering. So gauge-boson scattering at a lepton machine will have to wait for the NLC, possibly the TESLA project planned at DESY. For the aspects of W physics at a linear collider, see [Ze92].

The muon collider is, mildly put, a very long-term project, even though it possesses an interesting physics potential [BaBGH97].

In any case, it is no understatement to say that experimental data will soonest become available at least ten years from now.

Chapter 2

The Standard Model

The Standard Model (SM), also called Glashow-Salam-Weinberg theory [Gl61], is a spontaneously broken gauge theory which is able to phenomenologically describe very successfully the electromagnetic and weak fundamental forces with a single Lagrangian. It is also a minimal model in the sense that it includes no unnecessary degrees of freedom. Its particle content is summarized in the following table:

	Fermions				Bosons			
	Leptons		Quarks		Gauge bosons			Higgs
	e	ν_e	u	d	γ	Z	$W^\pm$	H
	μ	ν_μ	c	s				
	τ	ν_τ	t	b				
charge	-1	0	$\frac{2}{3}$	$-\frac{1}{3}$	0	0	± 1	0
spin	$\frac{1}{2}$	$\frac{1}{2}$	$\frac{1}{2}$	$\frac{1}{2}$	1	1	1	0

As of today, all of these particles except the scalar Higgs boson have been observed in nature and their properties have been determined, many of them with high precision.

2.1 Gauge principle

The basic idea behind a gauge theory is very simple. Consider a field theory that is invariant under a global transformation of some symmetry group, i.e. its Lagrangian does not change when the fields ψ undergo

$$\psi_i(x) \to \psi'_i(x) = \left(\mathrm{e}^{-\mathrm{i}\theta^a \tau^a}\right)_{ij} \psi_j(x) \tag{2.1}$$

where the τ^a are the generators of the symmetry group under consideration and the parameters θ^a are constants. Such a transformation is called a gauge transformation. For an abelian group it is merely a multiplication by a phase factor.

According to the gauge principle, a gauge theory should also be invariant under a *local* transformation, i.e. one in which the θ^a depend on x. This will in general not leave the Lagrangian invariant since it contains derivatives (e.g. in the kinetic part) which give rise to additional terms like the underlined:

$$\partial_\mu \mathrm{e}^{\mathrm{i}\theta^a\tau^a}\psi = \mathrm{e}^{-\mathrm{i}\theta^a\tau^a}\partial_\mu\psi + \underline{(-\mathrm{i}\tau^a\partial_\mu\theta^a)\,\mathrm{e}^{-\mathrm{i}\theta^a\tau^a}\psi}\,. \tag{2.2}$$

In order to re-establish invariance of the Lagrangian, the derivative is replaced by a new operator, the covariant derivative. It is defined as

$$D_\mu = \partial_\mu - \mathrm{i}gA_\mu \quad \text{with} \quad A_\mu \equiv A^a_\mu\tau^a\,. \tag{2.3}$$

The new dynamical quantity A_μ is called a gauge field and its purpose is to cancel the extra term that comes from the gauge transformation. To accomplish this, it must transform as

$$A'_\mu = \mathrm{e}^{-\mathrm{i}\theta^a\tau^a}A_\mu\,\mathrm{e}^{\mathrm{i}\theta^a\tau^a} + \frac{1}{\mathrm{i}g}(-\mathrm{i}\tau^a\partial_\mu\theta^a)\,. \tag{2.4}$$

Thus by postulating local gauge invariance, a new field comes into the theory that couples to the matter fields with a coupling constant g and whose exchange between matter fields can be interpreted as the mediation of a force.

As a dynamical object, the gauge field should also have its own kinetic term in the Lagrangian. This term, called the Yang-Mills term after Yang and Mills [YaM54], is

$$\mathcal{L}_{\mathrm{YM}} = -\frac{1}{2}\operatorname{Tr}F_{\mu\nu}F^{\mu\nu} = -\frac{1}{4}F^a_{\mu\nu}F^{a\mu\nu} \tag{2.5}$$

which is constructed from the field-strength tensor

$$\begin{aligned} F_{\mu\nu} \equiv \frac{\mathrm{i}}{g}[D_\mu, D_\nu] &= \partial_\mu A_\nu - \partial_\nu A_\mu - \mathrm{i}g[A_\mu, A_\nu] \\ &= \left(\partial_\mu A^a_\nu - \partial_\nu A^a_\mu + g f^{abc} A^b_\mu A^c_\mu\right)\tau^a \equiv F^a_{\mu\nu}\tau^a\,, \end{aligned} \tag{2.6}$$

where f^{abc} are the structure constants of the underlying group. The Yang-Mills term is gauge invariant owing to the cyclicity of the trace.

2.2 The Standard Model Lagrangian

2.2.1 Yang-Mills sector

To our present knowledge, there exist in nature four gauge bosons for the electroweak interaction: the photon, the Z boson, and the two $\mathrm{W}^{\pm}$ bosons. The gauge group is known from experiment not to be abelian, therefore the smallest group able to accomodate four gauge bosons is the composite group $\mathrm{SU}(2) \times \mathrm{U}(1)$. The general gauge transformation is in this case

$$\psi \to \mathrm{e}^{-\mathrm{i}\alpha^a \tau^a} \mathrm{e}^{-\mathrm{i}\beta/2} \psi \tag{2.7}$$

where $\tau^a = \sigma^a/2$ are the generators of $\mathrm{SU}(2)$ and σ^a the Pauli matrices. The covariant derivative is given by

$$D_\mu = \partial_\mu - \mathrm{i}g A^a_\mu \tau^a + \mathrm{i}g' B_\mu \tfrac{1}{2}\mathbf{1}\,. \tag{2.8}$$

Note that there are two coupling constants since the gauge group is composite. The Yang-Mills part of the Lagrangian reads

$$\mathcal{L}_{\mathrm{YM}} = -\frac{1}{4}(\partial_\mu A^a_\nu - \partial_\nu A^a_\mu + g\varepsilon^{abc} A^b_\mu A^c_\nu)^2 - \frac{1}{4}(\partial_\mu B_\nu - \partial_\nu B_\mu)^2\,. \tag{2.9}$$

2.2.2 Fermion sector

It is further known from experiment that left- and right-handed fermion fields interact differently, therefore they are assigned to different representations of the gauge group, the left-handed fields to $\mathrm{SU}(2)$ doublets,

$$L^L_i = \begin{pmatrix} \omega_-\, \nu_i \\ \omega_-\, \ell_i \end{pmatrix} \quad \text{and} \quad Q^L_i = \begin{pmatrix} \omega_-\, u_i \\ \omega_-\, d_i \end{pmatrix}, \tag{2.10}$$

and the right-handed fields to $\mathrm{SU}(2)$ singlets,

$$\ell^R_i = \omega_+\, \ell_i \quad \text{and} \quad u^R_i = \omega_+\, u_i\,, \;\; d^R_i = \omega_+\, d_i\,, \tag{2.11}$$

where $\omega_\pm = (\mathbf{1} \pm \gamma_5)/2$ are the chirality projectors and the index $i = 1, 2, 3$ counts the generations.

With this, the fermionic part of the Lagrangian takes the form

$$\begin{aligned} \mathcal{L}_{\mathrm{f}} = \sum_i\; & \bar{L}^L_i (\mathrm{i}\not{D}) L^L_i + \bar{Q}^L_i (\mathrm{i}\not{D}) Q^L_i \\ & + \bar{\ell}^R_i (\mathrm{i}\not{D}) \ell^R_i + \bar{u}^R_i (\mathrm{i}\not{D}) u^R_i + \bar{d}^R_i (\mathrm{i}\not{D}) d^R_i \end{aligned} \tag{2.12}$$

using the standard notation $\not{D} \equiv \gamma_\mu D^\mu$.

Since left- and right-handed fermions live in different representations, it is legitimate to think of them as distinct particles, which are mixed by the fermion mass terms (to be introduced below). Note that the massless fermionic Lagrangian is also invariant under chiral transformations $\psi \to \mathrm{e}^{-\mathrm{i}\theta\gamma_5}\psi$.

2.2.3 Higgs sector

Up to now, none of the terms in the Lagrangian is of the form $\frac{1}{2}m^2\bar{\psi}\psi$ or $\frac{1}{2}M^2 A_\mu A^\mu$, so neither fermions nor gauge bosons have a mass so far. Explicitly putting in such mass terms by hand would spoil renormalizability and gauge invariance. However, with the Higgs-Kibble-Goldstone mechanism [Hi66], masses may be introduced without ill side-effects by means of spontaneous symmetry breaking.

To this end, a new field Φ is introduced that transforms as an $\mathrm{SU}(2)$ doublet and has as its Lagrangian

$$\mathcal{L}_\mathrm{H} = \frac{1}{2}(D_\mu\Phi^\dagger)(D^\mu\Phi) - V[\Phi] \tag{2.13}$$

with the potential

$$V[\Phi] = \frac{\lambda}{4}(\Phi^\dagger\Phi)^2 - \mu^2\Phi^\dagger\Phi\,. \tag{2.14}$$

Assuming that λ and μ are positive, there are continuously many directions for Φ for which $V[\Phi]$ takes on its minimum, namely, all Φ for which $||\Phi||^2 = 2\mu^2/\lambda$. By assigning Φ a definite vacuum expectation value

$$\langle 0|\,\Phi\,|0\rangle = \frac{1}{\sqrt{2}}\begin{pmatrix}0\\ v\end{pmatrix} \quad \text{with} \quad \frac{v}{\sqrt{2}} = \sqrt{\frac{2\mu^2}{\lambda}} \tag{2.15}$$

the $\mathrm{SU}(2)\times\mathrm{U}(1)$ symmetry is broken down to a $\mathrm{U}(1)_\mathrm{em}$. The latter remains because Φ is still invariant under an electromagnetic gauge transformation since its generator,

$$Q = \tau^3 + \frac{1}{2}\mathbf{1} = \frac{1}{2}\begin{pmatrix}1 & 0\\ 0 & -1\end{pmatrix} + \frac{1}{2}\begin{pmatrix}1 & 0\\ 0 & 1\end{pmatrix} = \frac{1}{2}\begin{pmatrix}1 & 0\\ 0 & 0\end{pmatrix}\,, \tag{2.16}$$

does not act on the lower component of Φ.

Gauge-boson masses

Putting the vacuum expectation value into the kinetic term in $\mathcal{L}_\mathrm{H}$ makes the gauge bosons massive. The relevant terms are

$$\begin{aligned}\Delta\mathcal{L}_\mathrm{H} &= \frac{1}{2}(0\ \ v)\left(gA^a_\mu\tau^a - \frac{1}{2}g'B_\mu\right)\left(gA^{b\mu}\tau^b - \frac{1}{2}g'B^\mu\right)\begin{pmatrix}0\\ v\end{pmatrix}\\ &= \frac{1}{2}\frac{v^2}{4}\left[g^2(A^1_\mu)^2 + g^2(A^2_\mu)^2 + (gA^3_\mu + g'B_\mu)^2\right]\ .\end{aligned} \tag{2.17}$$

This shows that there are three massive and one massless boson, just as it is expected from the one remaining unbroken $\mathrm{U}(1)_\mathrm{em}$ symmetry. The mass eigenstates are denoted by

$$W^\pm_\mu = \frac{1}{\sqrt{2}}(A^1_\mu \mp \mathrm{i}A^2_\mu) \qquad \text{with mass } M_\mathrm{W} = g\frac{v}{2}\,, \tag{2.18}$$

$$Z_\mu = \frac{1}{\sqrt{g^2+g'^2}}(gA^3_\mu + g'B_\mu) \quad \text{with mass } M_\mathrm{Z} = \sqrt{g^2+g'^2}\,\frac{v}{2}\,, \tag{2.19}$$

and the massless field orthogonal to Z

$$A_\mu = \frac{1}{\sqrt{g^2+g'^2}}(g'A^3_\mu + gB_\mu) \quad \text{with mass } M_\gamma = 0\,. \tag{2.20}$$

The $W^\pm$ fields are chosen as charge eigenstates and the linear combinations of the other two fields amount to a rotation of the form

$$\begin{pmatrix}Z\\ A\end{pmatrix} = \begin{pmatrix}\cos\theta_\mathrm{W} & \sin\theta_\mathrm{W}\\ -\sin\theta_\mathrm{W} & \cos\theta_\mathrm{W}\end{pmatrix}\begin{pmatrix}A^3\\ B\end{pmatrix} \tag{2.21}$$

where θ_W is the so-called Weinberg mixing angle. Comparing with the expressions above, the sine and cosine of the mixing angle can be identified with

$$\cos\theta_\mathrm{W} = \frac{g}{\sqrt{g^2+g'^2}} \equiv c_\mathrm{W} \quad \text{and} \quad \sin\theta_\mathrm{W} = \frac{g'}{\sqrt{g^2+g'^2}} \equiv s_\mathrm{W}\,. \tag{2.22}$$

It then follows from (2.18) and (2.19) that the masses of the W and Z bosons are not independent, but satisfy

$$M_\mathrm{W} = c_\mathrm{W} M_\mathrm{Z}\,. \tag{2.23}$$

Furthermore, the coefficient of the electromagnetic interaction is just the electron charge, so

$$e = \frac{gg'}{\sqrt{g^2+g'^2}}\,. \tag{2.24}$$

Fermion masses

The fermions are assumed to couple to the Φ field via Yukawa terms, i.e.

$$\mathcal{L}_{\text{H–f}} = -\sum_{i,j} \left(G^{\ell}_{ij}\, \bar{L}^{L}_{i} \Phi\, \ell^{R}_{j} + G^{u}_{ij}\, \bar{Q}^{L}_{i} \Phi\, u^{R}_{j} + G^{d}_{ij}\, \bar{Q}^{L}_{i} \Phi\, d^{R}_{j} + \text{H.c.} \right) \tag{2.25}$$

where the sum subtends over all three generations. Again by inserting the vacuum expectation value of Φ the fermions become massive through terms of the form

$$\Delta\mathcal{L}_{\text{H–f}} = -\frac{1}{\sqrt{2}} G^{f}_{ij} \bar{f}^{L}_{i} f^{R}_{j}\,. \tag{2.26}$$

To arrive at mass eigenstates, the coupling matrices G^{f}_{ij} must be diagonalized by matrices U^{f}_{ij}. The fermion masses are then

$$m_{f,i} = U^{f,L}_{ik} G^{f}_{km} (U^{f,R}_{mi})^{\dagger} \frac{v}{\sqrt{2}}\,. \tag{2.27}$$

Since the neutrinos do not couple to the Φ (and therefore remain massless), the leptonic coupling matrix can be chosen diagonal from the beginning. Inserting the transformed quark fields $q'_i = U_{ij} q_j$ into $\mathcal{L}_{\text{f}}$ leads to quark mixing via the Cabibbo-Kobayashi-Maskawa matrix $V_{ij} = U^{u,L}_{ik} (U^{d,L}_{kj})^{\dagger}$ in the couplings of the quarks to the W boson.

Higgs mass

The standard parametrization for Φ is

$$\Phi = \begin{pmatrix} \varphi^{\dagger}(x) \\ \frac{1}{\sqrt{2}}[v + H(x) + \mathrm{i}\chi(x)] \end{pmatrix} \tag{2.28}$$

and inserting this into $V[\Phi]$, the physical Higgs field $H(x)$ also acquires the mass $M_{\text{H}} = \sqrt{2}\mu$ due to

$$\mu^2 H^2 + \text{(higher terms)} \tag{2.29}$$

where "(higher terms)" stands for tri- and quadrilinear terms in φ, χ, and H.

The complete, written-out SM Lagrangian can be found e.g. in [BoRS95].

2.3 The S matrix

An experimentalist generally prepares a state to have a definite particle content at $t \to -\infty$, and then measures what this state looks like at $t \to \infty$. It is assumed that far away from the collision point the particles behave as free particles. For the usual scattering geometry with stable particles in the initial and final states, this picture is clearly valid; just think of the CERN collider where the colliding particles approach each other in a ring with a circumference of some 27 km and are detected a macroscopic distance away from the interaction point.

It is less clear how valid this approach is when one considers particles that are first produced by some reaction, then interact, and subsequently decay very quickly into the final (stable) particles. For instance, the W boson decays approximately 3.2×10^{-25} seconds after its production. In this case it is a problematic assumption to directly take W bosons as initial and final particles, and doing so leaves its trace in the one-loop calculation (see Sect. 6.7).

A related complication is that the physical process observed at a collider is actually $f_1 \bar{f}_2 \to \mathrm{W}^+\mathrm{W}^- \to \mathrm{W}^+\mathrm{W}^- \to$ fermions, rather than $\mathrm{W}^+\mathrm{W}^- \to \mathrm{W}^+\mathrm{W}^-$, so in general the W bosons will not be on shell. This can be treated similar to the well-known Weizsäcker-Williams approximation for photonic reactions with a method known as the equivalent vector-boson method (see e.g. [Ku97] and references therein). The approximation consists in replacing the cross-section for virtual gauge bosons with the cross-section for real bosons, convoluted with the corresponding flux of the gauge bosons. Its accuracy has been assessed for Higgs-boson production. Analytical calculations [AlMP87] show good agreement for $\mathrm{W}^+\mathrm{W}^- \to \mathrm{H}$ for $M_\mathrm{H} \gtrsim$ 500 GeV, with errors $\lesssim \mathcal{O}(10\%)$ and decreasing with M_H and $\sqrt{s}$. Above 1 TeV the errors are very small. The estimate is expected to carry over to the case of W–W scattering.

Under these provisions the interesting question for a general scattering process is, how a free-particle state $|i_\text{in}\rangle$ in the remote past ($t \to -\infty$) evolves into a free-particle state $|f_\text{out}\rangle$ in the distant future ($t \to \infty$), where 'i' and 'f' label the particle content of the respective state. We postulate an operator that transforms an 'in' state into an 'out' state, called the S matrix. Formally,

$$\langle f_\text{out} | i_\text{in} \rangle = \langle f_\text{in} | \, S \, | i_\text{in} \rangle \ . \tag{2.30}$$

Perhaps it should be noted that 'in' and 'out' states do not inhabit two different

Hilbert spaces. They differ only in how they are labelled: by their appearance either at $t \to -\infty$ or $t \to \infty$. Any 'in' state can be expanded as a sum of 'out' states, with expansion coefficients given by the S matrix.

The physical content of the S matrix becomes more explicit when written as $S = U(t = \infty, t = -\infty)$, where U is the time evolution operator, $U = \mathrm{e}^{\mathrm{i}Ht/\hbar}$.

If there were no interactions then the initial and final states would be the same, and S would be just the identity. The rate for a reaction $i \to f$ is thus proportional to $|\langle f_{\mathrm{in}}| S - \mathbf{1} |i_{\mathrm{in}}\rangle|^2$. This is reflected by decomposing the S matrix into a trivial part, the unscattered beam, and a part responsible for the actual scattering,

$$S = \mathbf{1} + \mathrm{i}\, T\,, \tag{2.31}$$

where the on-shell matrix elements of the transition matrix T are given by

$$\langle f_{\mathrm{in}}| T |i_{\mathrm{in}}\rangle = (2\pi)^4\, \delta^{(4)}\Big(\sum k_i - \sum k_f\Big)\, \mathcal{M}_{fi}\,. \tag{2.32}$$

$\mathcal{M}_{fi}$ is called the invariant matrix element and is usually evaluated in perturbation theory.

2.4 Perturbative evaluation

The main tool for the manipulation of a field theory is an expansion in powers of coupling constants about some quadratic form, which is exactly soluble. Since this is basic lore in field theory it shall be sketched here rather briefly. For a more thorough description, see [Am84, Ry85].

The quantities one is interested in are the time-ordered products of field operators in the vacuum state. These are the Green functions

$$G^{(n)}(x_1, \ldots, x_n) = \langle 0| T\varphi(x_1) \cdots \varphi(x_n) |0\rangle \tag{2.33}$$

and they suffice to give the S matrix. T is the time-ordering operator and for simplicity, we are focusing here on only one species of fields, φ.

The Green functions may be computed as

$$G^{(n)}(x_1, \ldots, x_n) = \left(\frac{1}{\mathrm{i}}\frac{\delta}{\delta J(x_1)}\right) \cdots \left(\frac{1}{\mathrm{i}}\frac{\delta}{\delta J(x_n)}\right) Z[J]\bigg|_{J=0} \tag{2.34}$$

using the generating functional

$$Z[J] = N \int \mathcal{D}\varphi \, \mathrm{e}^{\mathrm{i}S[\varphi]} \, \mathrm{e}^{\mathrm{i}\int \mathrm{d}^4x \, J(x)\varphi(x)} \, . \tag{2.35}$$

This is so because each $\frac{1}{\mathrm{i}} \frac{\delta}{\delta J(x_i)}$ pulls down a factor $\varphi(x_i)$, and the time ordering is taken care of by the path integral. $N = 1/Z[0]$ is a normalization factor and $S = \int \mathrm{d}^4x \, \mathcal{L}$ is the action.

Now write $\mathcal{L} = \mathcal{L}_0 + \mathcal{L}_{\text{int}}$ with $\mathcal{L}_0$ the free and $\mathcal{L}_{\text{int}}$ the interacting part of the Lagrangian. Then by the same reasoning we can replace the argument of $\mathcal{L}_{\text{int}}$ with a functional derivative and Z becomes

$$Z[J] = N \exp\left\{ \mathrm{i} \int \mathrm{d}^4x \, \mathcal{L}_{\text{int}}\left(\frac{1}{\mathrm{i}} \frac{\delta}{\delta J(x)} \right) \right\} Z_0[J] \, , \tag{2.36}$$

where Z_0 denotes the generating functional for the free part. If $\mathcal{L}_0$ is a quadratic form, Z_0 is a Gaussian integral that can be done. Its solution is given in terms of the propagator $\Delta(x - y)$ of the φ field as

$$Z_0[J] = \exp\left\{ \frac{1}{2} \int \mathrm{d}^4x \, \mathrm{d}^4y \, J(x)\Delta(x-y)J(y) \right\} \, . \tag{2.37}$$

Hence it all reduces to calculating many derivatives of a Gaussian form, at the origin. Clearly, a derivative of the exponential brings down a factor of J. Thus, if the term is not to vanish when J is set to zero, another derivative must act to eliminate this factor. Consequently, the derivative terms must group in pairs, in all possible ways. For each such pair there will appear a factor $\Delta(x - y)$, where x and y are the coordinates of the J's in the pair.

Normally, the exponential in $\mathcal{L}_{\text{int}}$ is expanded in a perturbation series, e.g. for $\mathcal{L}_{\text{int}} = (\lambda/4!) \, \varphi^4$

$$Z[J] = N \sum_{n=0}^{\infty} \frac{\mathrm{i}^n}{n!} \left(\frac{\lambda}{4!} \right)^n \int \mathrm{d}^4x_1 \cdots \mathrm{d}^4x_n \left(\frac{\delta}{\delta J(x_1)} \right)^4 \cdots \left(\frac{\delta}{\delta J(x_n)} \right)^4 Z_0[J] \, . \tag{2.38}$$

In keeping track of the multitude of terms generated by such strings of derivatives, Feynman graphs serve as an invaluable device. The single terms are represented graphically by drawing a line for every propagator Δ and a dot (vertex) for every pairing. Conversely, one can derive a set of rules that allow the terms in the perturbation series to be recovered from the diagrams. The complete Feynman rules for the SM can be found in [De93].

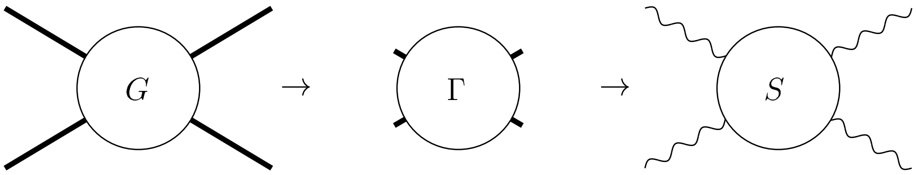

Figure 2.1: Schematical representation of the LSZ prescription for obtaining S-matrix elements from Green functions. The full Green function is denoted by G and the amputated one by Γ.

Since there may be more than one coupling constant, an expansion in the coupling constant is not necessarily a unique procedure. Instead, if we write out explicitly the $\hbar$ in the exponential, $\mathrm{e}^{\mathrm{i}S/\hbar}$, we find that the perturbative series is a consistent expansion in powers of $\hbar$, i.e. in the quantum corrections. Moreover, by a topological argument it can be shown that the diagrams corresponding to a particular power of $\hbar$ all have the same number of loops, therefore the expansion in $\hbar$ is simultaneously an expansion in the number of loops.

The S matrix is expressed in terms of the Green functions with their variables set on the mass shell and the part corresponding to the external particles extracted. This is the gist of the LSZ formula

$$S^{(n)}(x_1, \dots, x_n) = \prod_{i=1}^{n} Z_\varphi^{1/2} \varphi_{\mathrm{in}}(x_i) \left(-\partial_{x_i}^2 + m^2\right) G^{(n)}(x_1, \dots, x_n)\,, \tag{2.39}$$

named after Lehmann, Symanzik, and Zimmermann [LeSZ57]. The Klein-Gordon operator $(-\partial^2 + m^2)$ removes the external legs of the Green function and puts the respective particles on their mass shells and $Z_\varphi^{1/2}$ is the external field renormalization. In terms of the Feynman rules, this amounts to cutting off the external propagators and replacing them with the wave functions of the initial and final particles, φ_{in}, e.g. spinors for external fermions, or polarization vectors for external spin-1 bosons. Fig. 2.1 illustrates this schematically.

One final point to note is that so far, all pairings are admitted. Diagrammatically speaking these include diagrams which are only connected with the endpoints but not internally (so-called disconnected diagrams). They involve no interactions between the particles and hence contribute only to the "beam" part of the S matrix (the "$\mathbf{1}$" in Eq. (2.31)). Consequently, only connected diagrams need to be taken into account.

Chapter 3

Lowest-Order Cross-Section

3.1 Kinematics and notation

$\mathrm{W}^+\mathrm{W}^- \to \mathrm{W}^+\mathrm{W}^-$ is a short-hand for the two-body reaction

$$W^+(k_1,\lambda_1) + W^-(k_2,\lambda_2) \to W^+(k_3,\lambda_3) + W^-(k_4,\lambda_4)\,, \tag{3.1}$$

where the k_i and λ_i denote the momenta and helicities of the W bosons, respectively. In the following, the indices L, T and U denote longitudinal ($\lambda = 0$), transverse ($\lambda = \pm$) and unpolarized W bosons, respectively, and definite polarization combinations are denoted by a sequence of four letters, e.g. LTLT stands for $\mathrm{W}_\mathrm{L}^+\mathrm{W}_\mathrm{T}^- \to \mathrm{W}_\mathrm{L}^+\mathrm{W}_\mathrm{T}^-$.

The incoming particles travel along the z axis and are scattered into the x-z plane. In the centre-of-mass system (CMS) the momenta and polarization vectors $\varepsilon_i(\lambda_i)$ read explicitly

$$\begin{aligned}
k_1^\mu &= (E,\,0,\,0,\,-p)\,, & k_3^\mu &= (E,\,-p\sin\theta,\,0,\,-p\cos\theta)\,,\\
\varepsilon_1^\mu(0) &= (-p,\,0,\,0,\,E)\,/M_\mathrm{W}, & \varepsilon_3^{\mu,*}(0) &= (p,\,-E\sin\theta,\,0,\,-E\cos\theta)\,/M_\mathrm{W},\\
\varepsilon_1^\mu(\pm) &= (0,\,-1,\,\pm\mathrm{i},\,0)\,/\sqrt{2}, & \varepsilon_3^{\mu,*}(\pm) &= (0,\,-\cos\theta,\,\mp\mathrm{i},\,\sin\theta)\,/\sqrt{2},\\
k_2^\mu &= (E,\,0,\,0,\,p)\,, & k_4^\mu &= (E,\,p\sin\theta,\,0,\,p\cos\theta)\,,\\
\varepsilon_2^\mu(0) &= (-p,\,0,\,0,\,-E)\,/M_\mathrm{W}, & \varepsilon_4^{\mu,*}(0) &= (p,\,E\sin\theta,\,0,\,E\cos\theta)\,/M_\mathrm{W},\\
\varepsilon_2^\mu(\pm) &= (0,\,1,\,\pm\mathrm{i},\,0)\,/\sqrt{2}, & \varepsilon_4^{\mu,*}(\pm) &= (0,\,\cos\theta,\,\mp\mathrm{i},\,-\sin\theta)\,/\sqrt{2}
\end{aligned} \tag{3.2}$$

in terms of the energy E of the W bosons, their momentum $p = \sqrt{E^2 - M_\mathrm{W}^2}$, and the scattering angle θ. For the outgoing particles, the complex conjugate of the polarization vectors has to be taken.

The polarization vectors fulfill

$$\varepsilon_i \cdot \varepsilon_i^* = -1 \quad \text{and} \quad \varepsilon_i \cdot k_i = 0\,. \tag{3.3}$$

Observe especially that the longitudinal polarization vectors become increasingly (anti-)parallel to k_μ as k becomes large. In fact, for every component,

$$\varepsilon_i^\mu(0) = \mp\frac{k_i^\mu}{M_\mathrm{W}} + \mathcal{O}\left(\frac{M_\mathrm{W}}{E}\right) \tag{3.4}$$

with '$-$' for incoming ($i = 1, 2$) and '$+$' for outgoing ($i = 3, 4$) bosons. This peculiar behaviour can be dangerous to unitarity, see Sect. 4.2. The momenta and polarization vectors appear in the final formulas as scalar products of each other and contracted with Levi-Cività tensors.

The Mandelstam variables are defined as

$$\begin{aligned} s &= (k_1 + k_2)^2 = 4E^2\,, \\ t &= (k_1 - k_3)^2 = -4p^2 \sin^2\theta/2\,, \\ u &= (k_1 - k_4)^2 = -4p^2 \cos^2\theta/2\,. \end{aligned} \tag{3.5}$$

The polarized differential cross-section is expressed in terms of $\mathcal{M}$ as

$$\left(\frac{\mathrm{d}\sigma}{\mathrm{d}\Omega}\right)_{\lambda_1\lambda_2\lambda_3\lambda_4} = \frac{1}{64\pi^2 s}\left|\mathcal{M}_{\lambda_1\lambda_2\lambda_3\lambda_4}\right|^2 \tag{3.6}$$

and the unpolarized cross-section results from averaging over the incoming and summing over the outgoing particles,

$$\left(\frac{\mathrm{d}\sigma}{\mathrm{d}\Omega}\right)_\text{unpol} = \frac{1}{9}\sum_{\lambda_1,\lambda_2=-1}^{1}\ \sum_{\lambda_3,\lambda_4=-1}^{1}\left(\frac{\mathrm{d}\sigma}{\mathrm{d}\Omega}\right)_{\lambda_1\lambda_2\lambda_3\lambda_4}. \tag{3.7}$$

More generally, the correct average is obtained by multiplying with $1/3$ for each unpolarized W boson and by $1/2$ for each transverse W boson in the initial state.

The integrated cross-section is obtained by

$$\sigma = \int_0^{2\pi}\mathrm{d}\varphi\int_{\theta_\text{cut}}^{\pi-\theta_\text{cut}}\mathrm{d}\theta\,\sin\theta\,\frac{\mathrm{d}\sigma}{\mathrm{d}\Omega} \tag{3.8}$$

where θ_cut denotes an angular cut which is set to 10° in the numerical calculations.

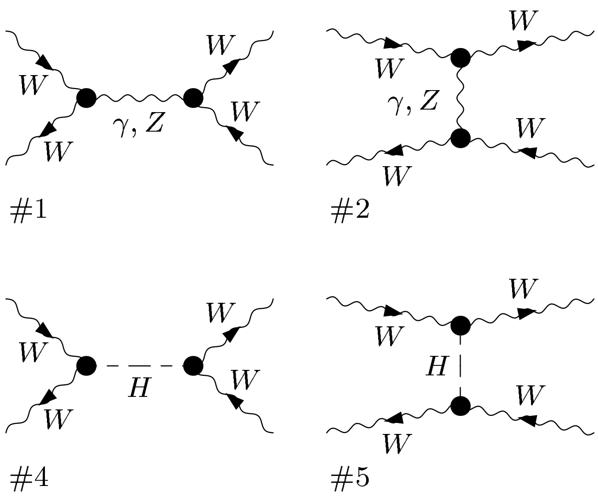

Figure 3.1: The lowest-order diagrams contributing to $\mathrm{W^+W^-} \to \mathrm{W^+W^-}$.

3.2 Analytical Born formulae

For $\mathrm{W^+W^-} \to \mathrm{W^+W^-}$ there exist in lowest order the seven diagrams shown in Fig. 3.1. Note that there is no u-channel due to charge conservation and therefore the cross-section is expected to have a forward-backward asymmetry. The amplitude resulting from these diagrams is

$$\begin{aligned}\mathcal{M}_{\mathrm{Born}} = & -e^2\left(\frac{1}{s}+\frac{c_{\mathrm{W}}^2}{s_{\mathrm{W}}^2}\frac{1}{s-M_{\mathrm{Z}}^2}\right)\mathcal{M}_1 - e^2\left(\frac{1}{t}+\frac{c_{\mathrm{W}}^2}{s_{\mathrm{W}}^2}\frac{1}{t-M_{\mathrm{Z}}^2}\right)\mathcal{M}_2 \\ & -\frac{e^2}{s_{\mathrm{W}}^2}\mathcal{M}_3 - \frac{e^2 M_{\mathrm{W}}^2}{s_{\mathrm{W}}^2}\frac{1}{s-M_{\mathrm{H}}^2}\,\mathcal{M}_4 - \frac{e^2 M_{\mathrm{W}}^2}{s_{\mathrm{W}}^2}\frac{1}{t-M_{\mathrm{H}}^2}\,\mathcal{M}_5\,. \end{aligned} \tag{3.9}$$

$\mathcal{M}_1$–$\mathcal{M}_5$ denote the matrix elements of the diagrams #1–#5 in Fig. 3.1. They contain the complete kinematical information and are given by

$$\begin{aligned}\mathcal{M}_1 = & \ (\varepsilon_1\cdot\varepsilon_2)(\varepsilon_3^*\cdot\varepsilon_4^*)(t-u) + \\ & 4\Big\{(\varepsilon_1\cdot\varepsilon_2)\big[(\varepsilon_3^*\cdot k_4)(\varepsilon_4^*\cdot k_2) - (\varepsilon_3^*\cdot k_2)(\varepsilon_4^*\cdot k_3)\big] \\ & + (\varepsilon_3^*\cdot\varepsilon_4^*)\big[(\varepsilon_1\cdot k_3)(\varepsilon_2\cdot k_4) - (\varepsilon_1\cdot k_4)(\varepsilon_2\cdot k_3)\big] \\ & - (\varepsilon_2\cdot k_1)\big[(\varepsilon_1\cdot\varepsilon_3^*)(\varepsilon_4^*\cdot k_3) - (\varepsilon_1\cdot\varepsilon_4^*)(\varepsilon_3^*\cdot k_4)\big] \\ & - (\varepsilon_1\cdot k_2)\big[(\varepsilon_2\cdot\varepsilon_4^*)(\varepsilon_3^*\cdot k_4) - (\varepsilon_2\cdot\varepsilon_3^*)(\varepsilon_4^*\cdot k_3)\big]\Big\}\,,\end{aligned} \tag{3.10}$$

$$\begin{aligned}
\mathcal{M}_2 = \; & (\varepsilon_1 \cdot \varepsilon_3^*)(\varepsilon_2 \cdot \varepsilon_4^*)(s-u) + \\
& 4\Big\{ (\varepsilon_1 \cdot k_3)\big[(\varepsilon_3^* \cdot \varepsilon_4^*)(\varepsilon_2 \cdot k_4) + (\varepsilon_2 \cdot \varepsilon_3^*)(\varepsilon_4^* \cdot k_2)\big] \\
& + (\varepsilon_3^* \cdot k_1)\big[(\varepsilon_1 \cdot \varepsilon_4^*)(\varepsilon_2 \cdot k_4) + (\varepsilon_1 \cdot \varepsilon_2)(\varepsilon_4^* \cdot k_2)\big] \\
& - (\varepsilon_1 \cdot \varepsilon_3^*)\big[(\varepsilon_2 \cdot k_3)(\varepsilon_4^* \cdot k_2) + (\varepsilon_2 \cdot k_4)(\varepsilon_4^* \cdot k_3)\big] \\
& - (\varepsilon_2 \cdot \varepsilon_4^*)\big[(\varepsilon_1 \cdot k_2)(\varepsilon_3^* \cdot k_4) - (\varepsilon_1 \cdot k_4)(\varepsilon_3^* \cdot k_2)\big] \Big\} ,
\end{aligned} \tag{3.11}$$

$$\mathcal{M}_3 = (\varepsilon_1 \cdot \varepsilon_2)(\varepsilon_3^* \cdot \varepsilon_4^*) + (\varepsilon_1 \cdot \varepsilon_3^*)(\varepsilon_2 \cdot \varepsilon_4^*) - 2(\varepsilon_1 \cdot \varepsilon_4^*)(\varepsilon_2 \cdot \varepsilon_3^*) , \tag{3.12}$$

$$\mathcal{M}_4 = (\varepsilon_1 \cdot \varepsilon_2)(\varepsilon_3^* \cdot \varepsilon_4^*) , \tag{3.13}$$

$$\mathcal{M}_5 = (\varepsilon_1 \cdot \varepsilon_3^*)(\varepsilon_2 \cdot \varepsilon_4^*) . \tag{3.14}$$

Explicit expressions for the various polarizations are listed in Table 3.1–3.3. Notice in particular that each longitudinal W boson enhances the individual matrix elements $\mathcal{M}_1$–$\mathcal{M}_5$ by a factor $\sqrt{s}/M_\mathrm{W}$.

3.3 t-channel singularity

For equal polarizations in the initial and final state, i.e. for $\lambda_1 = \lambda_3$ and $\lambda_2 = \lambda_4$, the lowest-order amplitude diverges for small momentum transfer t owing to the t-channel photon-exchange diagram. In fact, in this limit the lowest-order cross-section turns into the Rutherford cross-section $\propto 1/t^2 \propto 1/[p\sin(\theta/2)]^4$. If either $\lambda_1 = \lambda_3$ or $\lambda_2 = \lambda_4$, the cross-section has at most a $1/t$ singularity for small t, and for $\lambda_1 \neq \lambda_3$ and $\lambda_2 \neq \lambda_4$ it is regular.

Since experimentally the extreme forward direction cannot be observed, we use a finite angular cut-off θ_cut which excludes the singularity and renders the differential cross-section integrable.

Due to these Coulomb effects the total cross-section behaves as $(s - 4M_\mathrm{W}^2)^{-2}$ for $s \downarrow 4M_\mathrm{W}^2$ (i.e. it diverges at the threshold), provided the particles are stable. This comes about because near the threshold the relative velocity of the particles is small so that they have a long time to interact.

For unstable particles there is a substantial screening of this divergence if the lifetime $\tau \sim 1/\Gamma_\mathrm{W}$ is comparable to or smaller than the characteristic time of the Coulomb interaction $t_\mathrm{coul} \sim 1/\beta^2 M_\mathrm{W}$, where β is the relative velocity of the outgoing W bosons. Explicit calculations for this case can be found in

Polarization	$\mathcal{M}_1$	$\mathcal{M}_4$
LLLL	$\frac{(t-u)(s+2M_{\mathrm{W}}^2)^2}{4M_{\mathrm{W}}^4}$	$\frac{(s-2M_{\mathrm{W}}^2)^2}{4M_{\mathrm{W}}^4}$
LLL±, LL±L L±LL, ±LLL	$\frac{(s+2M_{\mathrm{W}}^2)\sqrt{2stu}}{2M_{\mathrm{W}}^3}$	0
LL±±, ±±LL	$-\frac{(t-u)(s+2M_{\mathrm{W}}^2)}{2M_{\mathrm{W}}^2}$	$\frac{s-2M_{\mathrm{W}}^2}{2M_{\mathrm{W}}^2}$
L±L±, ±L±L L±∓L, ±LL∓	$\frac{su}{M_{\mathrm{W}}^2}$	0
L±L∓, ±L∓L L±±L, ±LL±	$-\frac{st}{M_{\mathrm{W}}^2}$	0
L±±±, ±±±L ±±L±, ±L±± L±∓∓, ±±∓L ±L∓∓, ±±L∓	$-\frac{\sqrt{2stu}}{M_{\mathrm{W}}}$	0
±±±±, ±±∓∓	$t-u$	1
all others	0	0

Table 3.1: Analytical expressions for the matrix elements $\mathcal{M}_1$ and $\mathcal{M}_4$ in Eq. (3.9).

Polarization	$\mathcal{M}_2 = \text{(entry)} + (s-u)\mathcal{M}_5$	$\mathcal{M}_5$
LLLL	$-\frac{2st(t-2u)}{M_W^2\tilde{s}}$	$\frac{\left(s(t-u)-\tilde{s}^2\right)^2}{16M_W^4\tilde{s}^2}$
LLL±, LL±L L±LL, ±LLL	$-\frac{\left(st+2M_W^2(2t-u)\right)\sqrt{2stu}}{2M_W^3\tilde{s}}$	$\frac{\left(s(t-u)-\tilde{s}^2\right)\sqrt{2stu}}{8M_W^3\tilde{s}^2}$
LL±±, ±±LL L±±L, ±LL±	$\frac{t\left(s(t-u)-2M_W^2u\right)}{M_W^2\tilde{s}}$	$\frac{stu}{2M_W^2\tilde{s}^2}$
LL±∓, ±∓LL L±∓L, ±LL∓	$-\frac{tu(s+2M_W^2)}{M_W^2\tilde{s}}$	
L±L±, ±L±L	$-\frac{2tu(s+M_W^2)}{M_W^2\tilde{s}}$	$\frac{u\left(s(t-u)-\tilde{s}^2\right)}{4M_W^2\tilde{s}^2}$
L±L∓, ±L∓L	$\frac{t(st-2M_W^2u)}{M_W^2\tilde{s}}$	$-\frac{t\left(s(t-u)-\tilde{s}^2\right)}{4M_W^2\tilde{s}^2}$
L±±±, ±±±L ±L±±, ±±L±	$\frac{(2t-u)\sqrt{2stu}}{M_W\tilde{s}}$	$\frac{u\sqrt{2stu}}{2M_W\tilde{s}^2}$
L±∓±, ±∓±L ±L±∓, ±∓L∓	$-\frac{u\sqrt{2stu}}{M_W\tilde{s}}$	
L±±∓, ±∓∓L L±∓∓, ±±∓L ±L∓±, ±∓L± ±L∓∓, ±±L∓	$\frac{t\sqrt{2stu}}{M_W\tilde{s}}$	$-\frac{t\sqrt{2stu}}{2M_W\tilde{s}^2}$
±±±∓, ±∓∓∓ ±±∓±, ±∓±±	$\frac{2tu}{\tilde{s}}$	$-\frac{tu}{\tilde{s}^2}$
±±±±	$\frac{8tu}{\tilde{s}}$	$\frac{u^2}{\tilde{s}^2}$
±∓±∓	0	$\frac{u^2}{\tilde{s}^2}$
±±∓∓, ±∓∓±	0	$\frac{t^2}{\tilde{s}^2}$

Table 3.2: Analytical expressions for the matrix elements $\mathcal{M}_2$ and $\mathcal{M}_5$ in Eq. (3.9) where $\tilde{s} = s - 4M_W^2 = 4p^2$.

Polarization	$\mathcal{M}_3$		
LLLL	$\dfrac{s\big(stu-(2t-u)\tilde{s}^2\big)}{4M_\mathrm{W}^4\tilde{s}^2}$		
$\mathrm{LLL}\pm, \mathrm{LL}\pm\mathrm{L}$ $\mathrm{L}\pm\mathrm{LL}, \pm\mathrm{LLL}$	$-\dfrac{\big(s(t-u)+3\tilde{s}^2\big)\sqrt{2stu}}{8M_\mathrm{W}^3\tilde{s}^2}$		
$\mathrm{LL}\pm\pm, \pm\pm\mathrm{LL}$	$\dfrac{s(t^2+u^2)+\tilde{s}^3}{4M_\mathrm{W}^2\tilde{s}^2}$		
$\mathrm{LL}\pm\mp, \pm\mp\mathrm{LL}$	$-\dfrac{stu}{2M_\mathrm{W}^2\tilde{s}^2}$		
$\mathrm{L}\pm\pm\mathrm{L}, \pm\mathrm{LL}\pm$	$\dfrac{t(st+\tilde{s}^2)}{2M_\mathrm{W}^2\tilde{s}^2}$		
$\mathrm{L}\pm\mp\mathrm{L}, \pm\mathrm{LL}\mp$	$\dfrac{u(su-\tilde{s}^2)}{2M_\mathrm{W}^2\tilde{s}^2}$		
$\mathrm{L}\pm\mathrm{L}\pm, \pm\mathrm{L}\pm\mathrm{L}$	$-\dfrac{u\big(s(3t+u)+\tilde{s}^2\big)}{4M_\mathrm{W}^2\tilde{s}^2}$		
$\mathrm{L}\pm\mathrm{L}\mp, \pm\mathrm{L}\mp\mathrm{L}$	$-\dfrac{t\big(s(t+3u)-\tilde{s}^2\big)}{4M_\mathrm{W}^2\tilde{s}^2}$		
$\mathrm{L}\pm\pm\pm, \pm\pm\pm\mathrm{L}$ $\pm\mathrm{L}\pm\pm, \pm\pm\mathrm{L}\pm$	$\dfrac{(2t+u)\sqrt{2stu}}{2M_\mathrm{W}\tilde{s}^2}$		
$\mathrm{L}\pm\mp\pm, \pm\mp\pm\mathrm{L}$ $\pm\mathrm{L}\pm\mp, \pm\mp\mathrm{L}\mp$	$-\dfrac{u\sqrt{2stu}}{2M_\mathrm{W}\tilde{s}^2}$		
$\mathrm{L}\pm\pm\mp, \pm\mp\mp\mathrm{L}$ $\pm\mathrm{L}\mp\pm, \pm\mp\mathrm{L}\pm$	$\dfrac{t\sqrt{2stu}}{2M_\mathrm{W}\tilde{s}^2}$		
$\mathrm{L}\pm\mp\mp, \pm\pm\mp\mathrm{L}$ $\pm\mathrm{L}\mp\mp, \pm\pm\mathrm{L}\mp$	$-\dfrac{(t+2u)\sqrt{2stu}}{2M_\mathrm{W}\tilde{s}^2}$		
$\pm\pm\pm\mp, \pm\mp\mp\mp$ $\pm\pm\mp\pm, \pm\mp\pm\pm$	$\dfrac{tu}{\tilde{s}^2}$		
$\pm\pm\pm\pm$	$-\dfrac{t^2-2u(t+u)}{\tilde{s}^2}$	$\pm\pm\mp\mp$	$\dfrac{2t(t+u)-u^2}{\tilde{s}^2}$
$\pm\mp\mp\pm$	$-\dfrac{t^2}{\tilde{s}^2}$	$\pm\mp\pm\mp$	$-\dfrac{u^2}{\tilde{s}^2}$

Table 3.3: Analytical expressions for the matrix element $\mathcal{M}_3$ in Eq. (3.9) where $\tilde{s} = s - 4M_\mathrm{W}^2 = 4p^2$.

[BaBD93]. Here we shall neglect these effects since we are working in the approximation that the external W bosons are on-shell and stable.

3.4 Differential cross-section

All of the following figures are plotted for a Higgs mass of $M_{\mathrm{H}} = 100$ GeV. This value is in the range allowed by precision data, which favour a light Higgs boson, and in particular it lies below the threshold of $2M_{\mathrm{W}}$ so that the Higgs resonance needs not be treated. The latter is discussed in Sect. 4.5. Unless otherwise noted, an angular cut-off of $\theta_{\text{cut}} = 10°$ is used.

In Fig. 3.2 the differential lowest-order cross-section is shown for $\sqrt{s} = 200\,\mathrm{GeV}$, $1\,\mathrm{TeV}$, and $5\,\mathrm{TeV}$ for the dominating polarizations LLLL, LTLT, LLTT, TTTT, and for the unpolarized case UUUU. For all these polarizations except LLTT the curves display the strong forward peak owing to the t-channel pole. The figures show that the main contributions to the unpolarized cross-section in backward direction come from completely transversally polarized bosons. The sharp dips in the longitudinal cross-section correspond to zeros in the amplitude. To be precise, the longitudinal cross-section is a rational function in t and has four such zeros. For $\sqrt{s} \lesssim 274\,\mathrm{GeV}$ two of these zeros and for $\sqrt{s} \gtrsim 274\,\mathrm{GeV}$ one of them lie in the physical region; their contour is shown in Fig. 3.3. From the experimental point of view, these are of course completely negligible.

3.5 Total cross-section

Although the Born cross-section can be integrated analytically, the resulting formulae are rather long, so instead of giving the full expressions, we list only their leading term for $s \to \infty$ in Table 3.4. In Fig. 3.4 the integrated lowest-order cross-section is displayed for various polarizations. The curves reflect very nicely the high-energy behaviour of the analytical expressions.

The cross-sections for the polarizations LLLL, TTTT, LTLT, and LTTL behave as $1/s$ at high energies, all others are suppressed by additional factors $1/s$. Owing to the $1/t$ pole, the cross-sections with equal initial- and final-state polarizations, LLLL, TTTT, and LTLT, are enhanced by a factor $1/(1 - \cos^2\theta_{\text{cut}}) \approx 33$ for $\theta_{\text{cut}} = 10°$ and are therefore dominant. For these polarizations the con-

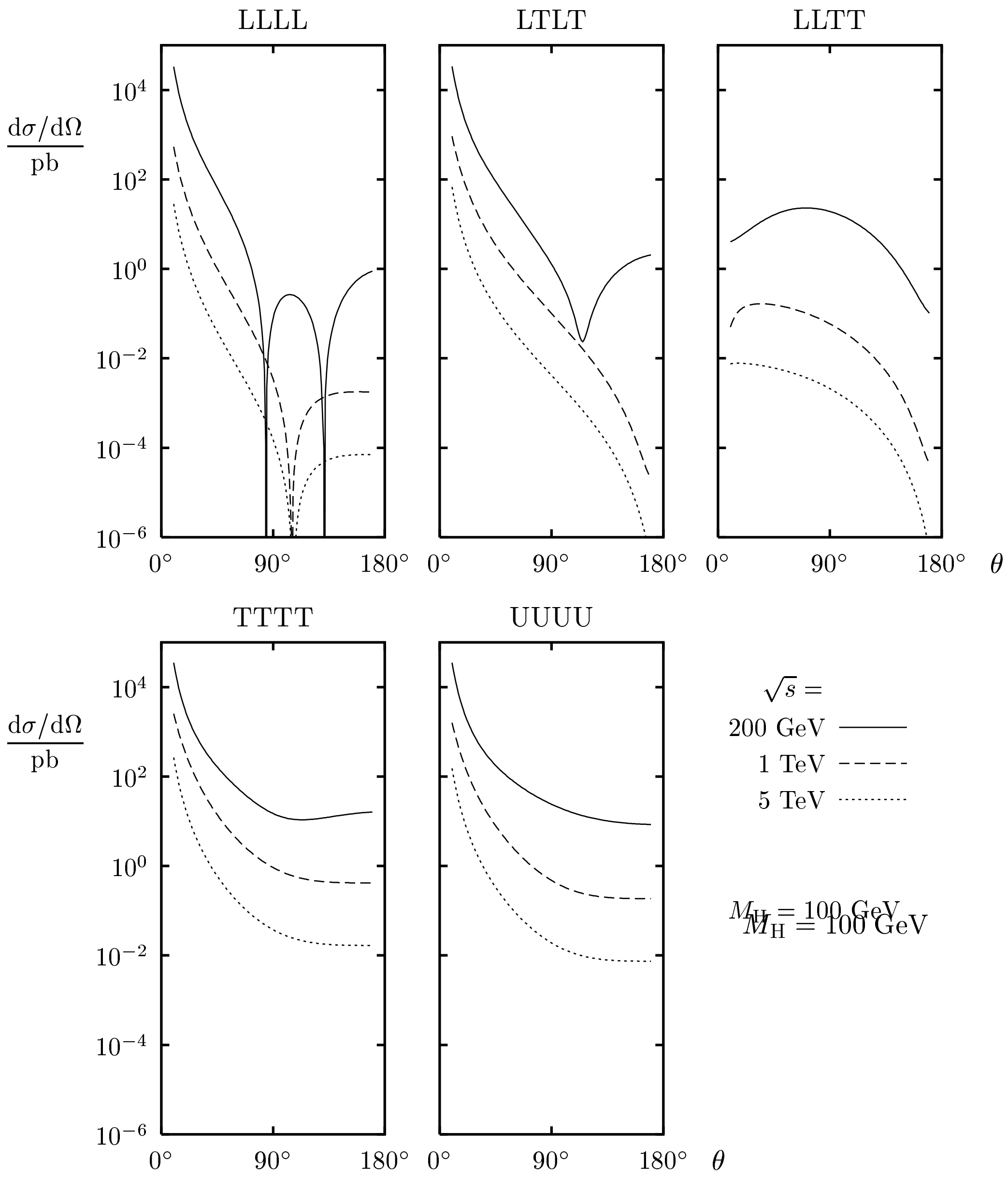

Figure 3.2: The differential lowest-order cross-section for various polarizations at different energies.

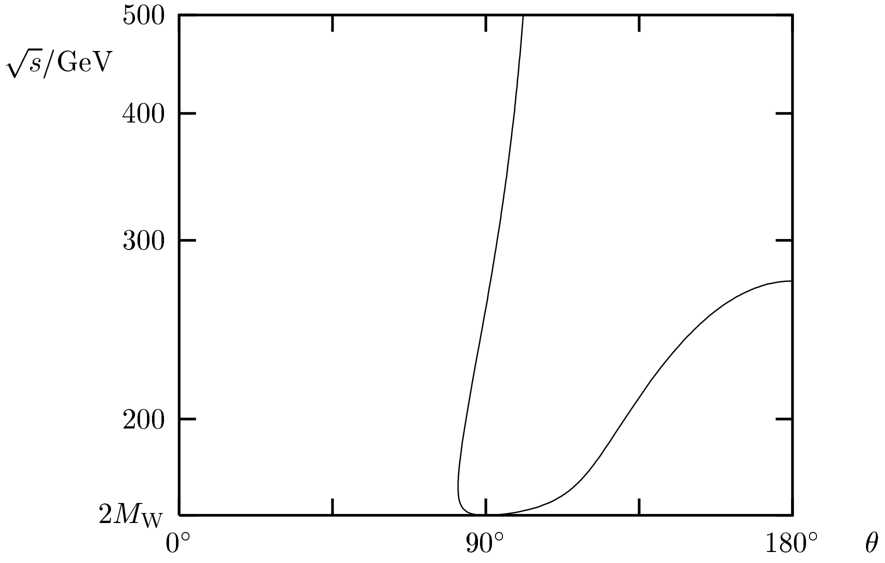

Figure 3.3: The contour of the zeros in the longitudinal cross-section as a function of energy. The lower branch approaches a constant ($\theta \approx 106^\circ$) in the high-energy limit.

tribution of the backward hemisphere is less than 1% for energies above $1\ \mathrm{TeV}$ and less than 3% for lower energies. Note that the size of the corresponding integrated cross-sections depends strongly on the angular cut, θ_{cut}, because of the t-channel singularity. This dependence is plotted in Fig. 3.5. For example, switching from $\theta_{\text{cut}} = 5^\circ$ to 10° changes the total cross-section roughly by a factor 4.

Polarization	$\sigma_{\text{Born}} = \pi\alpha^2/s_{\text{W}}^4 \cdot (\text{entry})$
LLLL	$\frac{1}{s}\left\{\frac{(M_{\text{H}}^2+M_{\text{Z}}^2)(2M_{\text{Z}}^2 L_c + M_{\text{H}}^2 c)}{4M_{\text{W}}^4} + \frac{c\,(75-26c^2-c^4)}{48c_{\text{W}}^4(1-c^2)}\right\}$
LLLT $= \text{LLTL}$ $= 2\,\text{LTLL}$ $= 2\,\text{TLLL}$	$\frac{1}{s^2}\left\{-\frac{(M_{\text{H}}^2+4M_{\text{W}}^2+M_{\text{Z}}^2)^2 L_c}{4M_{\text{W}}^2} - \frac{c\left[3\left(M_{\text{H}}^2+2(3M_{\text{W}}^2+M_{\text{Z}}^2)\right)^2-(6-c^2)(2M_{\text{W}}^2+M_{\text{Z}}^2)^2\right]}{12M_{\text{W}}^2}\right\}$
LLTT $= 4\,\text{TTLL}$	$\frac{1}{s}\frac{c\,(3+c^2)}{6}$
LTLT $= \text{TLTL}$	$\frac{1}{s}\left\{\frac{c\,(5-c^2)}{1-c^2}+2L_c\right\}$
LTTL $= \text{TLLT}$	$\frac{1}{s^3}\left\{\left[M_{\text{H}}^4+M_{\text{Z}}^4+2M_{\text{H}}^2(8M_{\text{W}}^2+M_{\text{Z}}^2)\right]L_c + \frac{c\,(5-c^2)(M_{\text{H}}^4+M_{\text{Z}}^4)}{2(1-c^2)} + \frac{c\,(8M_{\text{W}}^2+M_{\text{Z}}^2)\left[18M_{\text{H}}^2+(3+c^2)(8M_{\text{W}}^2+M_{\text{Z}}^2)\right]}{6}\right\}$
LTTT $= \text{TLTT}$ $= 2\,\text{TTLT}$ $= 2\,\text{TTTL}$	$\frac{1}{s^2}\left\{-M_{\text{W}}^2(29c+3c^3+20L_c)\right\}$
TTTT	$\frac{1}{s}\left\{\frac{c\,(75-26c^2-c^4)}{3(1-c^2)}+8L_c\right\}$

Table 3.4: Leading terms in s in the high-energy limit for integrated polarized lowest-order cross-sections. The following abbreviations are used: $c = \cos\theta_{\text{cut}}$ and $L_c = \ln\frac{1-c}{1+c}$. The relations between different polarizations in the left column are to be read e.g. as $\sigma_{\text{LTTT}} = 2\sigma_{\text{TTLT}}$, where the numerical prefactors originate from the different spin average.

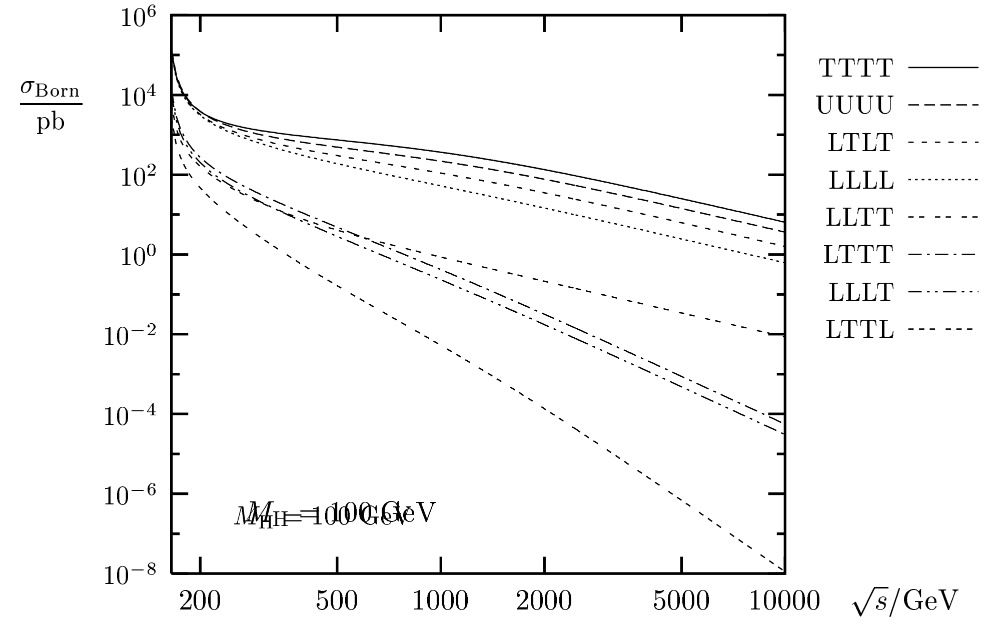

Figure 3.4: The integrated lowest-order cross-section for various polarizations.

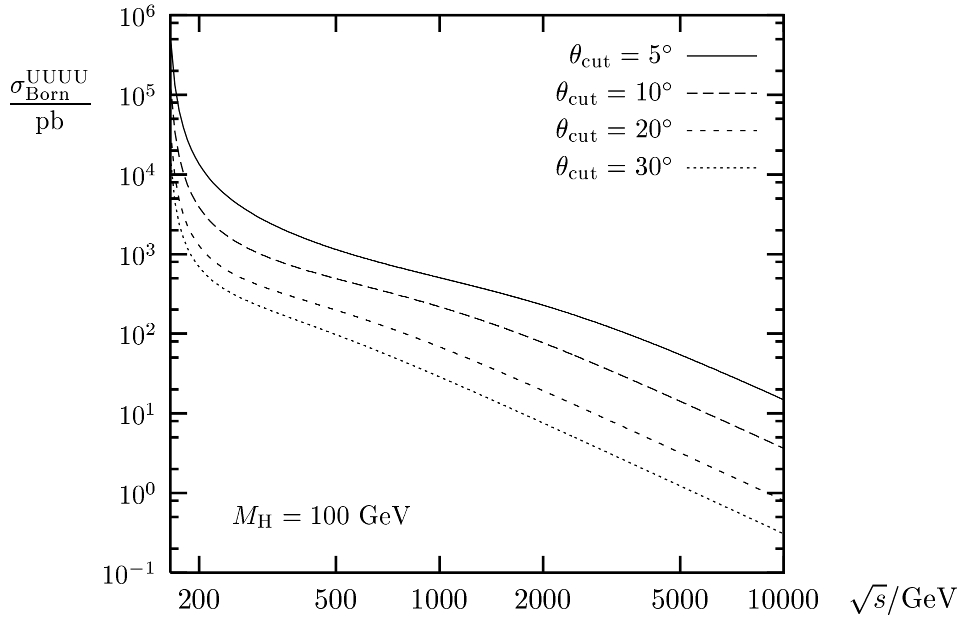

Figure 3.5: Angular cut-off dependence of the unpolarized integrated cross-section.

Chapter 4

Higgs Physics

4.1 Unitarity bound

The S matrix is unitary,

$$SS^\dagger = S^\dagger S = \mathbf{1}\,. \tag{4.1}$$

To investigate what constraints unitarity imposes on the cross-section, first take the matrix elements of (4.1) in 'in' states and insert a complete set of 'in' states between $S^\dagger$ and S:

$$\langle i_{\text{in}}|\, S^\dagger \sum_f |f_{\text{in}}\rangle \langle f_{\text{in}}|\, S \,|i_{\text{in}}\rangle = \sum_f |\langle f_{\text{in}}|\, S \,|i_{\text{in}}\rangle|^2 = 1\,. \tag{4.2}$$

The sum is understood to include the phase-space integration over the momenta of the particles. Eq. (4.2) illustrates that unitarity expresses probability conservation in the scattering process, for it shows that the probability that an initial state $|i_{\text{in}}\rangle$ is scattered into *any* final state is unity.

Now consider elastic scattering, that is $f = i$. Then

$$|\langle i_{\text{in}}|\, S \,|i_{\text{in}}\rangle|^2 = 1 - \sum_{f\neq i} |\langle f_{\text{in}}|\, S \,|i_{\text{in}}\rangle|^2 \leqslant 1 \tag{4.3}$$

implies that $\langle i_{\text{in}}|\, S \,|i_{\text{in}}\rangle$ is a complex number of modulus less than 1. From this it follows that $|\langle i_{\text{in}}|\, T \,|i_{\text{in}}\rangle|^2 = |-\mathrm{i}(\langle i_{\text{in}}|\, S \,|i_{\text{in}}\rangle - 1)|^2 \leqslant 4$.

Performing a partial wave expansion on the total cross-section yields

$$\sigma = \frac{\pi}{p^2} \sum_{J=0}^{\infty} (2J+1)\, |\langle i_{\text{in}}|\, T_J \,|i_{\text{in}}\rangle|^2 \tag{4.4}$$

The unitarity limit on the T matrix (of which T_J is the component with angular momentum J) constrains a single partial wave by

$$\sigma_J \leqslant \frac{4\pi}{p^2}(2J+1) \xrightarrow{s\to\infty} \frac{4\pi}{s/4}(2J+1) \propto \frac{1}{s} \tag{4.5}$$

since $p^2 = E^2 - M_{\mathrm{W}}^2 = s/4 - M_{\mathrm{W}}^2$. A crude estimate for the sum of the partial waves can be obtained as follows. If the range of the interaction is finite and equal to a, then for sufficiently high energy the sum is actually limited by $J_{\max} \simeq pa$. This in turn implies for the total cross-section

$$\sigma \leqslant \frac{4\pi}{p^2}\sum_{J=0}^{J_{\max}}(2J+1) \simeq 4\pi a^2 = \text{const}\,. \tag{4.6}$$

A detailed analysis entails the more permissive bound $\sigma \leqslant \text{const} \cdot \ln^2 s$. In gauge theories the cross-section will usually behave better, typically as $1/s$. This will be shown in the next section.

Eq. (4.5) is the so-called unitarity bound for a cross-section in the high-energy limit (see [We66] for a much more thorough treatment). It must be satisfied in principle by any S-matrix element for all values of the coupling constants and masses. However, this will generally only occur if the theory is treated to all orders. A perturbative expansion need not itself obey unitarity at a given order.

4.2 Unitarity in longitudinal W–W scattering at tree level

The unitarity bound turns out to be a nontrivial constraint for a theory. In fact, without the cancellations guaranteed by the gauge symmetry, the cross-section would grossly violate unitarity at high energies [Ve93].

Considering the dependence of the invariant matrix element $\mathcal{M}$ on s the following happens:

- Individual diagrams grow as s^2.
- The Yang-Mills structure of the three and four gauge-boson vertices leads to certain cancellations, and growth as s results.

- Diagrams involving Higgs exchange give further cancellations, and the total behaves as a constant.

As mentioned before, the longitudinal polarization vectors each give a factor $\sqrt{s}$. The WWWW vertex is momentum independent, as is the WWH vertex, while the WWγ and WWZ vertices are linear in the momenta. A propagator behaves as $1/s$ (or $1/t$). It is easy to see then that for longitudinally polarized external W bosons

(a) 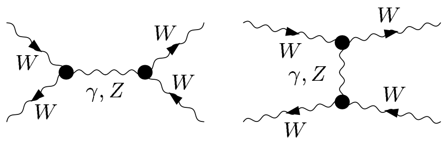

behave as s^2,

(b) 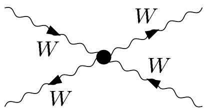

behaves as s^2, and

(c) 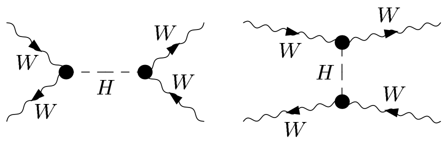

behave as s.

Since the total must (and indeed does) behave as a constant for large s we infer that the s^2 behaviour of diagrams (a) and (b) must cancel, while the remaining linear dependence on s must cancel against that of diagram (c). This is precisely what happens:

The denominators for photon and Z exchange may be combined to give

$$\frac{1}{s} + \frac{c_{\rm W}^2}{s_{\rm W}^2}\frac{1}{s - M_{\rm Z}^2} = \frac{1}{s_{\rm W}^2}\frac{1}{s} + \frac{c_{\rm W}^2}{s_{\rm W}^2}\frac{M_{\rm Z}^2}{s(s-M_{\rm Z}^2)} = \frac{1}{s_{\rm W}^2}\left(\frac{1}{s} + \frac{M_{\rm W}^2}{s^2}\right) + \mathcal{O}(s^{-3}) \tag{4.7}$$

and the other propagators are expanded similarly. To eliminate all misleading energy dependence, we use the Mandelstam relation $u = 4M_{\rm W}^2 - s - t$, and replace $t = (4M_{\rm W}^2 - s)\sigma$ where $\sigma = \sin^2\theta/2$. From the Born formula, Eq. (3.9), and the matrix elements for longitudinal bosons from Tables 3.1–3.3 we get for

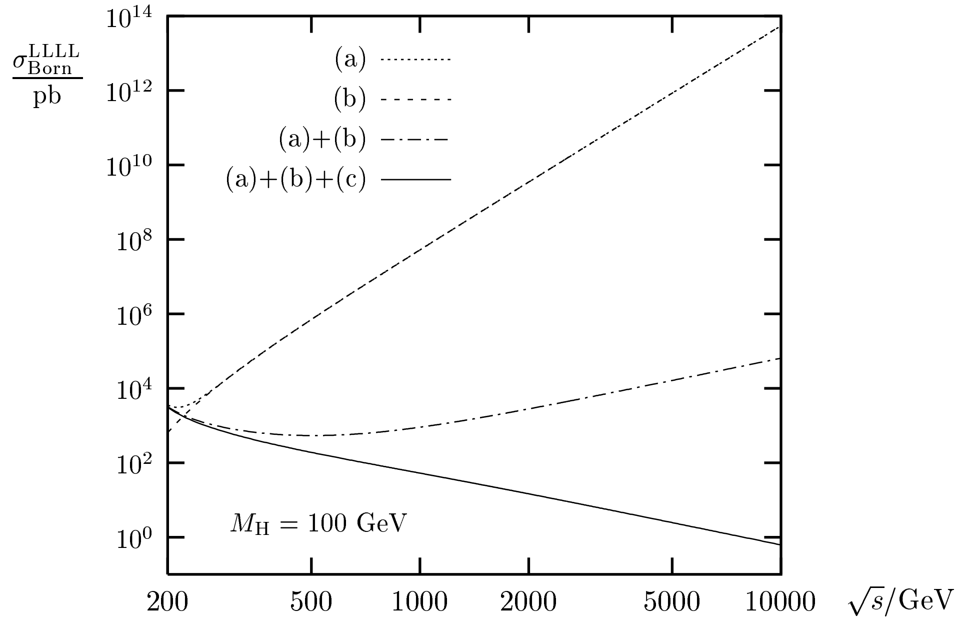

Figure 4.1: The cross-sections for longitudinal gauge-boson scattering resulting from subsets of the tree-level diagrams: (a) diagrams involving only three-gauge-boson couplings, (b) diagram involving only four-gauge-boson couplings, (c) diagrams involving Higgs bosons.

the leading terms in s (apart from an overall factor $-e^2/s_{\mathrm{W}}^2$):

$$
\begin{array}{rl}
\text{(a)} = & \frac{s^2}{M_{\mathrm{W}}^4}\frac{\sigma^2-4\sigma+1}{4} + \frac{s}{M_{\mathrm{W}}^2}\frac{13\sigma-5}{4} + \mathcal{O}(1) \\
\text{(b)} = & \frac{s^2}{M_{\mathrm{W}}^4}\frac{-\sigma^2+4\sigma-1}{4} + \frac{s}{M_{\mathrm{W}}^2}\frac{-12\sigma+4}{4} + \mathcal{O}(1) \\
\hline
\text{(a)}+\text{(b)} = & \frac{s}{M_{\mathrm{W}}^2}\frac{\sigma-1}{4} + \mathcal{O}(1) \\
\text{(c)} = & \frac{s}{M_{\mathrm{W}}^2}\frac{-\sigma+1}{4} + \mathcal{O}(1)
\end{array}
\tag{4.8}
$$

Without gauge symmetry, the diagrams with three and four gauge-boson vertices would be independent of each other and any cancellation would be incidental.

The gauge cancellations are demonstrated graphically in Fig. 4.1 for the total cross-section. The cancellations are already quite substantial at a few hundred GeV.

4.3 Possibility of a strongly interacting Higgs sector

From the results of the previous section we see that virtual Higgs-boson exchange is needed to prevent the $2 \to 2$ scattering amplitudes of longitudinal gauge bosons from violating the (perturbative) unitarity bound at high energies. In turn, the requirement of unitarity can be used to derive bounds on the Higgs-boson mass below which the SM remains weakly interacting and treatable in low-order perturbation theory [DiM73, LeQT77]. These bounds are of the order of 1 TeV and are slightly strengthened by including the $\mathcal{O}\big(\alpha/s_{\mathrm{W}}^2(M_{\mathrm{H}}^2/M_{\mathrm{W}}^2)\big)$ radiative corrections to gauge-boson scattering [DaW89]. As already pointed out in [Pa85], all these bounds are only qualitative, since they are obtained by applying perturbation theory in a region where it breaks down. The bounds on M_{H} can be related to a scale of new physics, which is necessary to avoid the Landau pole in the scalar self-interaction [MaVW89] (see Fig. 4.2). If these bounds are not satisfied the Higgs sector becomes strongly interacting. Let us go into this a little further.

As the mass of the Higgs boson becomes very large, the analysis of the Higgs sector undergoes a qualitative change. Consider the Higgs self-couplings in the SM,

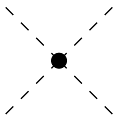 $\propto \dfrac{M_{\mathrm{H}}^2}{M_{\mathrm{W}}^2}$ and 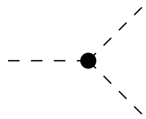 $\propto \dfrac{M_{\mathrm{H}}^2}{M_{\mathrm{W}}}\,,$ (4.9)

both of which are seen to grow with the square of the Higgs mass, scaled by M_{W}. For $M_{\mathrm{H}} \gg M_{\mathrm{W}}$, we enter the domain of strong coupling. A perturbative expansion in a coupling proportional to M_{H}^2 is no longer a sensible procedure, and it is for this reason that the above vertices are sometimes referred to as 'nonperturbative.'

Because of these large couplings one might expect that radiative corrections [GuHKD90] will be large as M_{H} grows. However, Veltman [Ve77] pointed out that for processes without external Higgs bosons there is a screening mechanism which secures that at one-loop order there are only $\mathcal{O}\big(\alpha/s_{\mathrm{W}}^2 \ln(M_{\mathrm{H}}/M_{\mathrm{W}})\big)$ corrections, while at two or more loops, there are corrections of order $\alpha^2/s_{\mathrm{W}}^4(M_{\mathrm{H}}^2/M_{\mathrm{W}}^2)$. Radiative corrections which are dependent

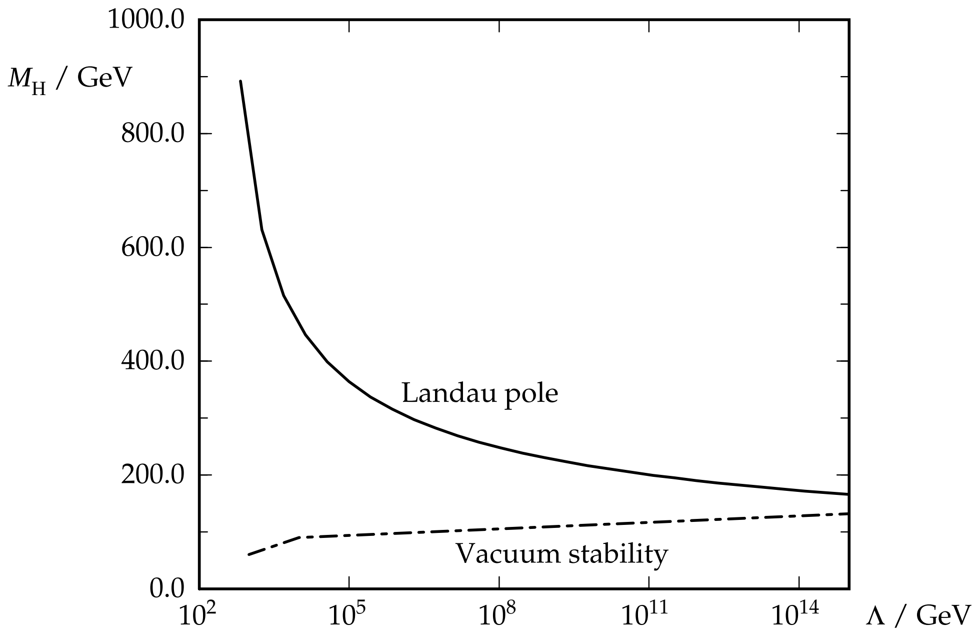

Figure 4.2: Bounds on the mass of the Higgs boson in the SM. Λ denotes the energy scale at which the Higgs–gauge-boson system of the SM would become strongly interacting; it can be thought of as the scale at which new physics arises and the SM is no longer a valid theory. The upper bound is derived from the condition that the running quartic Higgs self-coupling $\lambda(Q)$ (cf. Eq. (2.14)) be finite (i.e. that there be no Landau pole) up to the scale Λ. The lower bound follows from the requirement of vacuum stability, i.e. that the scalar potential be bounded from below, $\lambda(Q) > 0$. (Figure taken from [Da97].)

on the Higgs mass are thus of the form

$$\frac{\alpha}{s_{\mathrm{W}}^2}\ln\frac{M_{\mathrm{H}}}{M_{\mathrm{W}}}+\left(\frac{\alpha}{s_{\mathrm{W}}^2}\right)^2\frac{M_{\mathrm{H}}^2}{M_{\mathrm{W}}^2}+\ldots \tag{4.10}$$

For large values of M_{H}, the theory is strongly coupled, but the effects of the strong interactions are screened by an extra factor of α/s_{W}^2. This explains why observables at up to LEP energies are relatively insensitive to the Higgs mass and why experiments so far failed to either confirm or rule out a strongly interacting Higgs sector, although the present data ($M_{\mathrm{H}}=159^{+153}_{-86}$ GeV [LEP96]) seem to favour a weakly interacting Higgs sector.

This screening is not accidental. The underlying reason is that since the Higgs potential is in exact correspondence (upon ignoring fermions) with the linear sigma model, it has the symmetry structure $\mathrm{SU}(2)_L\times\mathrm{SU}(2)_R$, which is larger than the gauge symmetry $\mathrm{SU}(2)_L\times\mathrm{U}(1)_Y$, containing an extra, so-called custodial, $\mathrm{SU}(2)$ [SiSVZ80].

As a side remark, for a very heavy Higgs boson ($M_{\mathrm{H}}\gg M_{\mathrm{W}},M_{\mathrm{Z}}$), which is a good approximation for a Higgs mass in the range of the unitarity limit, ~ 1 TeV, there exists an effective theory, obtained by integrating out the Higgs field in the path integral [DiG96]. This theory allows leading one-loop Higgs contributions to be easily derived from the effective Lagrangian.

4.4 The equivalence theorem

Although initially a complex doublet of Higgs fields (i.e. four degrees of freedom) is introduced, there remains only one physical scalar Higgs field following spontaneous symmetry breaking. To be specific, we have four Higgs fields and eight gauge-field components before symmetry breaking, and one Higgs field and eleven gauge-field components afterwards. So there is a transfer of three degrees of freedom from the Higgs sector to the gauge sector. In this sense these Higgs fields become the longitudinal spin modes of the massive vector bosons.

This intuitive statement may be given a more precise meaning by the so-called equivalence theorem (ET), which states that S-matrix elements involving longitudinal gauge bosons are equivalent to those of the unphysical Higgs up to $\mathcal{O}(M_\mathrm{W}/E)$ corrections, i.e.

$$S(W_\mathrm{L}^+, W_\mathrm{L}^-, Z_\mathrm{L}, \dots) = S(\varphi^+, \varphi^-, \chi, \dots) + \mathcal{O}\left(\frac{M_\mathrm{W}}{E}\right) . \tag{4.11}$$

The proof of this statement relies basically on a Ward identity and has been worked out to various levels of rigour in [CoLT74]. The outline of the proof is the following.

The Ward identity $k^\mu \langle J_\mu \rangle = 0$ satisfied by a gauge-current matrix element between on-shell states expresses the conservation of the gauge current. It can be represented diagrammatically as

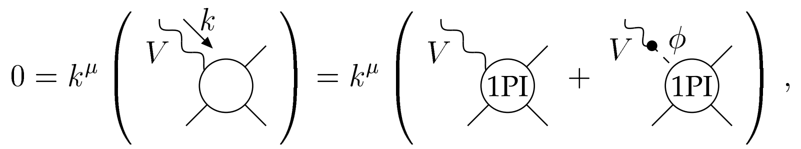

(4.12)

where we have in anticipation of Sect. 5.1.1 set $\xi_V = 0$ (Lorentz gauge) in order that the Goldstone fields ϕ do not enter into the gauge-fixing terms in Eq. (5.8) and contribute extra terms.

The second term in Eq. (4.12) in which the gauge boson V couples to the Goldstone field ϕ is responsible for the mass of the gauge boson. If we write the matrix element of the gauge current as

$$\langle 0 | \, J_\mu \, | \phi(k) \rangle = -\mathrm{i} F k_\mu \, . \tag{4.13}$$

then the gauge-boson mass is given by $M_V = gF$, where g is the gauge-boson coupling constant. Writing each term in Eq. (4.12) in terms of the corresponding 1PI amputated Green function, we find

$$k^\mu \langle \Gamma_\mu^V(k) \rangle + k^\mu \langle (\mathrm{i} g F k_\mu) \frac{\mathrm{i}}{k^2} \Gamma^\phi(k) \rangle = k^\mu \langle \Gamma_\mu^V(k) \rangle - M_V \langle \Gamma^\phi(k) \rangle = 0 \, . \tag{4.14}$$

Since the gauge-boson vertex Γ_μ^V is 1PI, the momenta of propagators inside the vertex are not, in general, collinear with k^μ and this allows to replace k^μ by $M_V \varepsilon_\mathrm{L}^\mu$ in the high-energy limit via Eq. (3.4). (If the momenta were collinear, the replacement would be incorrect because of the transversality condition $\varepsilon \cdot k = 0$.) The final result is then

$$\varepsilon_\mathrm{L}^\mu(k) \langle \Gamma_\mu^V(k) \rangle = \langle \Gamma^\phi(k) \rangle + \mathcal{O}\left(\frac{M_\mathrm{W}}{E}\right) . \tag{4.15}$$

This displays the nature of the connection between the longitudinal gauge bosons and the charged Higgs fields. It is this relation which in the absence of a direct Higgs signal could make longitudinal gauge-boson scattering the best tool for investigating the Higgs sector. Either $W_{\mathrm{L}}^{\pm}$ or $\varphi^{\pm}$ (or Z_{L} or χ), properly normalized, can serve as a good field variable for the longitudinal modes; the renaming does not change the physics.

4.5 Treatment of the Higgs resonance

Diagrams that involve a Higgs-boson propagator in the s-channel have a pole at $s = M_{\mathrm{H}}^2$. At Born level there is only one resonant diagram:

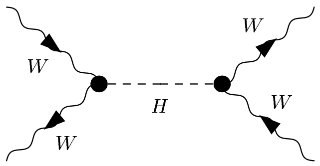

$$= -\frac{e^2 M_{\mathrm{W}}^2}{s_{\mathrm{W}}^2}\frac{\mathcal{M}_4}{s - M_{\mathrm{H}}^2} \tag{4.16}$$

where $\mathcal{M}_4 = (\varepsilon_1 \cdot \varepsilon_2)(\varepsilon_3 \cdot \varepsilon_4)$ (see Eq. (3.9)). The resonance is in no sense 'small' compared to the free-particle case and therefore perturbation theory breaks down in this region, a fact that is indicated by the pole. If $M_{\mathrm{H}} > 2M_{\mathrm{W}}$ a proper treatment of the resonance is necessary to render the cross-section finite and meaningful.

For a resonant diagram of the form $F(s)/(s - M_{\mathrm{H}}^2)$ the numerator is in general gauge dependent. Therefore, naive introduction of a finite Higgs-boson width as well as naive Dyson summation may invalidate the Ward identities and thus spoil the gauge invariance of the S matrix. The introduction of a finite width in the propagator, viz.

$$\frac{F(s)}{s - M_{\mathrm{H}}^2} \longrightarrow \frac{F(s)}{s - M_{\mathrm{H}}^2 + \mathrm{i}M_{\mathrm{H}}\Gamma_{\mathrm{H}}}\,, \tag{4.17}$$

does violate the Ward identities by adding terms proportional to $F(s)\Gamma_{\mathrm{H}}/(s - M_{\mathrm{H}}^2)/(s - M_{\mathrm{H}}^2 + \mathrm{i}M_{\mathrm{H}}\Gamma_{\mathrm{H}})$. These could in principle violate unitarity, but even for longitudinal W bosons (LLLL) fortunately behave as a constant. For a more comprehensive discussion of this issue, see [DeDH97].

The decay width is defined as

$$\Gamma_{\mathrm{H}} = \mathrm{Im}\,\Sigma_H(s = M_{\mathrm{H}}^2)/M_{\mathrm{H}}\,. \tag{4.18}$$

Σ_H is the Higgs self-energy and is given to one-loop order by

$$\begin{aligned}\Sigma_H(s) = \frac{\alpha}{32\pi s_{\mathrm{W}}^2 M_{\mathrm{W}}^2}\Big\{ & 3M_{\mathrm{H}}^2 \left[3M_{\mathrm{H}}^2\, B_0(s, M_{\mathrm{H}}^2, M_{\mathrm{H}}^2) + A_0(M_{\mathrm{H}}^2)\right] \\ & + 2\left(M_{\mathrm{H}}^4 - 4M_{\mathrm{W}}^2(s - 3M_{\mathrm{W}}^2)\right) B_0(s, M_{\mathrm{W}}^2, M_{\mathrm{W}}^2) \\ & + 2\left(6M_{\mathrm{W}}^2 + M_{\mathrm{H}}^2\right) A_0(M_{\mathrm{W}}^2) - 24M_{\mathrm{W}}^4 \\ & + \left(M_{\mathrm{H}}^4 - 4M_{\mathrm{Z}}^2(s - 3M_{\mathrm{Z}}^2)\right) B_0(s, M_{\mathrm{Z}}^2, M_{\mathrm{Z}}^2) \\ & + \left(6M_{\mathrm{Z}}^2 + M_{\mathrm{H}}^2\right) A_0(M_{\mathrm{Z}}^2) - 12M_{\mathrm{Z}}^4 \\ & + \sum_f 4N_{\mathrm{c}}^f m_f^2 \left[\left(s - 4m_f^2\right) B_0(s, m_f^2, m_f^2) - 2A_0(m_f)\right]\Big\}\end{aligned} \tag{4.19}$$

where f runs over all flavours and N_{c}^f is a colour factor that is 1 for leptons and 3 for quarks. A_0 and B_0 are the one- and two-point one-loop integrals, respectively (see Sect. 5.4.1). The Higgs decay width increases steeply with its mass; it is plotted in Fig. 4.3.

Fig. 4.4 shows the total unpolarized cross-section for various values of M_{H}. For Higgs masses exceeding the threshold of $2M_{\mathrm{W}}$ the resonance is clearly a prominent feature in the cross-section. Likewise, the above mentioned increase of the Higgs decay width with its mass can easily be observed. In fact, even in the curve for the large value of $M_{\mathrm{H}} = 900$ GeV (which is though not favoured from the present data), the resonance remains a distinguishable peak over the non-resonant background.

It must be realized that the decay width is of $\mathcal{O}(\alpha)$ when Σ_H is evaluated to one-loop accuracy. This means, since the real part of the denominator vanishes at the resonance, that in the overall precision of the calculation one order in α is lost at the resonance. It should further be noted that the finite width does not affect the gauge cancellations necessary for a decent high-energy behaviour of the $2 \to 2$ amplitudes. This can readily be seen from Eq. (4.8): inclusion of a decay width amounts to the substitution $M_{\mathrm{H}}^2 \to M_{\mathrm{H}}^2 - \mathrm{i}M_{\mathrm{H}}\Gamma_{\mathrm{H}}$ and the leading terms in s coming from the Higgs diagrams cannot (and do not) depend on M_{H}, otherwise they could never cancel the contributions from the gauge sector.

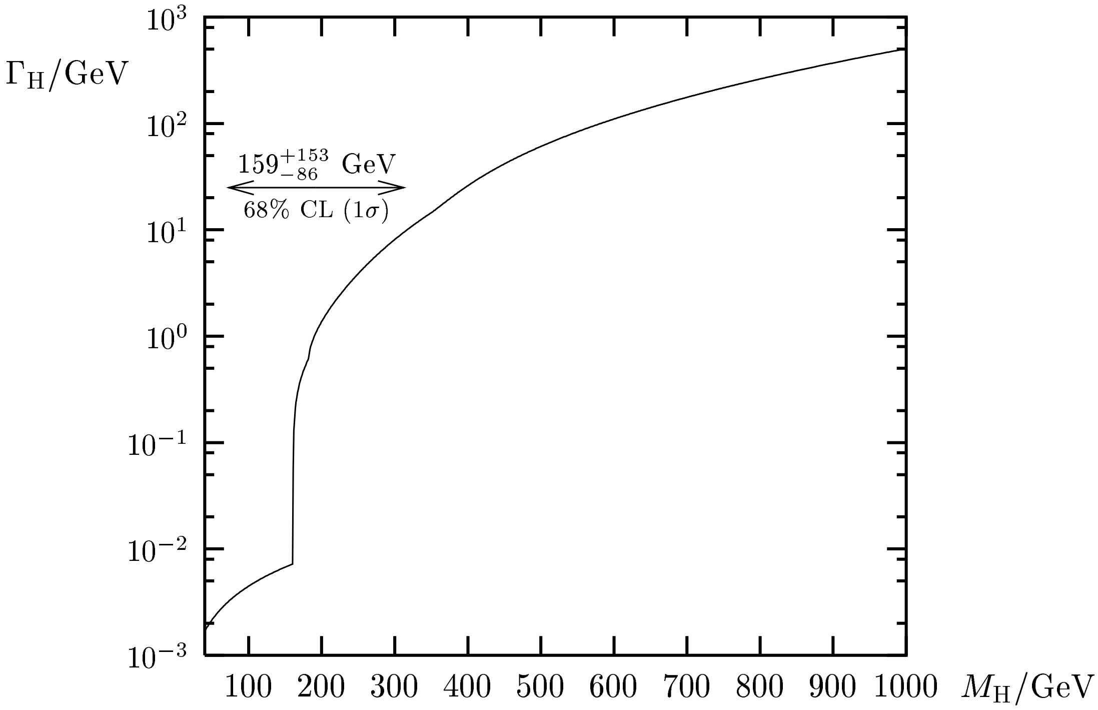

Figure 4.3: The Higgs-boson decay width $\Gamma_{\mathrm{H}} = \mathrm{Im}\,\Sigma_H(s = M_{\mathrm{H}}^2)/M_{\mathrm{H}}$ as a function of its mass. At $M_{\mathrm{H}} \gtrsim 1$ TeV the width becomes comparable to the mass. Since above this point the width of the resonance is bigger than its mass it is difficult to speak then of a reasonably well defined object. For the presently favoured mass range indicated by the arrow the width lies between 3 MeV and 9 GeV which would result in a narrow resonance. The two kinks at ~ 160 and ~ 180 GeV correspond to the thresholds for $\mathrm{H} \to \mathrm{W}^+\mathrm{W}^-$ and $\mathrm{H} \to \mathrm{ZZ}$, respectively.

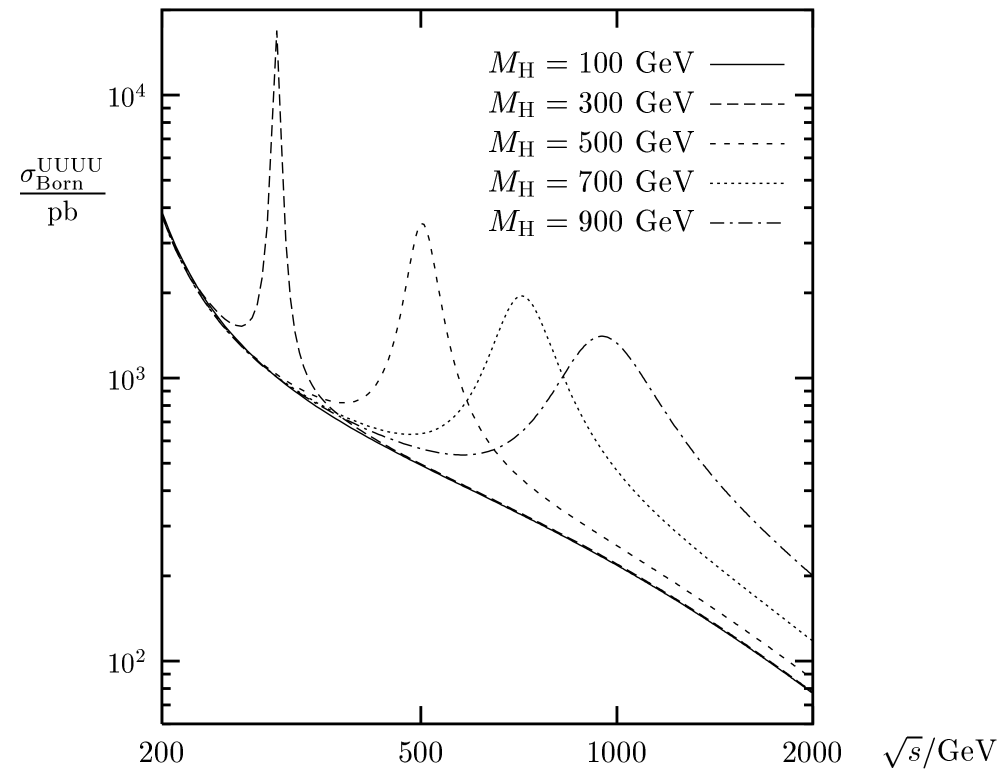

Figure 4.4: The unpolarized Born cross-section for various values of $M_{\rm H}$. Note that for the lowest displayed value, $M_{\rm H} = 100$ GeV, there is no peak since it lies below the threshold for $W^+W^- \to W^+W^-$.

Chapter 5

One-loop Corrections

5.1 Quantization and Gauge Fixing

Quantizing the classical Lagrangian assembled in Sect. 2.2 by means of the path integral is not straightforward owing to the gauge invariance of the action. Consider the path integral

$$\int \mathcal{D}A\, \mathrm{e}^{\mathrm{i}S[A]} \tag{5.1}$$

where A generically denotes all gauge fields in the theory.

Now the integral runs over all field configurations including those which are related by a gauge transformation. To see why this is a problem, take a particular field configuration A_0 for which $S[A_0] = 0$, then the integrand is 1 for all configurations that are gauge-equivalent to A_0 and since these constitute a non-denumerable set, the integral is badly divergent. Fig. 5.1 illustrates this situation.

Realizing that this sort of overcounting comes from the gauge invariance of the action, the solution is to fix a particular gauge. To begin, choose a gauge condition, symbolically written as

$$G[A] = 0\,. \tag{5.2}$$

For instance, the Lorentz gauge would correspond to $G[A] = \partial_\mu A^\mu$.

This gauge condition is inserted into the path integral with the help of the identity

$$1 = \int \mathcal{D}\alpha\, \delta(G[A^\alpha])\, \det\left(\frac{\delta G[A^\alpha]}{\delta\alpha}\right) \tag{5.3}$$

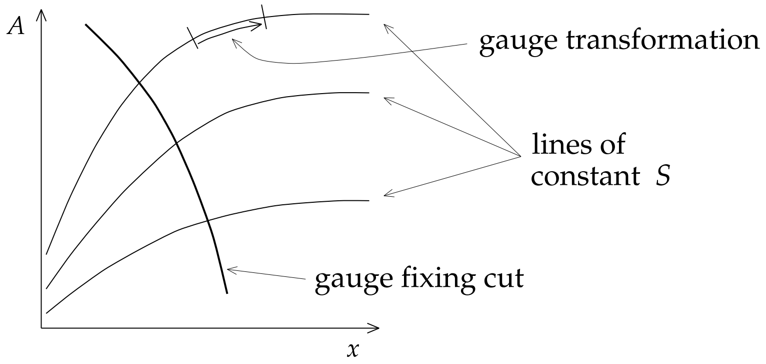

Figure 5.1: Before gauge fixing, there are infinitely many field configurations belonging to the same value of the action functional S, all related by gauge transformations. The gauge fixing procedure cuts through these lines of constant S and fixes a unique field configuration for each value of the action.

which is the functional analytic generalization of the well-known formula $1 = \int \mathrm{d}x\, \delta(g(x)) \frac{\partial g(x)}{\partial x}$. The above integral extends over all gauge transformations α, A^α being the field A transformed by α.

Inserting the identity (5.3) into the path integral (5.1) and interchanging the order of the functional integrals over A and α results in

$$\int \mathcal{D}A\, \mathrm{e}^{\mathrm{i}S[A]} = \int \mathcal{D}\alpha \int \mathcal{D}A\, \mathrm{e}^{\mathrm{i}S[A]}\, \delta(G[A^\alpha])\, \det\left(\frac{\delta G[A^\alpha]}{\delta\alpha}\right) . \tag{5.4}$$

In the inner integral, A may be replaced with A^α since $S[A]$ is gauge invariant anyway, and the measure is invariant because the infinitesimal version of the gauge-transformed field A^α,

$$(A^\alpha)^a_\mu = A^a_\mu + \frac{1}{g}\partial_\mu \alpha^a + f^{abc} A^b_\mu \alpha^c = A^a_\mu + \frac{1}{g} D_\mu \alpha^a , \tag{5.5}$$

consists of a linear shift of the A^a_μ, followed by a unitary rotation of the various components of the symmetry multiplet $A^a_\mu(x)$ at each point. Neither of these operations change the measure, hence $\mathcal{D}A = \mathcal{D}A^\alpha$.

Note that as long as the gauge-fixing functional $G[A]$ is linear in A, the functional derivative $\delta G/\delta\alpha$ is independent of α. This means that the path integral can be written as

$$\int \mathcal{D}A\, \mathrm{e}^{\mathrm{i}S[A]} = \left(\int \mathcal{D}\alpha\right) \int \mathcal{D}A^\alpha\, \mathrm{e}^{\mathrm{i}S[A^\alpha]}\, \delta(G[A^\alpha])\, \det\left(\frac{\delta G[A^\alpha]}{\delta\alpha}\right) . \tag{5.6}$$

The first part is responsible for the overcounting that caused the divergence, now nicely factored out and ready to be cancelled by normalization. The second part is actually independent of α since A^α is only an integration variable that can be renamed at will, e.g. back to A.

To evaluate the determinant it is useful to rewrite it as a functional integral over anticommuting fields, thus

$$\det\left(\frac{\delta G[A^\alpha]}{\delta\alpha}\right) = \int \mathcal{D}c\,\mathcal{D}\bar{c}\,\exp\left[\mathrm{i}\int \mathrm{d}^4x\,\bar{c}\left(-g\frac{\delta G[A^\alpha]}{\delta\alpha}\right)c\right]. \tag{5.7}$$

This means that the gauge fixing condition is now incorporated in the Lagrangian at the price of two new degrees of freedom, c and $\bar{c}$. Since these arise from a mathematical manipulation they are unphysical and therefore named Faddeev-Popov ghosts [FaP67].

The gauge-fixed Lagrangian is of course no longer gauge invariant. However, it still possesses a smaller symmetry, called the BRST symmetry. This symmetry is important in proving the renormalizability of a theory (see e.g. [PeS95, We96]).

5.1.1 't Hooft-Feynman gauge

A particularly convenient class of gauges are the 't Hooft gauges which are defined by

$$\begin{aligned} G_\pm &= \partial^\mu W^\pm_\mu \mp \mathrm{i}M_\mathrm{W}\xi_\mathrm{W}\varphi^\pm\,, \\ G_\mathrm{Z} &= \partial^\mu Z_\mu - M_\mathrm{Z}\xi_\mathrm{Z}\chi\,, \\ G_\mathrm{A} &= \partial^\mu A_\mu\,. \end{aligned} \tag{5.8}$$

The gauge-fixing terms for this gauge are

$$\mathcal{L}_\mathrm{fix} = -\frac{1}{2}\left[\frac{1}{\xi_\mathrm{A}}G_\mathrm{A}^2 + \frac{1}{\xi_\mathrm{Z}}G_\mathrm{Z}^2 + \frac{2}{\xi_\mathrm{W}}G_+G_-\right]. \tag{5.9}$$

The gauge is linear and the gauge-fixing Lagrangian is especially engineered to cancel mixing terms of the form $\varphi\,\partial^\mu V_\mu$ between gauge and unphysical Higgs bosons.

The parameters ξ_W, ξ_Z and ξ_A are gauge parameters. They can be viewed as Lagrangian multiplicators that enforce the choice of gauge as a subsidiary condition to the action.

Putting $\xi_\mathrm{W} = \xi_\mathrm{Z} = \xi_\mathrm{A} = 1$ results in the so-called Feynman gauge. This is the most convenient gauge for higher-order computations, mainly because the gauge-field propagator takes on the very simple form

$$\Delta^V_{\mu\nu}(k) = \mathrm{i}\,\frac{-g_{\mu\nu}}{k^2 - M_V^2 + \mathrm{i}\varepsilon}\,. \tag{5.10}$$

One could speculate that it would be even more convenient to have the unphysical Higgs fields eliminated. Indeed, it is possible to achieve this by choosing the unitary gauge which is derived from (5.8) by taking the limit $\xi_V \to \infty$ ($V = \mathrm{W}, \mathrm{Z}, \mathrm{A}$). The propagators of the unphysical Higgs fields vanish in that limit, but the drawback is that the gauge-field propagator becomes

$$\Delta^V_{\mu\nu}(k)\big|_{\text{unitary}} = \mathrm{i}\,\frac{-g_{\mu\nu} + k_\mu k_\nu / M_V^2}{k^2 - M_V^2 + \mathrm{i}\varepsilon} \tag{5.11}$$

and has an unacceptable high-energy behaviour due to the $k_\mu k_\nu$ term.

5.2 Background field method

The background field method (BFM) is based on the observation that gauge fixing is actually needed only for the quantum fields, i.e. those appearing in loops, and that for the remaining fields appearing at tree level (the so-called background fields) it is not necessary to destroy gauge invariance. The choice of appropriate background fields can simplify practical calculations considerably.

In BFM, the usual gauge field is decomposed into a quantum field A and a background field $\hat{A}$,

$$A \to A + \hat{A}\,. \tag{5.12}$$

The quantum fields are the variables of integration in the path integral. Since the background field $\hat{A}$ is held fixed, the measure is unchanged, i.e.

$$\mathcal{D}A_{\text{conv}} = \mathcal{D}A_{\text{BFM}}\,. \tag{5.13}$$

The gauge fixing is then carried out in the usual manner for the quantum fields and breaks only the gauge invariance of the quantum fields. The action is manifestly invariant under gauge transformations of the background fields.

The details of this method applied to the SM including the full renormalization and a complete set of Feynman rules have been worked out in [DeDW95].

To show in what way BFM simplifies calculations, consider the following diagram where we focus on the WWWW vertex:

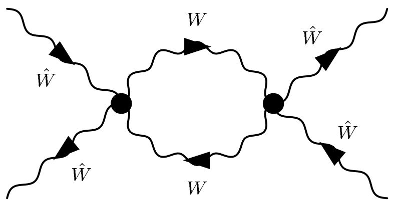

In the conventional formalism all fields are quantum fields, and the vertex has the structure

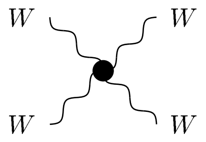

$$\propto \; 2g_{\mu\nu}g_{\rho\sigma} - g_{\mu\rho}g_{\nu\sigma} - g_{\mu\sigma}g_{\nu\rho} \, . \tag{5.14}$$

In BFM the W's in the loop are quantum fields whereas the external W's are background fields, denoted by a hat. The structure of the vertex is now

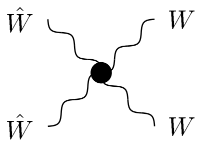

$$\propto \; 2g_{\mu\nu}g_{\rho\sigma} - g_{\mu\rho}g_{\nu\sigma}\left(1 - \frac{1}{\xi_Q}\right) - g_{\mu\sigma}g_{\nu\rho}\left(1 - \frac{1}{\xi_Q}\right) , \tag{5.15}$$

so that for a suitable choice of the quantum gauge parameter, i.e. Feynman gauge, $\xi_Q = 1$, two of the three terms disappear. The above diagram provides a drastic example, where the number of terms in BFM is only $1/9$ compared to the conventional formalism.

Moreover, one often observes strong compensations between different diagrams spoiling the numerical stability of evaluations. These so-called gauge cancellations are reduced in BFM due to the gauge invariance of the background part of the action, i.e. only the quantum fields contribute to the cancellations. Numerically, this works out to roughly one order of magnitude and has a noticeable effect on the numerical stability, particularly at high energies.

When using the ET in higher-order calculations one has to be careful to include all correction factors that result from renormalization and amputation [YaY88]. It has been found in [DeD96] that this is particularly easy within the BFM. In this formalism the matrix elements for external longitudinal vector bosons are directly obtained from the amputated Green functions with the corresponding Higgs fields multiplied with the wave-function renormalization constants of the gauge bosons.

5.3 Renormalization

5.3.1 Ultraviolet divergences

In loop calculations one encounters the problem that some diagrams lead to divergent results. Take as a concrete example the following self-energy diagram:

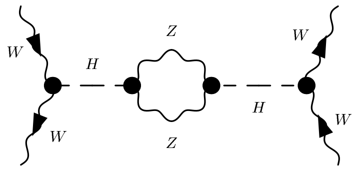

$$\propto \int \frac{\mathrm{d}^4k}{[k^2 - M_\mathrm{Z}^2]\,[(k-k_1-k_2)^2 - M_\mathrm{Z}^2]}\,. \tag{5.16}$$

where k_1 and k_2 are the incoming momenta as defined in Eq. (3.2). Its leading term for large k is

$$\int \frac{\mathrm{d}^4k}{k^4} = \int \mathrm{d}\Omega \int^{\Lambda} \frac{k^3\mathrm{d}k}{k^4} \propto \ln\Lambda \qquad (\Lambda \to \infty) \tag{5.17}$$

and diverges logarithmically. If this were a physical result, the theory's predicting power would be limited to tree level, and indeed, this would be a very questionable and unsatisfactory situation.

However, at a closer look we realize that the parameters in the Lagrangian have no immediate physical relevance beyond the tree approximation. For instance, the physical mass of a particle is obtained from the position of the pole of the full propagator of the field corresponding to that particle, which includes all higher-order corrections. There obviously is a relation between the physical mass and the parameters in the Lagrangian, but this is nontrivial and is plagued by the infinities mentioned above. Since one insists on a theory which yields a set of finite physical masses and finite coupling constants, the only possibility is to take the point of view that the original parameters in the (regularized) Lagrangian are infinite.

Although initially all amplitudes are calculated in terms of the parameters that occur in the Lagrangian, we may subsequently re-express everything in terms of a set of new parameters. The choice of these new parameters is not unique. For instance, the amplitudes may be expressed in terms of the physical masses rather than the Lagrangian mass parameters. We then insist that the new parameters are finite, and check whether the amplitudes expressed in terms of them still contain divergences. If not, we have succeeded in absorbing all the infinities generated by the loop corrections into the original parameters of the Lagrangian. This criterion, renormalizability, is a crucial and stringent requirement for every meaningful quantum field theory. In spite of the fact that such theories have infinities, they yield sensible predictions.

The fact that the original parameters are then regarded as infinite should be of no concern, because they are no longer relevant and cannot be measured experimentally. In other words, they correspond to just one particular parametrization of the theory, which is only convenient in lowest-order perturbation theory.

Step 1: Isolating the divergences

In order to carry out the renormalization procedure in an explicit fashion it is obviously necessary to deal with the infinities in some well-defined mathematical way. To this end, a regularization procedure is used which renders the potentially divergent integrals finite. The regularization is defined in terms of a parameter which, at the end of the calculation, is taken to a certain limit in which the divergences will again become manifest. This limiting procedure allows one to unambigously calculate the various Feynman diagrams, and absorb the infinities according to the chosen renormalization prescription. There are many ways to regularize the loop diagrams, each expressing the infinities in a characteristic way.

In the present work, the so-called dimensional regularization procedure [tHV72] is employed. It is based on the observation that the degree of divergence of Feynman integrals depends on the number of space-time dimensions. Instead of working in four dimensions, one analytically continues to an arbitrary dimension other than four, $d = 4 - \varepsilon$, in which case the divergences show up as terms proportional to $1/\varepsilon$. More generally, the arbitrary dimensional Feynman integral may have poles as the dimension approaches an integer for which the original integral was divergent. The important advantage of this method is that the Feynman rules and almost all symmetries of the theory do not depend on the specific number of space-time dimensions.

Step 2: Absorbing the infinities

We must now re-express the parameters of the Lagrangian in terms of new, finite parameters. The renormalized parameters are introduced by the following transformation where the original ("bare") parameters are denoted by a subscripted 0.

$$
\begin{aligned}
M^2_{\mathrm{W},0} &= M^2_{\mathrm{W}} + \delta M^2_{\mathrm{W}}\,, \\
M^2_{\mathrm{Z},0} &= M^2_{\mathrm{Z}} + \delta M^2_{\mathrm{Z}}\,, \\
M^2_{\mathrm{H},0} &= M^2_{\mathrm{H}} + \delta M^2_{\mathrm{H}}\,, \\
m_{f,i,0} &= m_{f,i} + \delta m_{f,i}\,, \\
e_0 &= (1+\delta e)e\,, \\
\begin{pmatrix} Z_0 \\ A_0 \end{pmatrix} &= \begin{pmatrix} 1+\frac{1}{2}\delta Z_{ZZ} & \frac{1}{2}\delta Z_{ZA} \\ \frac{1}{2}\delta Z_{AZ} & 1+\frac{1}{2}\delta Z_{AA} \end{pmatrix} \begin{pmatrix} Z \\ A \end{pmatrix}\,, \\
W^{\pm}_0 &= \left(1+\tfrac{1}{2}\delta Z_{WW}\right) W^{\pm}\,, \\
H_0 &= \left(1+\tfrac{1}{2}\delta Z_{H}\right) H\,, \\
f^L_{i,0} &= \left(\delta_{ij}+\tfrac{1}{2}\delta Z^{f,L}_{ij}\right) f^L_j\,, \\
f^R_{i,0} &= \left(\delta_{ij}+\tfrac{1}{2}\delta Z^{f,R}_{ij}\right) f^R_j\,.
\end{aligned}
\tag{5.18}
$$

δM, δe, and δZ are renormalization constants. Inserting the transformation into the "bare" Lagrangian $\mathcal{L}_0$ we get

$$\mathcal{L} = \mathcal{L}_0 - \delta\mathcal{L}\,. \tag{5.19}$$

$\delta\mathcal{L}$, termed counter-term Lagrangian, must have essentially the same structure as $\mathcal{L}_0$, otherwise the divergences would not cancel order by order. This is only true if the theory is renormalizable. For the SM, renormalizability was proved by 't Hooft [tH71].

The renormalized parameters and hence the renormalization constants are not fixed yet since, roughly speaking, subtracting two infinite quantities does not lead to a unique finite result. They are determined by imposing certain conditions. One very convenient scheme to work in is to choose for the finite parameters the physical masses and coupling constants. This is called the on-shell renormalization scheme and was introduced by Ross et al. [RoT71, De93]. The on-shell renormalization conditions are:

- The pole of the full propagator $(p^2 - M_x^2 + \Sigma_{xx})^{-1}$ determines the physical mass of the particle x; this forces the renormalized self-energy to fulfill

$$\mathrm{Re}\,\Sigma^{\mathrm{ren}}_{xx}(p^2 = M_x^2) = 0 \tag{5.20}$$

  and fixes δM_x.

- The radiative corrections for the $ee\gamma$ vertex vanish in the Thomson limit of vanishing momentum transfer, i.e.

$$\bar{u}(p)\Gamma_\mu^{ee\gamma}(p,p)u(p)\Big|_{p^2=m_\mathrm{e}^2} = \mathrm{i}e\,\bar{u}(p)\gamma_\mu u(p)\,. \tag{5.21}$$

  This condition is equivalent to requiring that the electron charge be the same as in low-energy ordinary electrodynamics and fixes δe.

- The residue of the propagator is unity; this guarantees the correct normalization of the fields and fixes δZ_x by

$$\mathrm{Re}\,\frac{\partial\Sigma_{xx}^{\mathrm{ren}}(p^2)}{\partial p^2}\bigg|_{p^2=M_x^2} = 0\,. \tag{5.22}$$

- There is no γ–Z mixing at the Z pole which implies

$$\mathrm{Re}\,\Gamma_{AZ}^{\mu\nu}(k)\varepsilon_\nu(k)\Big|_{k^2=0} = 0 \quad \text{and} \quad \mathrm{Re}\,\Gamma_{AZ}^{\mu\nu}(k)\varepsilon_\nu(k)\Big|_{k^2=M_\mathrm{Z}^2} = 0\,. \tag{5.23}$$

An abridged set of renormalization constants needed for the calculations in this thesis is (see [De93] for the others)

$$\begin{aligned}
\delta M_\mathrm{W}^2 &= \mathrm{Re}\,\Sigma_{WW}^\perp(p^2=M_\mathrm{W}^2)\,, & \delta Z_{WW} &= -\,\mathrm{Re}\,\frac{\partial\Sigma_{WW}^\perp(p^2)}{\partial p^2}\bigg|_{p^2=M_\mathrm{W}^2}\,,\\
\delta M_\mathrm{Z}^2 &= \mathrm{Re}\,\Sigma_{ZZ}^\perp(p^2=M_\mathrm{Z}^2)\,, & \delta Z_{ZZ} &= -\,\mathrm{Re}\,\frac{\partial\Sigma_{ZZ}^\perp(p^2)}{\partial p^2}\bigg|_{p^2=M_\mathrm{Z}^2}\,,\\
\delta M_\mathrm{H}^2 &= \mathrm{Re}\,\Sigma_{H}(p^2=M_\mathrm{H}^2)\,, & \delta Z_{H} &= -\,\mathrm{Re}\,\frac{\partial\Sigma_{H}(k^2)}{\partial p^2}\bigg|_{p^2=M_\mathrm{H}^2}\,,\\
\delta Z_{AZ} &= -2\,\mathrm{Re}\,\frac{\Sigma_{AZ}^\perp(p^2=M_\mathrm{Z}^2)}{M_\mathrm{Z}^2}\,, & \delta Z_{AA} &= -\,\mathrm{Re}\,\frac{\partial\Sigma_{AA}^\perp(p^2)}{\partial p^2}\bigg|_{p^2=0}\,,\\
\delta Z_{ZA} &= 2\,\frac{\Sigma_{AZ}^\perp(p^2=0)}{M_\mathrm{Z}^2}\,, & \delta e &= -\frac{1}{2}\left(\delta Z_{AA}+\frac{s_\mathrm{W}}{c_\mathrm{W}}\delta Z_{ZA}\right)\,,\\
\delta s_\mathrm{W}^2 &= c_\mathrm{W}^2\left(\frac{\delta M_\mathrm{Z}^2}{M_\mathrm{Z}^2}-\frac{\delta M_\mathrm{W}^2}{M_\mathrm{W}^2}\right)\,,
\end{aligned} \tag{5.24}$$

where $\Sigma^\perp$ denotes the transverse part of the respective self-energy. The renormalization of the coupling constant, δe, is usually obtained from the vertex function but can be expressed in terms of the self-energies via the Ward identity.

5.3.2 Infrared divergences

At the other end of the spectrum, at very low energies, there are also divergences which appear in the charge form factor. They originate from photonic contributions and are intrinsically related to the masslessness of the photon. Consider the following diagram:

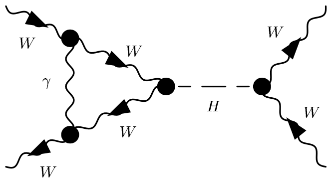

$$\propto \int \frac{\mathrm{d}^4 k}{k^2\,[(k+k_1)^2 - M_{\mathrm{W}}^2]\,[(k-k_2)^2 - M_{\mathrm{W}}^2]} \tag{5.25}$$

where k_1 and k_2 are the momenta of the incoming particles as given by Eq. (3.2). Using the mass shell condition $k_1^2 = M_{\mathrm{W}}^2$ and ignoring terms in k^2 the second factor in the denominator becomes

$$(k+k_1)^2 - M_{\mathrm{W}}^2 = 2\,k\cdot k_1 + k_1^2 - M_{\mathrm{W}}^2 + \mathcal{O}(k^2) = 2\,k\cdot k_1 + \mathcal{O}(k^2) \tag{5.26}$$

and therefore the integral is logarithmically divergent in the limit of small k because

$$\int \frac{\mathrm{d}^4 k}{k^2(2\,k\cdot k_1)(-2\,k\cdot k_2)} = \\ \int \mathrm{d}\Omega \int_\omega \frac{k^3 \mathrm{d}k}{k^4}\,\frac{-1}{2k_1(1-\cos\theta_1)\,2k_2(1-\cos\theta_2)} \propto \ln\omega \qquad (\omega\to 0)\,. \tag{5.27}$$

It is obvious that this divergence does not occur if the photon is replaced by a massive particle. In the actual calculations a regulator mass ("photon mass") λ is introduced to render the integrals finite. The IR divergences then appear in the form $\ln(\lambda/M_{\mathrm{W}})$.

More generally, diagrams are infrared divergent when a photon line running in a loop is joined on both sides with propagators whose masses squared equal the external momentum squared entering at the respective vertex, like in the following diagram.

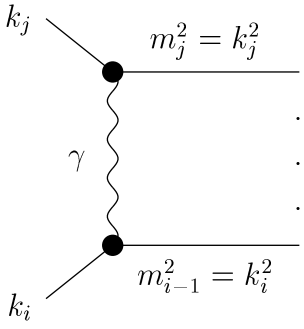

The resolution of the infrared divergence problem is found in the observation that it is not really possible to measure the rate for a reaction involving definite numbers of photons and charged particles, because photons of very low energy can always escape undetected. Since the photons are massless their energies can be arbitrarily small and thus less than the resolution of any detector. What can be measured is the rate for such a reaction to take place with no unobserved photon having an energy greater than some small quantity ΔE, and with a total energy carried away by unobserved photons less than E_{tot}.

For these observable processes the divergences have to cancel. The diagrams where a real photon is emitted from an external leg are called bremsstrahlung diagrams, schematically drawn here as

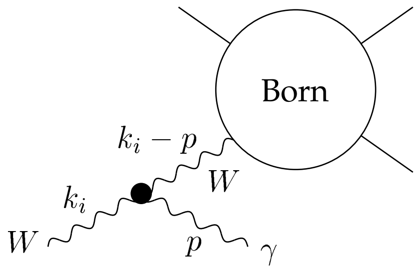

The infrared divergent terms coming from the bremsstrahlung diagrams exactly cancel those from the virtual photonic diagrams. This cancellation takes place order by order [BlN37]. If the virtual corrections are evaluated at one-loop level, then to stay consistently within the same order in α one has to take only single photon radiation off the Born diagrams into account.

Writing the Born matrix element as

$$\mathcal{M}_{\text{Born}} = \varepsilon_i^\mu(k_i)\mathcal{M}_\mu(k_i) \tag{5.28}$$

and denoting by ε_γ the photon polarization vector, the amplitude for the emission of a photon from the ith incoming line is

$$\begin{aligned}\mathcal{M}_{\text{soft}} = {} & \varepsilon_i^\mu(k_i)\, \varepsilon_\gamma^\rho(p) \\ & \times \mathrm{i}eQ_i \big[g_{\mu\nu}(2k_i - p)_\rho - g_{\nu\rho}(k_i - 2p)_\mu - g_{\mu\rho}(k_i + p)_\nu \big] \\ & \times \mathrm{i}\, \frac{-g^{\nu\sigma} + (k_i - p)^\nu (k_i - p)^\sigma / M_\mathrm{W}^2}{(k_i - p)^2 - M_\mathrm{W}^2}\, \mathcal{M}_\sigma(k_i)\,,\end{aligned} \tag{5.29}$$

where $Q_i = \pm 1$ is the charge of the ith W boson. Note that we are working in unitary gauge (Eq. (5.11)) to avoid having to calculate also the corresponding diagram with a φ in the propagator.

In the soft-photon limit we neglect all terms proportional to p in the numerator and transform the denominator similar to Eq. (5.26). Together with the transversality condition $\varepsilon_i \cdot k_i = 0$ this yields

$$\mathcal{M}_{\text{soft}} = -eQ_i \frac{k_i \cdot \varepsilon_\gamma}{k_i \cdot p} \mathcal{M}_{\text{Born}} \,. \tag{5.30}$$

The same result applies also for an outgoing line but with an additional minus sign. It is interesting to observe that only the convection current is needed. Other contributions, like the magnetic-moment term, are not IR singular and are neglected in the soft-photon approximation. This makes Eq. (5.30) universal, i.e. it is correct for scalar particles, fermions, vector bosons, etc.

Since the photon is unobserved, we must sum over its polarizations and integrate over its phase space for energies less than ΔE. We use the following identity, valid if the photon couples to a conserved current

$$\sum_{\lambda=\pm} \left|\varepsilon_\gamma^\mu(\lambda) A_\mu\right|^2 = A \cdot A^* \,. \tag{5.31}$$

Summing over soft-photon emission from all external lines we obtain

$$\left(\frac{\mathrm{d}\sigma}{\mathrm{d}\Omega}\right)_{\text{soft}} = \left(\frac{\mathrm{d}\sigma}{\mathrm{d}\Omega}\right)_{\text{Born}} \left\{-\frac{e^2}{(2\pi)^3} \int_{|\vec{p}|\leqslant\Delta E} \frac{\mathrm{d}^3 p}{2\omega_p} \sum_{i,j=1}^{4} \frac{\pm Q_i Q_j \, k_i \cdot k_j}{(k_i \cdot p)(k_j \cdot p)}\right\} . \tag{5.32}$$

Owing to the universality of the convection current, the soft-photon cross-section is always proportional to the Born cross-section. The proportionality constant is called the soft-photon factor δ_{soft} and depends only on the charges and momenta of the external particles. The sign is '$+$' if particles i and j are both either incoming or outgoing, and '$-$' otherwise. The same regulator mass λ that was used in the virtual photonic contributions is also introduced in the photon energy term

$$\omega_p = \sqrt{\vec{p}^{\,2} + \lambda^2} \tag{5.33}$$

and singles out the IR divergences in the form $\ln(\Delta E/\lambda)$. After adding the diagrams with virtual and real photon emission, the λ-dependent terms cancel. In return, the amplitude now depends on ΔE and hence on the experimental set-up. It should be realized, however, that this dependence is only logarithmic. Note also that the result is no longer Lorentz invariant due to the integration region.

The basic integrals needed for the soft-photon factor have been worked out e.g. by 't Hooft and Veltman [tHV79]. For the case of $\mathrm{W}^+\mathrm{W}^- \to \mathrm{W}^+\mathrm{W}^-$ the soft-photon factor becomes

$$\begin{aligned}\delta_{\text{soft}} = -\frac{2\alpha}{\pi}\bigg\{&\ln\frac{4\Delta E^2}{\lambda^2} + \frac{E}{p}\ln\frac{E-p}{E+p} \\ &- (s-2M_{\mathrm{W}}^2)\,\mathcal{I}\Big(s+\sqrt{s(s-4M_{\mathrm{W}}^2)}\Big) \\ &- (2M_{\mathrm{W}}^2-t)\,\mathcal{I}\Big(4M_{\mathrm{W}}^2-t+\sqrt{t(t-4M_{\mathrm{W}}^2)}\Big) \\ &+ (2M_{\mathrm{W}}^2-u)\,\mathcal{I}\Big(4M_{\mathrm{W}}^2-u+\sqrt{u(u-4M_{\mathrm{W}}^2)}\Big)\bigg\}\end{aligned} \tag{5.34}$$

where the function $\mathcal{I}(x)$ is defined as

$$\begin{aligned}\mathcal{I}(x) = \frac{2(x-2M_{\mathrm{W}}^2)}{x(x-4M_{\mathrm{W}}^2)}\bigg\{&\ln\frac{4\Delta E^2}{\lambda^2}\ln\frac{x-2M_{\mathrm{W}}^2}{2M_{\mathrm{W}}^2} \\ &+ \mathrm{Li}_2\bigg(1-\frac{4E(E-p)}{x}\,\frac{x-2M_{\mathrm{W}}^2}{2M_{\mathrm{W}}^2}\bigg) \\ &+ \mathrm{Li}_2\bigg(1-\frac{4E(E+p)}{x}\,\frac{x-2M_{\mathrm{W}}^2}{2M_{\mathrm{W}}^2}\bigg) \\ &- \mathrm{Li}_2\bigg(1-\frac{4E(E-p)}{x}\bigg) \\ &- \mathrm{Li}_2\bigg(1-\frac{4E(E+p)}{x}\bigg)\bigg\}\end{aligned} \tag{5.35}$$

and Li_2 is the dilogarithm function (see App. D of [dWS86] and references therein)

$$\mathrm{Li}_2(z) = \int_z^0 \mathrm{d}t\,\frac{\ln(1-t)}{t}\,. \tag{5.36}$$

5.4 Structure of the one-loop amplitudes

5.4.1 Scalar and tensor one-loop integrals

Whereas at Born level all momenta running along the internal lines of a Feynman diagram are fixed by the overall momentum conservation, at one-loop level there remains one momentum which must be integrated over. Similarly, at two-loop level there are two integration momenta, etc.

A typical one-loop diagram looks like

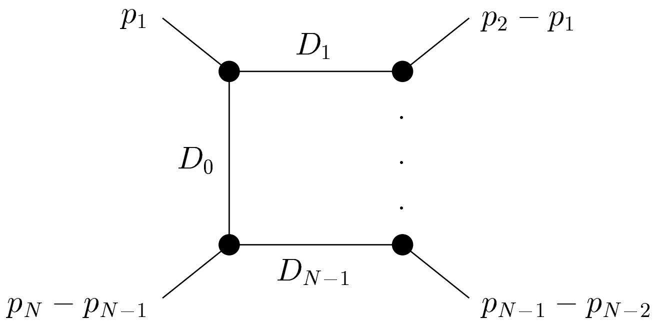

and the basic form of integral corresponding to such a diagram is

$$T^N_{\mu_1 \dots \mu_P} = \frac{(2\pi\mu)^{4-d}}{\mathrm{i}\pi^2} \int \mathrm{d}^d q \, \frac{q_{\mu_1} \cdots q_{\mu_P}}{D_0 D_1 \cdots D_{N-1}} \tag{5.37}$$

with

$$\begin{aligned} D_0 &= q^2 - m_0^2 + \mathrm{i}\varepsilon \,, \\ D_i &= (q + p_i)^2 - m_i^2 + \mathrm{i}\varepsilon \,, \quad i = 1, \dots, N-1 \,. \end{aligned} \tag{5.38}$$

The denominators arise from the propagators running in the loop. μ is an arbitrary reference mass that keeps track of the correct dimension of the integral in d space–time dimensions. Eventually, the renormalized amplitude must be independent of μ.

P, the number of q's in the numerator determines the Lorentz tensor structure of the whole integral, e.g. $P = 0$ denotes a scalar integral, $P = 1$ a vector integral, etc. From the definition it is obvious that the integrals are symmetric under permutation of the Lorentz indices. The q's arise from fermion propagators or from vertices that correspond to terms with derivatives in the Lagrangian.

The usual nomenclature is A for T^1, B for T^2, etc. The scalar integrals are denoted by a subscripted zero: A_0, B_0, etc.

5.4.2 Reduction of the tensor integrals

The integrals with a tensor structure can be reduced to linear combinations of scalar integrals [PaV79, De93]. This reduction is performed in two steps.

Step 1: The integrals are symmetric, Lorentz-covariant tensors, i.e. they transform in a definite way under Lorentz transformations. This allows them to be decomposed into a tensor basis formed from the linear independent momenta p_i and the metric tensor $g_{\mu\nu}$. The choice of this basis is not unique; in the present work, the basis is chosen such that the coefficients are totally symmetric in their indices. For the integrals up to the four-point function this decomposition reads explicitly

$$B_\mu = p_{1\mu} B_1 \,, \tag{5.39}$$

$$B_{\mu\nu} = g_{\mu\nu} B_{00} + p_{1\mu} p_{1\nu} B_{11} \,, \tag{5.40}$$

$$C_\mu = p_{1\mu} C_1 + p_{2\mu} C_2 = \sum_{i=1}^{2} p_{i\mu} C_i \,, \tag{5.41}$$

$$C_{\mu\nu} = g_{\mu\nu} C_{00} + \sum_{i,j=1}^{2} p_{i\mu} p_{j\nu} C_{ij} \,, \tag{5.42}$$

$$C_{\mu\nu\rho} = \sum_{i=1}^{2} \big(g_{\mu\nu} p_{i\rho} + g_{\nu\rho} p_{i\mu} + g_{\mu\rho} p_{i\nu}\big) C_{00i} + \sum_{i,j,k=1}^{2} p_{i\mu} p_{j\nu} p_{k\rho} C_{ijk} \,, \tag{5.43}$$

$$D_\mu = \sum_{i=1}^{3} p_{i\mu} D_i \,, \tag{5.44}$$

$$D_{\mu\nu} = g_{\mu\nu} D_{00} + \sum_{i,j=1}^{3} p_{i\mu} p_{j\nu} D_{ij} \,, \tag{5.45}$$

$$D_{\mu\nu\rho} = \sum_{i=1}^{2} \big(g_{\mu\nu} p_{i\rho} + g_{\nu\rho} p_{i\mu} + g_{\mu\rho} p_{i\nu}\big) D_{00i} + \sum_{i,j,k=1}^{2} p_{i\mu} p_{j\nu} p_{k\rho} D_{ijk} \,, \tag{5.46}$$

$$\begin{aligned} D_{\mu\nu\rho\sigma} = {} & (g_{\mu\nu} g_{\rho\sigma} + g_{\mu\rho} g_{\nu\sigma} + g_{\mu\sigma} g_{\nu\rho}) D_{0000} \\ & + \sum_{i,j,k=1}^{3} \big(g_{\mu\nu} p_{i\rho} p_{j\sigma} + g_{\nu\rho} p_{i\mu} p_{j\sigma} + g_{\mu\rho} p_{i\nu} p_{j\sigma} \\ & \qquad + g_{\mu\sigma} p_{i\nu} p_{j\rho} + g_{\nu\sigma} p_{i\mu} p_{j\rho} + g_{\rho\sigma} p_{i\mu} p_{j\nu}\big) D_{00ij} \\ & + \sum_{i,j,k,\ell=1}^{3} p_{i\mu} p_{j\nu} p_{k\rho} p_{\ell\sigma} D_{ijk\ell} \,. \end{aligned} \tag{5.47}$$

Step 2: To reduce the number of Lorentz indices one contracts with p_k^μ or with $g^{\mu\nu}$. Contracting a q_μ from the numerator with p_k^μ yields

$$\begin{aligned} 2 q_\mu p_k^\mu &= (q + p_k)^2 - q^2 - p_k^2 \\ &= \big[(q + p_k)^2 - m_k^2\big] - \big[q^2 - m_0^2\big] - p_k^2 + m_k^2 - m_0^2 \\ &= D_k - D_0 - p_k^2 + m_k^2 - m_0^2 = D_k - D_0 - f_k \end{aligned} \tag{5.48}$$

with $f_k = p_k^2 - m_k^2 + m_0^2$, and similarly

$$g^{\mu\nu} q_\mu q_\nu = q^2 - m_0^2 + m_0^2 = D_0 + m_0^2 \,. \tag{5.49}$$

Hence we find

$$\begin{aligned} p_k^{\mu_P} T^N_{\mu_1\ldots\mu_P} &= \frac{1}{2} \frac{(2\pi\mu)^{4-d}}{\mathrm{i}\pi^2} \int \mathrm{d}^d q \, \frac{q_{\mu_1} \cdots q_{\mu_{P-1}} (D_k - D_0 - f_k)}{D_0 \cdots D_{N-1}} \\ &= \frac{1}{2} \left(T^{N-1,\not k}_{\mu_1\ldots\mu_{P-1}} - T^{N-1,\not 0}_{\mu_1\ldots\mu_{P-1}} - f_k T^N_{\mu_1\ldots\mu_{P-1}} \right) =: R^{N,k}_{\mu_1\ldots\mu_{P-1}} \end{aligned} \tag{5.50}$$

and

$$\begin{aligned} g^{\mu_{P-1}\mu_P} T^N_{\mu_1\ldots\mu_P} &= \frac{(2\pi\mu)^{4-d}}{\mathrm{i}\pi^2} \int \mathrm{d}^d q \, \frac{q_{\mu_1} \cdots q_{\mu_{P-2}} (D_0 + m_0^2)}{D_0 \cdots D_{N-1}} \\ &= T^{N-1,\not 0}_{\mu_1\ldots\mu_{P-2}} + m_0^2 T^N_{\mu_1\ldots\mu_{P-2}} =: R^{N,00}_{\mu_1\ldots\mu_{P-2}} \end{aligned} \tag{5.51}$$

where $\not k$ indicates that D_k has been cancelled. Altogether we have now N linear equations

$$\begin{aligned} R^{N,k}_{\mu_1\ldots\mu_{P-1}} &= p_k^{\mu_P} T^N_{\mu_1\ldots\mu_P} \,, \qquad k = 1, \ldots, N-1 \,, \\ R^{N,00}_{\mu_1\ldots\mu_{P-2}} &= g^{\mu_P\mu_{P-1}} T^N_{\mu_1\ldots\mu_P} \end{aligned} \tag{5.52}$$

relating the rank P tensors with rank $P-1$ and $P-2$ tensors. Inserting into these the decompositions from step 1 yields linear relations between the coefficient functions $T^N_{i_1\ldots i_P}$ and $R^{N,k}_{i_1\ldots i_{P-1}}$ and $R^{N,00}_{i_1\ldots i_{P-2}}$ with scalar products of the external momenta as coefficients. Finally, this set of equations must be solved for the $T^N_{i_1\ldots i_P}$. The solution is given in d dimensions by

$$\begin{aligned} T^N_{00 i_1\ldots i_{P-2}} &= \frac{1}{d + P - N - 1} \left[R^{N,00}_{i_1\ldots i_{P-2}} - \sum_{k=1}^{N-1} R^{N,k}_{k i_1\ldots i_{P-2}} \right] , \\ T^N_{k i_1\ldots i_{P-1}} &= (X^{-1}_{N-1})_{kk'} \left[R^{N,k'}_{i_1\ldots i_{P-2}} - \sum_{r=1}^{P-1} \delta_{i_r k'} T^N_{00 i_1\ldots i_{r-1} i_{r+1}\ldots i_{P-1}} \right] , \end{aligned} \tag{5.53}$$

provided the Gram matrix

$$X_{N-1} = \begin{pmatrix} p_1^2 & p_1 p_2 & \ldots & p_1 p_{N-1} \\ p_2 p_1 & p_2^2 & \ldots & p_2 p_{N-1} \\ \vdots & & \ddots & \vdots \\ p_{N-1} p_1 & p_{N-1} p_2 & \ldots & p_{N-1}^2 \end{pmatrix} \tag{5.54}$$

is nonsingular. The Gram matrix becomes singular e.g. if the external momenta are linearly dependent, which happens for exact forward or backward scattering ($\theta = 0, \pi$). Eq. (5.53) gives $T_{i_1 \dots i_P}$ in terms of lower-rank tensor coefficients. Clearly, this procedure can be iterated until all tensor coefficients are reduced to scalar functions.

A word on the numerical implementation: The scalar integrals can all be worked out [tHV79], their main constituents are logarithms and dilogarithms. In four dimensions only A_0 and B_0 are divergent; they depend, in dimensional regularization, on the scale parameter μ. There exists a very thorough and robust implementation of the scalar one-loop functions in Fortran in a library package called FF by G.J. van Oldenborgh [vOV90].

In this thesis, step 1 of the tensor reduction is performed analytically and step 2 numerically. Expectably the expressions are much more compact, but also the coefficient functions turn out to be more stable when evaluated numerically. Presumably this comes about because as $\theta \to 0, \pi$, the inverse of the Gram matrix conjures up expressions that behave as 0/0 and cancellations appear to be somewhat obstructed by the analytical reduction. Nevertheless, that region of phase space is delicate to handle in any case (even in the numerical implementation quadruple precision is needed for some intermediate values to yield an acceptable accuracy in the final result), so to avoid problems, a cut-off with $\theta_{\text{cut}} = 10^\circ$ is used in the actual calculations.

Chapter 6

Numerical Results

6.1 One-loop diagram gallery

At one-loop level, roughly 1000 diagrams contribute to $\mathrm{W}^+\mathrm{W}^- \to \mathrm{W}^+\mathrm{W}^-$. The diagrams can be classified as self-energy corrections, vertex corrections, and box corrections. The self-energy corrections and the vertex corrections can be further divided into s- and t-channel contributions, the box corrections involve in addition u-channel contributions. The t-channel contributions can be obtained from the s-channel contributions via crossing, i.e. via the interchange of the outgoing W^- boson with the incoming W^+ boson.

The s-channel self-energy corrections are shown in Fig. 6.1. They consist of insertions of the Z-boson and photon self-energies and the γ–Z-boson mixing energy into diagram #1 of Fig. 3.1 and Higgs-boson self-energy insertions into diagram #4 of Fig. 3.1.

To avoid presenting hundreds of diagrams in Fig. 6.1 and the following figures, similar diagrams have been combined. Each combination of particle labels on the internal lines corresponds to an extra diagram, where those have to be omitted that violate charge or lepton-number conservation or involve one of the following vertices: $\gamma\gamma HH$, $\gamma\gamma\chi\chi$, γZHH, $\gamma Z\chi\chi$, $W^+W^-\chi H$, χHH, $Z\chi\chi$, ZHH, $\gamma\chi\chi$, $\gamma\chi H$, γHH, $\gamma\nu\nu$, which do not exist in the SM.

For example, diagram #1 of Fig. 6.1 represents a ϕ-loop contribution to the photon self-energy and to the γZ and $Z\gamma$ mixing, and ϕ-, χ-, and H-loop contributions to the Z-boson self-energy. In addition, fermionic diagrams are shown only for the first fermion generation.

The s-channel vertex corrections consist of corrections to the γWW, ZWW

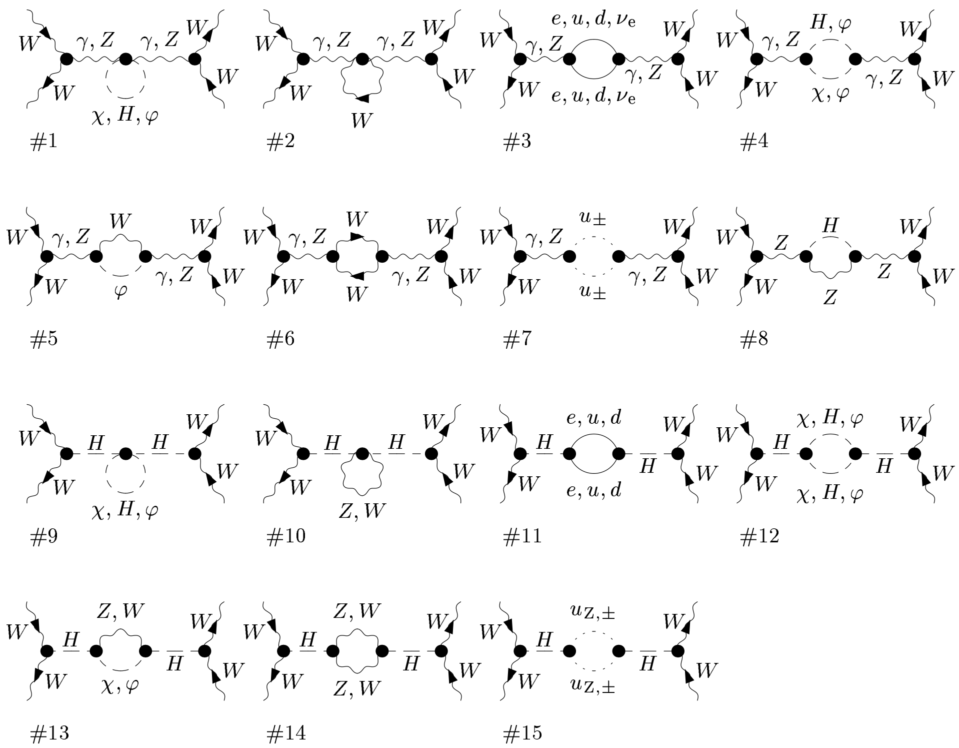

Figure 6.1: The s-channel self-energy diagrams.

and HWW vertices in diagrams #1 and #4 of Fig. 3.1. The corrections to the final-state vertices in these diagrams are shown in Fig. 6.2.

The box diagrams are shown in Figs. 6.3, 6.4, and 6.5. While the t-channel boxes are obtained from the s-channel boxes via crossing, the u-channel boxes are different owing to the different charge flow. In particular, there are no fermionic u-channel diagrams. For this reason, the Landau singularity that plagues the corrections to $\mathrm{ZZ} \to \mathrm{ZZ}$ [DeDH97] does not show up in $\mathrm{W}^+\mathrm{W}^- \to \mathrm{W}^+\mathrm{W}^-$.

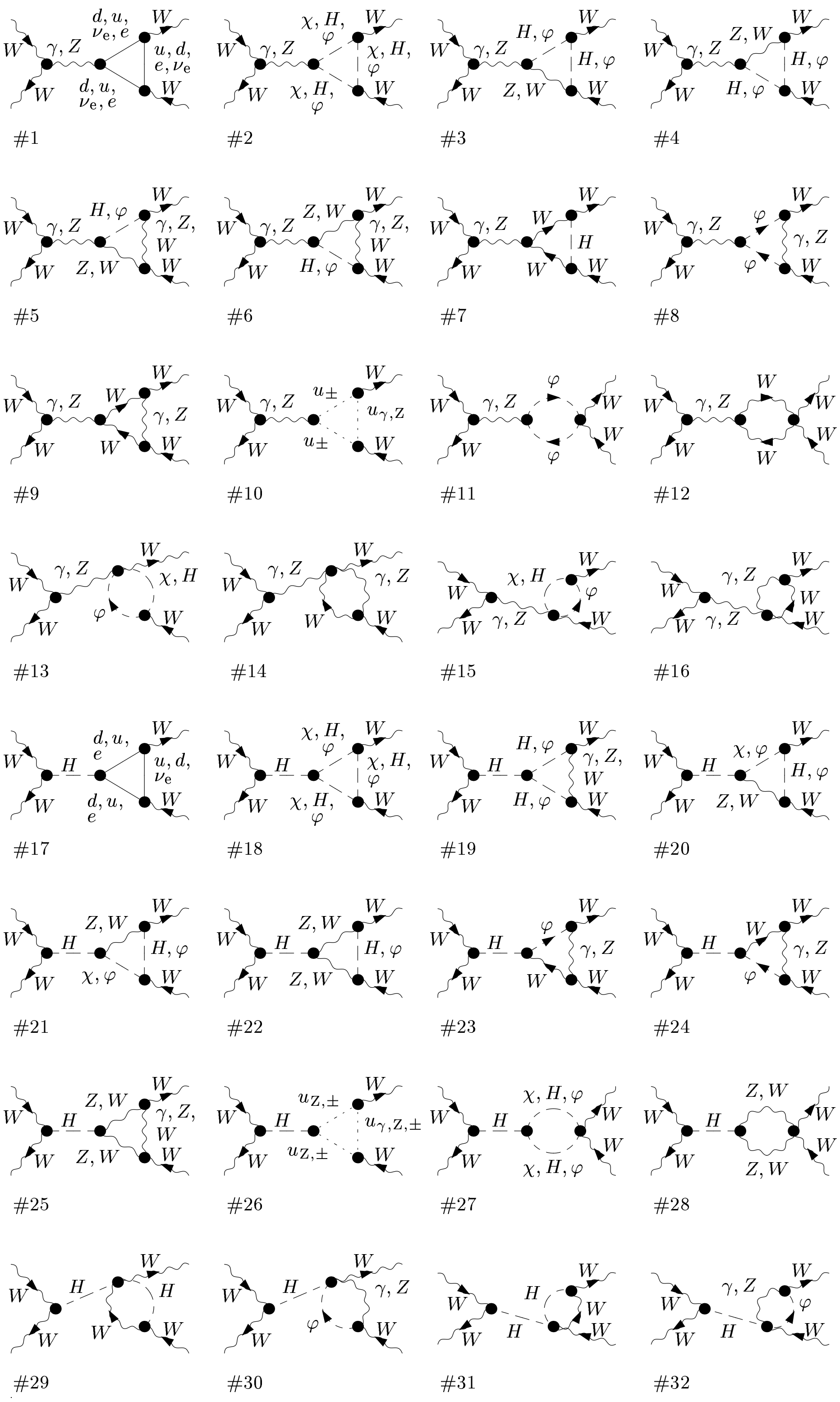

Figure 6.2: The s-channel vertex diagrams for the final-state vertex.

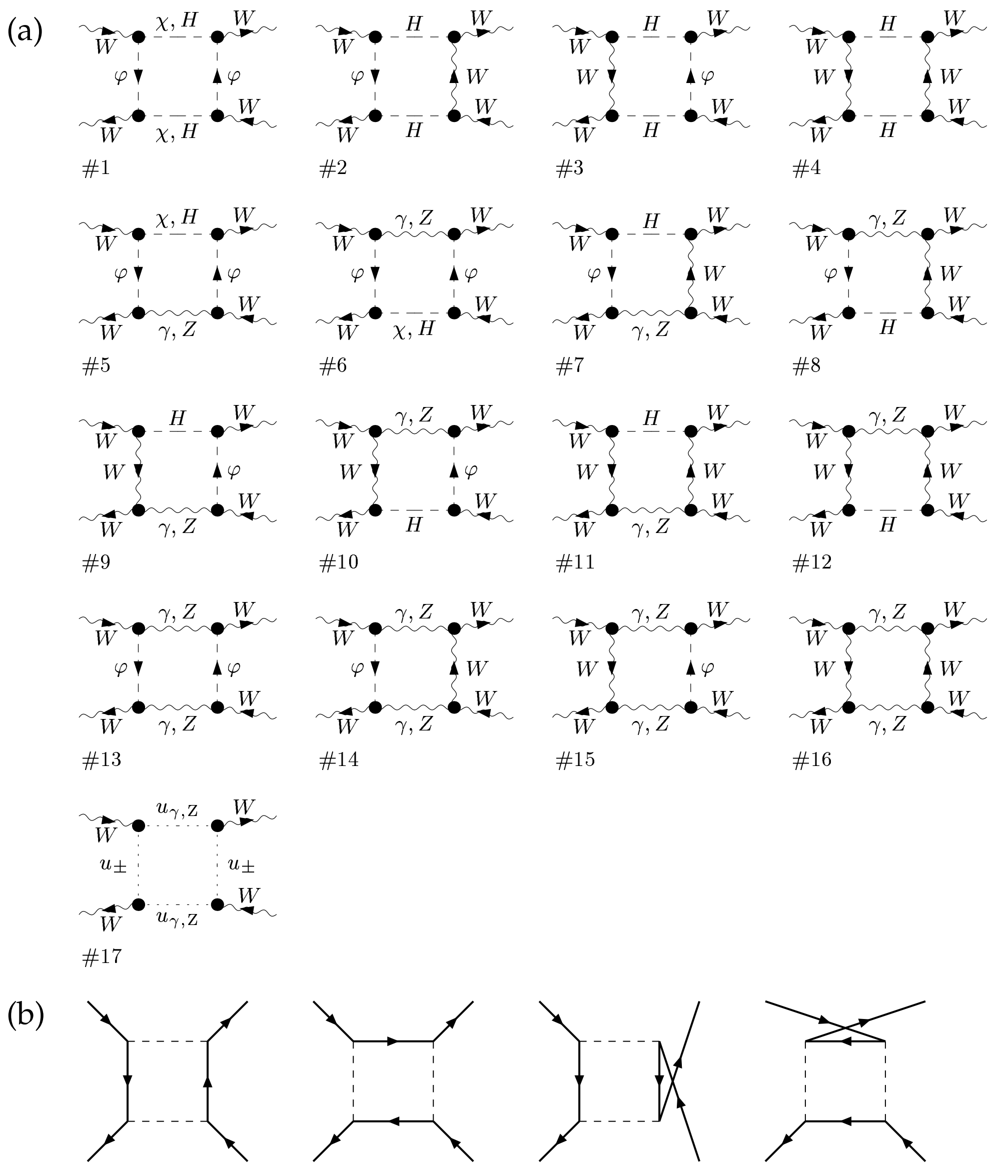

Figure 6.3: Genuine box diagrams that appear in the s, t, and u channel. Each diagram in (a) represents actually four diagrams with different charge flows shown in (b), i.e. one s-channel, one t-channel, and two u-channel diagrams.

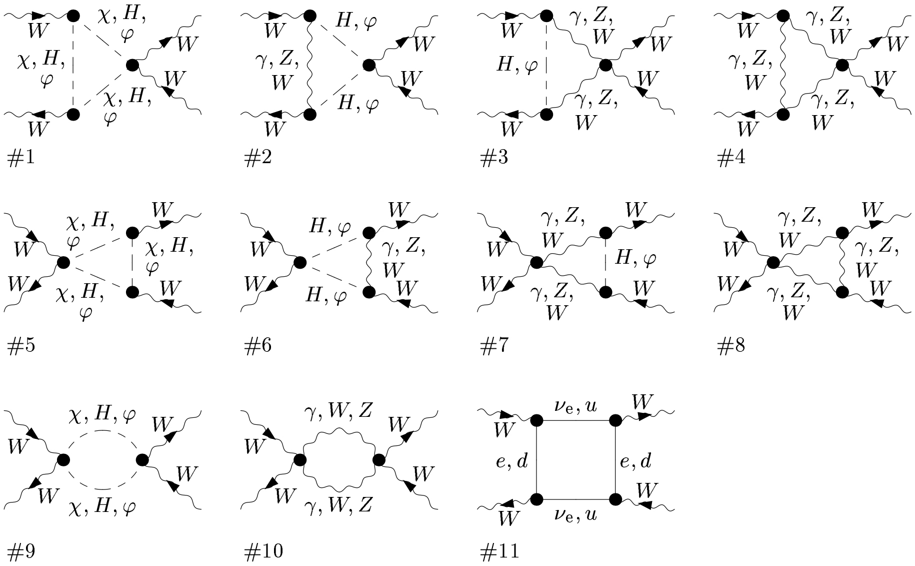

Figure 6.4: Further s-channel box diagrams. For every diagram there exists a t-channel analogue (obtained by exchanging the lower left and upper right leg).

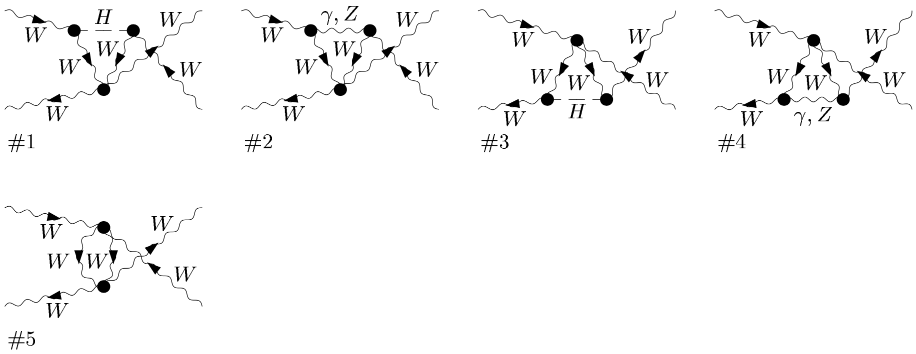

Figure 6.5: Further u-channel box diagrams.

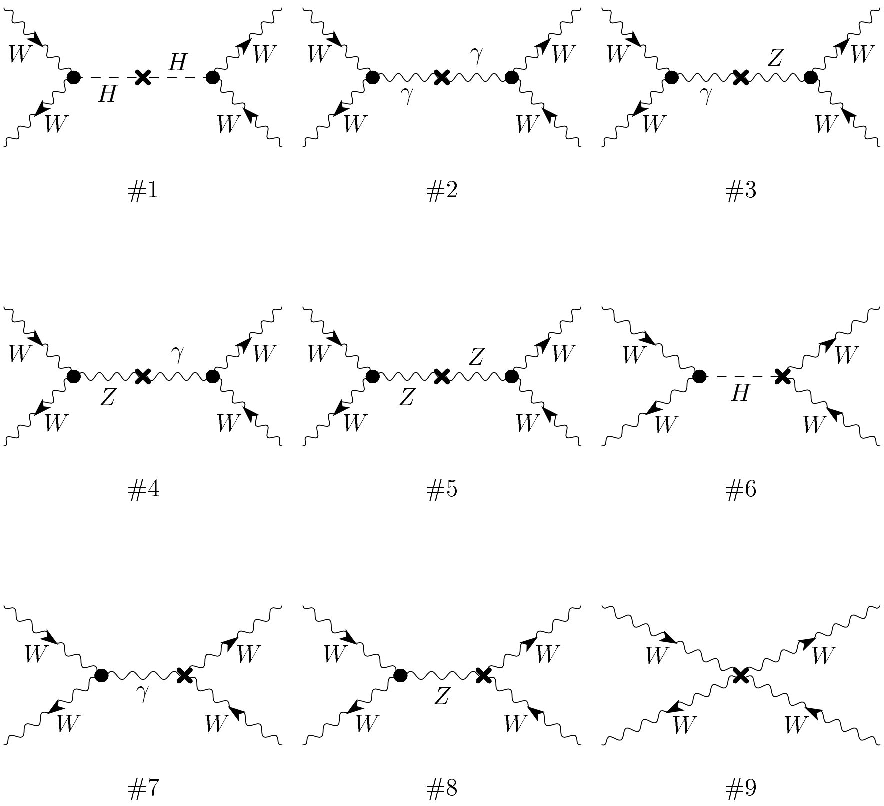

Figure 6.6: The counter-term diagrams. Omitted are the t-channel diagrams and those with the cross on the left vertex.

6.2 Differential cross-section

The $\mathcal{O}(\alpha^3)$-corrected differential cross-section including bremsstrahlung corrections is computed as

$$|\mathcal{M}_{\text{Born}}|^2 + 2\,\mathrm{Re}\,(\mathcal{M}^*_{\text{Born}}\delta\mathcal{M}) + |\mathcal{M}_{\text{soft}}|^2 \\ = |\mathcal{M}_{\text{Born}}|^2\,(1+\delta_{\text{soft}}) + 2\,\mathrm{Re}(\mathcal{M}^*_{\text{Born}}\delta\mathcal{M})\ , \qquad (6.1)$$

where $\delta\mathcal{M}$ is the sum of the one-loop Feynman diagrams.

As before, a Higgs-boson mass of $M_{\mathrm{H}} = 100\,\mathrm{GeV}$ is used in all plots and the integrated cross-sections are evaluated for an angular cut $\theta_{\text{cut}} = 10°$.

In the soft-photon approximation the corrections depend on the soft-photon cut-off energy ΔE via logarithms of the form $\ln(\Delta E/E)$. For small ΔE, where the soft-photon approximation is valid, these terms give rise to large corrections, which are, however, cancelled if hard-photon bremsstrahlung is taken into account. In order to avoid artificially large soft-photon effects, we have chosen to discard all terms involving $\ln(\Delta E/E)$ in the corrections.* The elimination of the cut-off-dependent terms can be simply achieved by choosing $\Delta E = E$. The corrections defined in this way can be viewed as a suitable measure of the purely weak corrections, which cannot be separated from the electromagnetic corrections on the basis of Feynman diagrams in a gauge-invariant way [DeD93, DeDS95].

The lowest-order and corrected differential cross-sections for the dominant polarizations LLLL, LTLT, LLTT, TTTT, and UUUU are shown in Fig. 6.7 for $\sqrt{s} = 200\,\mathrm{GeV}$, $1\,\mathrm{TeV}$, and $5\,\mathrm{TeV}$. The corrections are small at low energies for all scattering angles but get large at high energies, in particular in the backward direction. This is due to the fact that the contributions of the u-channel box diagrams to the cross-section involve terms that behave as $1/|u|$ for $M_{\mathrm{W}}^2 \ll |u| \ll s$ and approach a constant of the order of $1/M_{\mathrm{W}}^2$ for $|u| \ll M_{\mathrm{W}}^2$ while the lowest-order cross-section is of order $1/s$ for $|u| \ll s$. Hence the relative corrections in the backward direction are typically enhanced by a factor $s/|u|$ compared to the corrections in forward direction or to the total cross-section and can easily reach 100% at $\sqrt{s} = 5\,\mathrm{TeV}$. Since $|\delta\mathcal{M}|^2$ is missing in (6.1), the cross-section can formally become even negative in this case. We ignore this problem in the following, since the cross-sections are small in this

*Of course, these terms have to be reinstalled in a complete calculation involving hard-photon bremsstrahlung.

region, and, as has been stated above, the total cross-section is dominated by the forward region. Note that the large corrections in the backward direction do not indicate a breakdown of perturbation theory because no additional enhancement factors s/u should appear in higher orders.

6.3 Total cross-sections

In Fig. 6.8, the integrated cross-sections in lowest order and including $\mathcal{O}(\alpha)$ corrections as well as the relative $\mathcal{O}(\alpha)$ corrections are plotted for the dominant polarizations LLLL, LTLT, LLTT, TTTT, and UUUU. For small energies the corrections are positive and roughly 10%. With increasing energy the corrections become large and negative and reach the order of the lowest-order cross-sections around $10\,\mathrm{TeV}$. The large corrections at high energies originate from logarithms of the form $\alpha/\pi\ln^2(s/M_\mathrm{W}^2)$, which are additionally enhanced by numerical factors.

To demonstrate that the numerical precision is reliable at least for the dominating polarizations, the ratio of the cross-section integrated from 10° to 90° to the one integrated from 10° to 170° (the usual integration region) is shown in Fig. 6.9. It can be seen that the backward directions account for less than 3% of the total cross-section.

The dependency on the soft-photon cut-off energy ΔE is assessed in Fig. 6.10. We compare the value taken for the calculations, $\Delta E = E$, with the experimentally more reasonable choices $\Delta E = 10\%E$ and $\Delta E = M_\mathrm{W}$. Generally, all three values of ΔE agree for low energies but deviate at high energies. Nevertheless, the dependence on ΔE is nowhere as substantial as the dependence on the angular cut-off θ_cut (compare Fig. 3.5).

6.4 Accuracy of the equivalence-theorem predictions

The calculations of enhanced corrections to longitudinal gauge-boson scattering usually have been done [Pa85, DaW89] with the help of the equivalence theorem (ET) [CoLT74].

We calculated the matrix element for $\varphi^+\varphi^- \to \varphi^+\varphi^-$ to one-loop order in

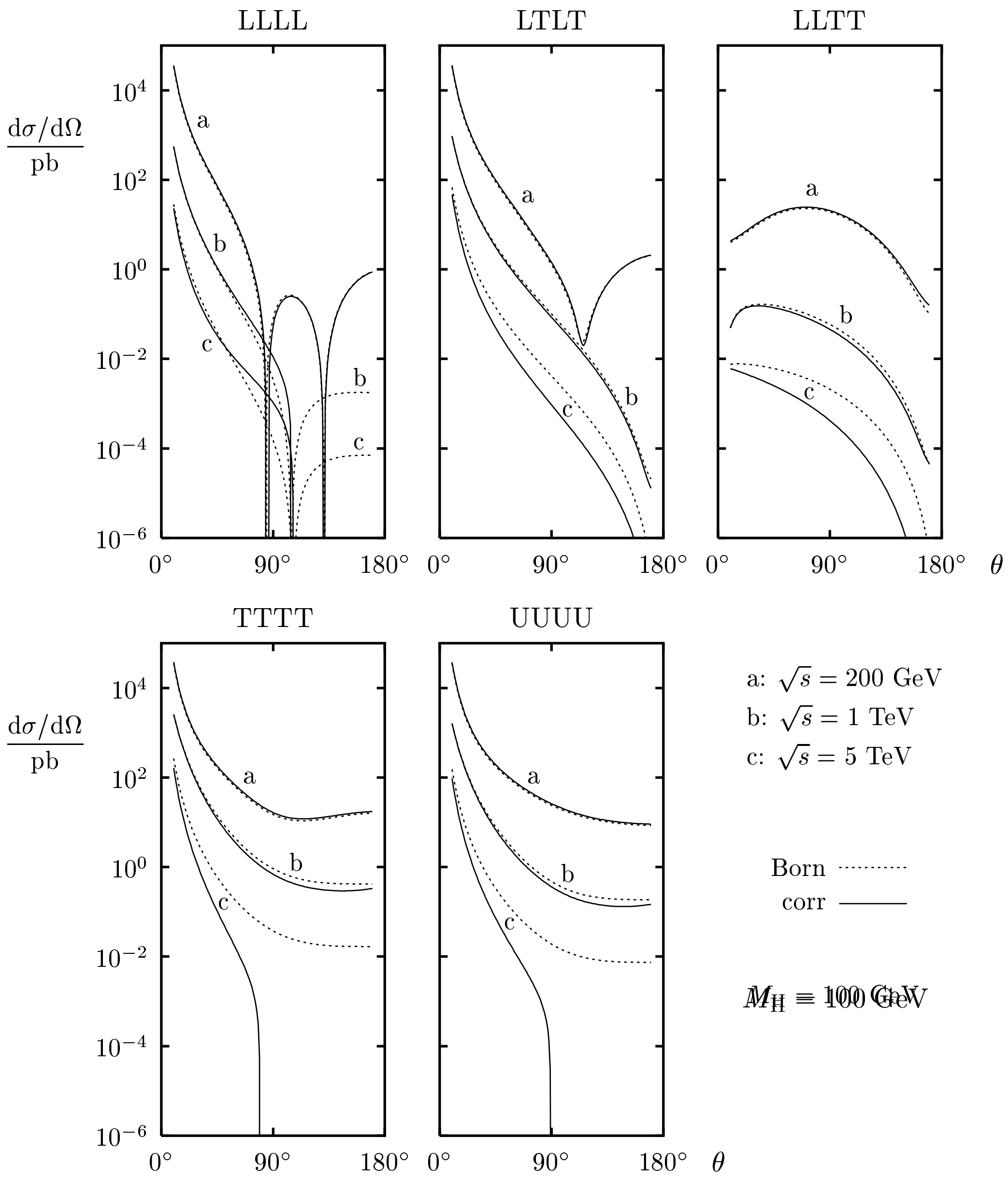

Figure 6.7: The differential cross-sections for the dominant polarizations at $\sqrt{s} = 200\,\mathrm{GeV}$, $1\,\mathrm{TeV}$, and $5\,\mathrm{TeV}$ in lowest order (Born) and including the $\mathcal{O}(\alpha)$ corrections (corr). Note that in some regions of phase space the corrected cross-sections become formally negative and are therefore not visible in these logarithmic plots.

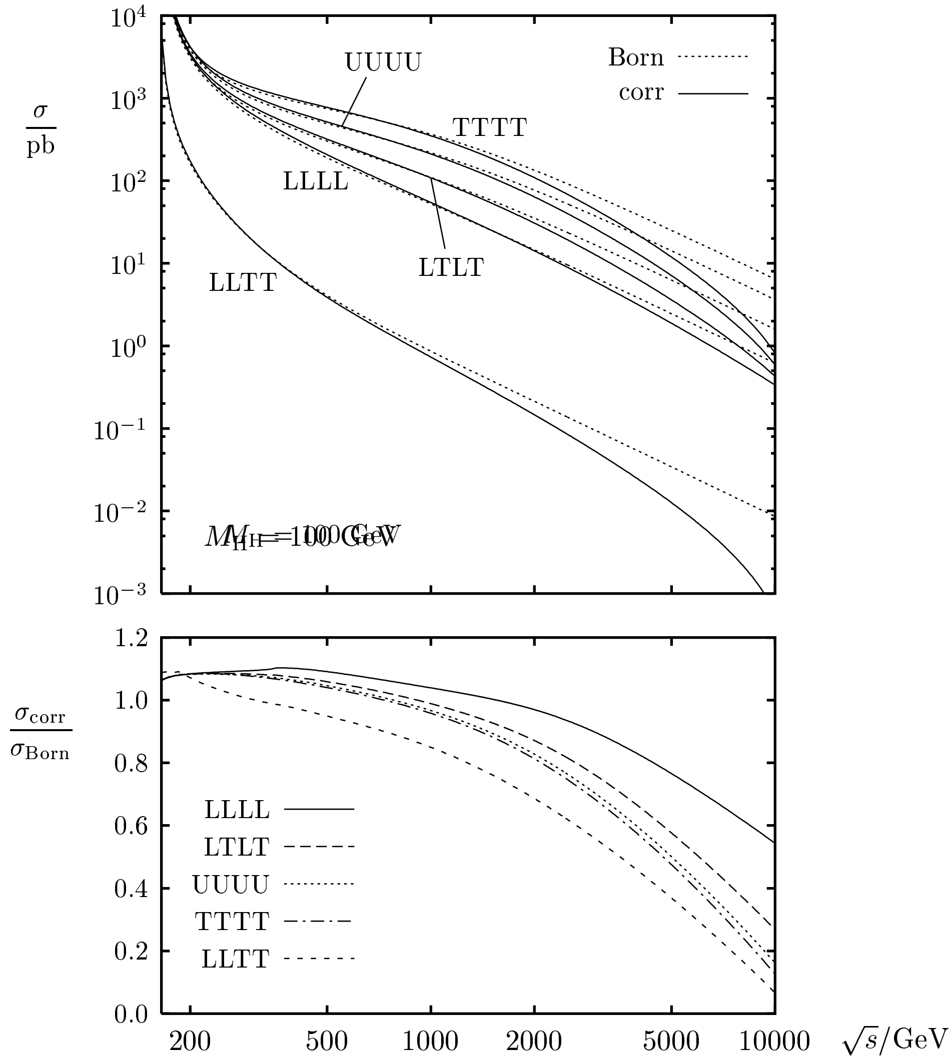

Figure 6.8: Upper plot: The integrated cross-sections for the dominant polarizations in lowest order (Born) and including the $\mathcal{O}(\alpha)$ corrections (corr). Lower plot: Relative corrections for the same polarizations.

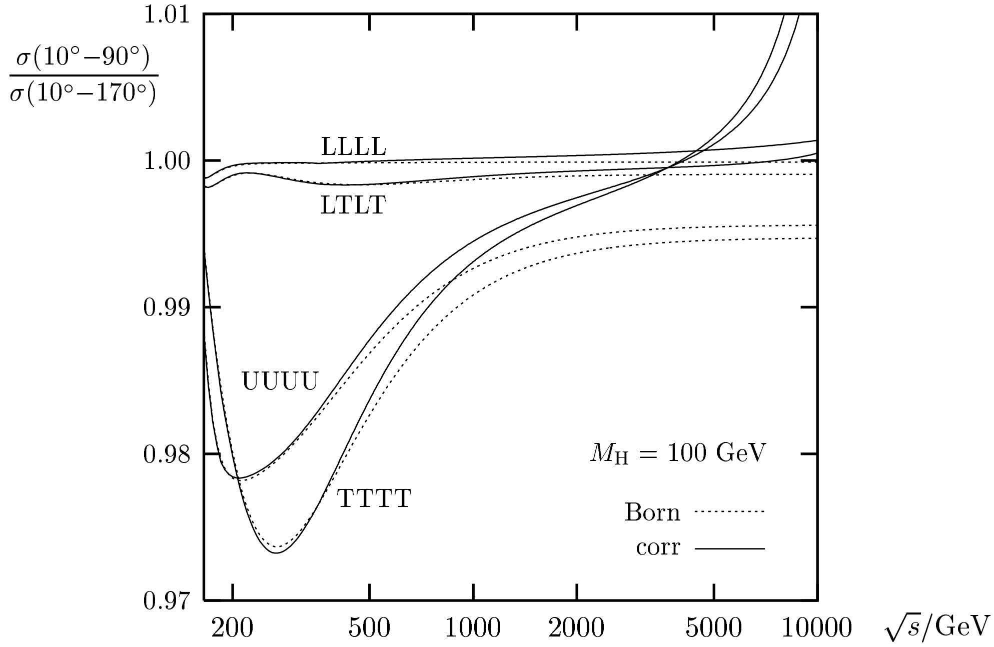

Figure 6.9: The ratio of the cross-section integrated over $\theta = 10° \ldots 90°$ to the one integrated over $\theta = 10° \ldots 170°$ (the usual integration region). As expected from the differential cross-sections, the contributions from scattering angles larger than $90°$ are negligibly small ($< 3\%$). For a strictly positive cross-section the ratio should never grow larger than 1. Where this happens it consequently indicates that the $\mathcal{O}(\alpha^3)$ approximation to the cross-section has developed negative values in parts of the region $\theta = 90° \ldots 170°$. Though quantitatively small, the figure suggests that these pathologic negative bits become more pronounced with increasing energy.

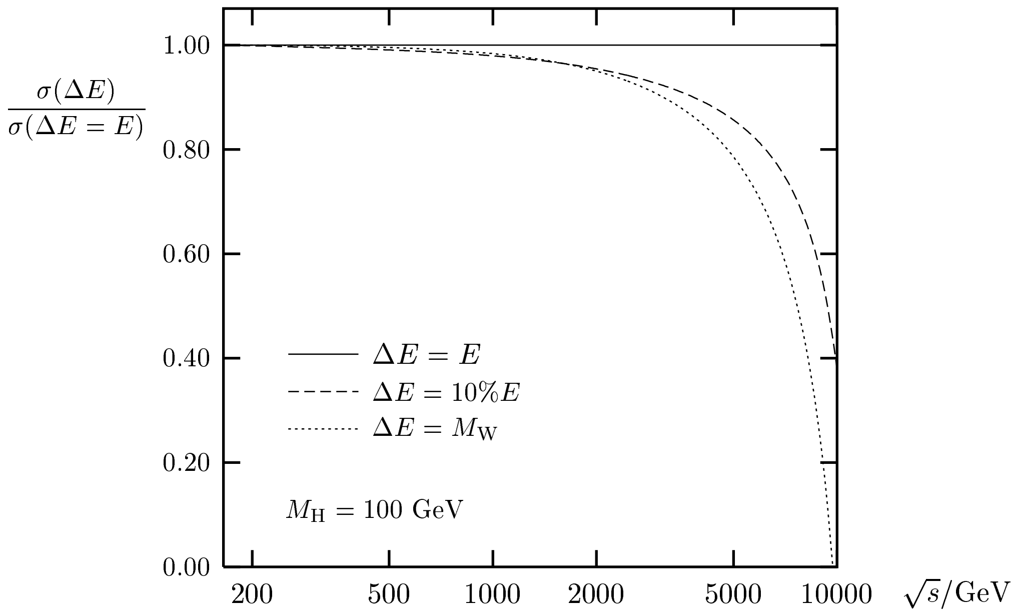

Figure 6.10: Dependence of the integrated cross-section on the choice of the soft-photon cut-off energy ΔE.

the BFM and from this the ET prediction for the cross-section for $\mathrm{W_L^+W_L^-} \to \mathrm{W_L^+W_L^-}$

$$\left(\frac{\mathrm{d}\sigma}{\mathrm{d}\Omega}\right)_{\mathrm{ET}} = \frac{1}{64\pi^2 s}\Bigg[\left|\mathcal{M}_{\mathrm{Born}}^{\varphi^+\varphi^-\to\varphi^+\varphi^-}\right|^2(1+\delta_{\mathrm{soft}}) \\ + 2\,\mathrm{Re}\Big\{\big(\mathcal{M}_{\mathrm{Born}}^{\varphi^+\varphi^-\to\varphi^+\varphi^-}\big)^*\delta\mathcal{M}^{\varphi^+\varphi^-\to\varphi^+\varphi^-}\Big\}\Bigg]. \quad (6.2)$$

Since $\varphi^+\varphi^- \to \varphi^+\varphi^-$ and $\varphi^+\varphi^- \to \varphi^+\varphi^-\gamma$ are no physical processes, the cross-section (6.2) is not well-defined at finite energies. The ET is valid only for high energies and guarantees Eq. (6.2) to provide a sensible cross-section only in the high-energy limit, i.e. up to terms of order M_{W}/E. In fact (6.2) is gauge-dependent and the IR singularities between the virtual and real corrections do not cancel exactly. In the analytic results, which are obtained for an infinitesimal photon mass λ, terms proprotional to $(M_{\mathrm{W}}/E)\ln(\lambda^2/s)$ and gauge-dependent terms proprotional to (M_{W}/E) remain. In order to avoid an enhancement of the IR-singular terms we have chosen a photon mass equal to the energy of the W bosons, $\lambda = E$. This ensures that the artifical IR-singular logarithms do not lead to enhanced contributions.

Since also the soft-photon corrections factor corresponding to $\varphi^+\varphi^- \to$

	$\frac{\sigma(\varphi^+\varphi^- \to \varphi^+\varphi^-)}{\sigma(\mathrm{W_L^+W_L^-} \to \mathrm{W_L^+W_L^-})} - 1$		
$\sqrt{s}$	Born	corr	mixed
$500\,\mathrm{GeV}$	-6.40%	-2.65%	3.22%
$1\,\mathrm{TeV}$	-3.02%	0.78%	3.68%
$2\,\mathrm{TeV}$	-1.01%	0.29%	1.33%
$5\,\mathrm{TeV}$	-0.18%	-0.62%	-0.39%
$10\,\mathrm{TeV}$	-0.05%	-0.22%	-0.13%

Table 6.1: Relative deviations of the ET predictions for $\mathrm{W_L^+W_L^-} \to \mathrm{W_L^+W_L^-}$.

$\varphi^+\varphi^-$ is gauge-dependent we have chosen to use directly the soft-photon correction factor for $\mathrm{W^+W^-} \to \mathrm{W^+W^-}$. We stress that despite the gauge-dependences and the IR-singularities contained in Eq. (6.2), our results are valid at the same level as all ET results, i.e. up to terms of order M_W/E.

In order to improve the accuracy of the ET calculation the lowest-order cross-section for $\mathrm{W_L^+W_L^-} \to \mathrm{W_L^+W_L^-}$ is combined with the $\mathcal{O}(\alpha)$ corrections from $\varphi^+\varphi^- \to \varphi^+\varphi^-$ as follows

$$\left(\frac{\mathrm{d}\sigma}{\mathrm{d}\Omega}\right)_{\text{mixed}} = \frac{1}{64\pi^2 s}\Bigg[\left|\mathcal{M}_{\text{Born}}^{\mathrm{W_L^+W_L^-}\to\mathrm{W_L^+W_L^-}}\right|^2 + \left|\mathcal{M}_{\text{Born}}^{\varphi^+\varphi^-\to\varphi^+\varphi^-}\right|^2\delta_{\text{soft}} \\ + 2\,\mathrm{Re}\Big\{\left(\mathcal{M}_{\text{Born}}^{\varphi^+\varphi^-\to\varphi^+\varphi^-}\right)^*\delta\mathcal{M}^{\varphi^+\varphi^-\to\varphi^+\varphi^-}\Big\}\Bigg]. \quad (6.3)$$

In this way the error originating from the use of the ET is suppressed by an order of α.

The accuracy of the ET predictions for the scattering of longitudinal W bosons is investigated in Fig. 6.11 and Table 6.1. We show the lowest-order cross-section (Born) for $\varphi^+\varphi^- \to \varphi^+\varphi^-$ normalized to the lowest-order cross-section for $\mathrm{W_L^+W_L^-} \to \mathrm{W_L^+W_L^-}$ and the corrected cross-section (corr) calculated from the ET according to Eq. (6.2) and according to the 'mixed' formula Eq. (6.3), both normalized to the corrected cross-section for $\mathrm{W_L^+W_L^-} \to \mathrm{W_L^+W_L^-}$.

Above $\sqrt{s} \gtrsim 500\,\mathrm{GeV}$ the deviations are all below 7% and become smaller at higher energies. Above $\sim 2\,\mathrm{TeV}$ they are less than 1%. For high energies, where the ET is valid, the approximation (6.3) is in fact better than the pure ET prediction.

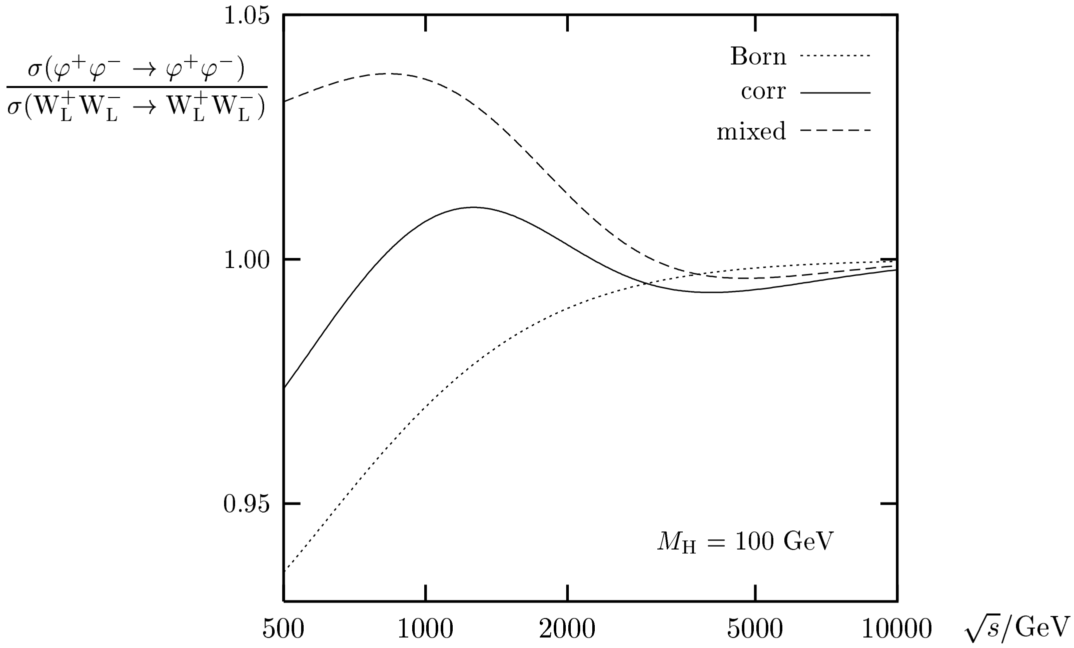

Figure 6.11: Relative deviations of the ET predictions for $W_L^+W_L^- \to W_L^+W_L^-$. 'Born' and 'corr' label the deviations for the tree-level and $\mathcal{O}(\alpha)$-corrected cross-sections, respectively. For the curve marked 'mixed' the ET is used only for the corrections [cf. Eq. (6.3)].

6.5 Evaluation with the computer

Evaluating some 1000 diagrams is a task nobody in his or her right mind would attempt to do by hand. Fortunately, the methods for one-loop calculations are by now broadly developed. The basic calculational scheme is summarized in Fig. 6.12. The following sections are intended to give an idea of what the individual steps are like.

6.5.1 Generating the diagrams with *FeynArts*

FeynArts [KüBD91] is a program package based on *Mathematica* [Wo96] for generating Feynman diagrams.

To generate Feynman diagrams, the first step is to find all possible topologies for a given number of external legs and internal loops. The necessary commands are

```
tops = CreateTopologies[ 1, 2 -> 2,
  ExcludeTopologies -> {Tadpoles, WFCorrections} ];
countertops = CreateCTTopologies[ 1, 2 -> 2,
  ExcludeTopologies -> {CTTad, ExtCTSE} ];
```

The first two lines generate the topologies for the loop diagrams, the other two for the counterterm diagrams. Their arguments are similar and are interpreted as “Generate all topologies for a $2 \to 2$ process with 1 loop, thereby excluding tadpoles (`Tadpoles`, `CTTad`) and loop insertions on the external legs (`WFCorrections`, `ExtCTSE`).” The symbolic expressions specifying the topologies are then stored in the variables `tops` and `countertops`, respectively.

In a second step, the actual fields need to be inserted into the generic topologies. Given the model specific information (i.e. the propagators and couplings allowed within the theory), *FeynArts* can produce diagrams for practically any model. Here the SM is used:

```
ins = InsertFields[ tops,
  {V[3],-V[3]} -> {V[3],-V[3]}, Model -> "SM",
  InsertionLevel -> Particles,
  Restrictions -> {NoQuarkMixing,
    NoGeneration2, NoGeneration3} ];
```

FeynArts $\sim 1/2$ h	Generate $W^+W^- \to W^+W^-$ diagrams Generate self-energy diagrams for renormalization Create topologies $\downarrow$ Insert fields $\downarrow$ Generate amplitudes
FormCalc $\sim 1/2$ h	Algebraic simplifications – calculate traces – contract indices – reduce tensor integrals – introduce abbreviations
NumPrep *num.F* ~ 30 ms for 1 point	– numerically stable algorithms (scalar and tensor integrals) – optimized for speed (avoid multiple calculations etc.) – flexibility (e.g. conv., BFM) – easy checking possible

Figure 6.12: Calculational scheme for evaluation of one-loop corrections on the computer. The quoted timings are for the complete set of diagrams for $W^+W^- \to W^+W^-$ on an HP 9000/735 workstation with 128 MB of memory.

This command instructs *FeynArts* to insert fields into the topologies stored in `tops`. The external fields are specified to be W^-, W^+, W^-, and W^+ where `V[3]` is a W^- boson in *FeynArts* terminology, and `-V[3]` its antiparticle, W^+. Both the topologies and the inserted diagrams may be drawn with

```
Paint[ tops ];  Paint[ ins ];
```

Lastly, the diagrams must be translated into amplitudes using the Feynman rules. This is accomplished by

```
amp1 = CreateFeynAmp[ ins ];
amp2 = PickLevel[Particles][ amp1 ];
```

The amplitudes created this way are symbolic *Mathematica* expressions, specifically designed to be in a readable form. Here is an example for the output of *FeynArts*, corresponding to the diagram

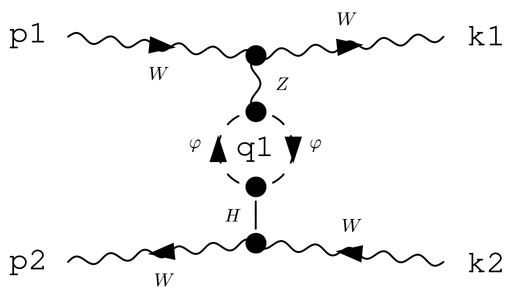


```
I*EL^4*MH^2*(-CW^2 + SW^2)/(64*Pi^4*SW^4)*
PolarizationVector[p1, li1]*
PolarizationVector[p2, li2]*
Conjugate[PolarizationVector[k1, li3]]*
Conjugate[PolarizationVector[k2, li4]]*
(FourVector[-k1 - p1, li6]*MetricTensor[li1, li3] +
  FourVector[-k1 + 2*p1, li3]*MetricTensor[li1, li6] +
  FourVector[2*k1 - p1, li1]*MetricTensor[li3, li6])*
FourVector[k1 - p1 + 2*q1, li5]*MetricTensor[li5, li6]*
MetricTensor[li2, li4]*
FeynAmpDenominator[PropagatorDenominator[q1, MW],
  PropagatorDenominator[k1 - p1 + q1, MW]]*
PropagatorDenominator[-k1 + p1, MH]*
PropagatorDenominator[-k1 + p1, MZ]
```

p1 and p2 are the incoming and k1 and k2 the outgoing momenta. The structure of the diagram can easily be recounted: the polarization vectors from the external bosons, the coupling structure consisting of FourVectors and MetricTensors, and the denominators coming from the propagators. The loop propagators are wrapped in the head FeynAmpDenominator.

6.5.2 Algebraic simplification with *FormCalc*

For one-loop calculations, the resulting formulae tend to get rather large, so usually they are evaluated numerically and the results are then plotted or similar. The *FeynArts* output, nice as it is, is still not well suited for direct numerical evaluation. For instance, Lorentz indices need to be contracted, Dirac traces calculated, as well as a lot of simple algebra performed like factoring terms etc.

Particularly adapted to this kind of algebra needed in high-energy physics is *Form*, a computer algebra program by J. Vermaseren [Ve91]. Unfortunately, *Form* is not directly compatible to *Mathematica* (and also less user friendly), therefore a program called *FormCalc* was developed by the author of this thesis. The basic idea behind *FormCalc* can be seen from the following diagram:

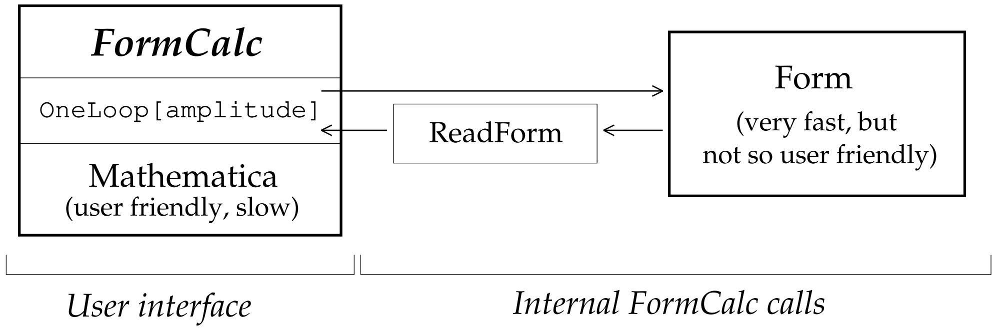

This way, the user gets maximum speed, for the heavy algebra is passed on to *Form*, but retains the flexibility to handle, select and rearrange the expressions with the powerful instruction set of *Mathematica*.

The user input required to process a file containing Feynman amplitudes generated by *FeynArts* is minimal:

```
<< FormCalc.m;
ProcessFile["wwww.self.amp","results/self"];
ProcessFile["wwww.vert.amp","results/vert"];
ProcessFile["wwww.box.amp","results/box"];
Abbreviations >> "results/abbr";
```

Here, the files `wwww.self.amp` etc. are assumed to contain the amplitudes from *FeynArts*, and the output is written e.g. to `results/self.m` (bosonic part) and `results/selfF.m` (fermionic part).

The last line of the previous example reveals that *FormCalc* automatically introduces abbreviations. This is an invaluable device for handling large mathematical expressions. The abbreviations are sums and products of standard matrix elements, which are scalar products of and Levi-Cività tensors contracted with polarization and momentum four-vectors.

The following example is a brief excerpt of the *FormCalc* output for $\mathrm{W^+W^-} \to \mathrm{W^+W^-}$; more precisely, it comes from diagrams of the type 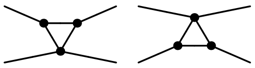 .

```
(-4*a2*MW2*O2 - 2*a2*MW2*P401 - 6*a2*P471*S
  - 2*a2*P472*S + a2*P473*S + a2*P470*T)
   *C0i[cc1, MW2, MW2, T, 0, MW2, 0]
- (-2*a2*MW2*P417*S2 + 4*a2*O14*S*S2 - 6*a2*O23*S*S2
  - 2*a2*P456*S*S2 + a2*P457*S*S2
  + (a2*O2*S2*T)/2 + a2*O3*S2*T
  - O1*(-4*a2*MW2*S2 + 2*a2*S2*T))
    *C0i[cc1, MW2, MW2, T, MW2, 0, MW2]
+ (a2*O42*S*S4)/2
    *(C0i[cc12, MW2, MW2, T, MH2, MW2, MH2] +
      C0i[cc2, MW2, MW2, T, MH2, MW2, MH2] +
      C0i[cc22, MW2, MW2, T, MH2, MW2, MH2])
```

The structure of this expression is characteristic for all one-loop amplitudes: a linear combination of scalar and tensor one-loop integrals†. The coefficients contain parameters of the SM like `a2` $= \alpha^2$, `S4` $= s_{\mathrm{W}}^{-4}$, etc. and the above mentioned abbreviations like `O2`, `P456`, etc. In order to demonstrate the usefulness of introducing abbreviations, consider `P457` from the above example, and see for yourself of how many expressions it is composed:

```
P457 = O24 - O41 + O8
```

with

†The computer uses a generalized notation: `C0i[cc12, ...]` $= C_{12}(\dots)$ is the coefficient of $p_{1\mu}p_{2\nu}$ in the three-point tensor function.

```
O24 = e13*k21*k43
O41 = e24*k13*k31
O8  = e34*k13*k21
```

with

```
e13 = Pair[e[1],e[3]]
e24 = Pair[e[2],e[4]]
k21 = Pair[e[2],k[1]]
k43 = Pair[e[4],k[3]]
k13 = Pair[e[1],k[3]]
k31 = Pair[e[3],k[1]]
k21 = Pair[e[2],k[1]]
```

(`Pair[a,b]` denotes the scalar products of the four-vectors `a` and `b`.)

6.5.3 Final numerical evaluation in Fortran

After processing through *FormCalc* the expressions need only very little further modification to cast them into Fortran code. Basically, numerical constants need to be inserted and the expression broken up into chunks which the compiler can handle. This task is accomplished by a program called *NumPrep*. It takes the algebraically simplified amplitudes as input and produces

- several modules of Fortran code (e.g. `self.F`, `box.F`),
- a subroutine for calculating the abbreviations (`abbr.F`),
- a special control file with which to set and/or modify parameters of the calculation (`feyn.h`), and
- a so-called `makefile` that allows to compile the whole bundle with only a few keystrokes.

Together with a driver program (`num.F`), the package is able to calculate differential and total cross-sections for any given boson polarization (including partially or totally unpolarized bosons) in any energy range. Special effort has gone into the ability to control every step of the computation with as little manual (error-prone) interference as possible. Fortran has been chosen since it is the most efficient language for “number crunching,” i.e. evaluating huge formulae.

Here is an example of the code:

```
#include <defs.h>
        double complex function box()
        implicit logical (a-s,u-z)
        implicit double complex (t)
#include <vars.h>
        box=(0.0097507818121657581221448O3*O220*S +
     -     0.0016251303020276263536908004*P505*S -
     -     0.0024376954530414395305362007*P506*S -
     -     0.0032502606040552527073816O1*O1*U +
     -     0.00081256515101381317684540O2*P1*U)
     -     *Cval(cc22,cd20) -
     -  0.00052445142186901827884821 5*O43*S*
     -   (Cval(cc12,cd11) + Cval(cc12,cd21) +
     -     Cval(cc2,cd11) + Cval(cc2,cd21) +
     -     Cval(cc22,cd11) + Cval(cc22,cd21))
...
```

The one-loop integrals are calculated in a separate step and are subsequently retrieved from an array (`Cval` here). In particular scattering-angle independent integrals are evaluated outside of the loop over θ, a procedure which saves a considerable amount of time.

The control file `feyn.h` mentioned above allows the user to easily modify settings (only one file needs to be re-compiled) like the IR regulator mass λ or the dimensional parameter μ, e.g.

```
#define LAMBDA 1D10
#define MUDIM 1D10
```

and it also lets the user select which modules (and which fermion generations) to include in the calculation by modifying a line like

```
        oneloop=box()+boxFDUT8()+boxFET8()
     -    +boxT7()+boxT8()+boxT9()
     -    +self()+selfF()+tri()+triF()
```

6.6 Parameters and Calculational Details

For the calculations the following parameter set is used [PDG]:

$$\begin{aligned}
\alpha^{-1} &= 137.0359895, & M_\mathrm{Z} &= 91.188\,\mathrm{GeV}, & M_\mathrm{W} &= 80.401\,\mathrm{GeV}, \\
m_\mathrm{e} &= 0.51099906\,\mathrm{MeV}, & m_\mathrm{u} &= 47.0\,\mathrm{MeV}, & m_\mathrm{d} &= 47.0\,\mathrm{MeV}, \\
m_\mu &= 105.658389\,\mathrm{MeV}, & m_\mathrm{c} &= 1.55\,\mathrm{GeV}, & m_\mathrm{s} &= 150\,\mathrm{MeV}, \\
m_\tau &= 1771.1\,\mathrm{MeV}, & m_\mathrm{t} &= 175.5\,\mathrm{GeV}, & m_\mathrm{b} &= 4.5\,\mathrm{GeV}.
\end{aligned} \tag{6.4}$$

The masses of the light quarks are adjusted such that the experimentally measured hadronic vacuum polarization is reproduced [EiJ95].

Several cross-checks have been performed to ascertain the correctness of our calculation. In particular, we checked

- the algebraic simplification of the Feynman diagrams by comparing the *FormCalc* results with those obtained from *FeynCalc* [MeBD91] for selected diagrams (analytically),
- the numerical evaluation of the Feynman diagrams by comparing the evaluation of selected diagrams in *Fortran* and in *Mathematica* (numerically),
- the evaluation of the scalar one-loop integrals by comparing the results of the *FF* routines with Ansgar Denner's routines (numerically),
- the gauge and renormalization-scheme independence of the results by comparing the results in conventional formalism and background-field formalism (numerically),
- the UV finiteness by proving independence of the scale parameter of dimensional regularization μ (analytically),
- the IR finiteness by testing independence of the regulator mass λ (numerically).

Numerical computations were done using extended precision (`REAL*16`) with a mantissa of approximately 33 digits. The relative deviation between numerical results from different calculational methods was less than 10^{-16}. A double precision calculation is in general sufficient up to about $10\,\mathrm{TeV}$. For higher energies the gauge cancellations become so strong that double precision does not give reliable results any more.

6.7 Difficulties beyond $\mathcal{O}(\alpha^3)$ accuracy

In Sect. 6.2 it was demonstrated that $\mathcal{O}(\alpha^3)$ accuracy is not sufficient in regions where the tree-level amplitude becomes small, namely for large scattering angles at high energies. A consistent $\mathcal{O}(\alpha^4)$ calculation would require calculation of the two-loop amplitudes, which is a formidable task. One might be tempted to simply replace

$$|\mathcal{M}_{\text{Born}}|^2 + 2\,\mathrm{Re}\,(\mathcal{M}^*_{\text{Born}}\delta\mathcal{M}) \longrightarrow |\mathcal{M}_{\text{Born}} + \delta\mathcal{M}|^2 \,. \tag{6.5}$$

This, of course, comprises only an incomplete set of higher-order diagrams. There are two severe problems this approach brings with it and therefore it was not used in this thesis.

Firstly, with the soft-photon factor δ_{soft} evaluated to $\mathcal{O}(\alpha)$, only the combination in Eq. (6.1) is IR finite in the limit $\lambda \to 0$. Including $|\delta\mathcal{M}|^2$ would require $\mathcal{M}_{\text{soft}}$ to $\mathcal{O}(\alpha^2)$, i.e. it would include two-photon emission off the Born diagrams as well as single-photon emission off the one-loop diagrams.

The second, more severe difficulty is closely related to the instability of the W boson. When calculating the one-loop diagrams for $\mathrm{W}^+_\mathrm{L}\mathrm{W}^-_\mathrm{L} \to \mathrm{W}^+_\mathrm{L}\mathrm{W}^-_\mathrm{L}$ one finds that not all terms proportional to s cancel. The left-over terms proportional to s in the unrenormalized amplitude can be expressed in terms of the transverse W self-energy:

$$\delta\mathcal{M}^{\text{unren.}}_{\mathcal{O}(s)} = \frac{4\pi\alpha}{s^2_\mathrm{W}}\cos^2\frac{\theta}{2}\frac{s}{M^2_\mathrm{W}}\frac{\Sigma^W_\mathrm{T}(M^2_\mathrm{W})}{M^2_\mathrm{W}}\,. \tag{6.6}$$

The counter terms, in fact only the W-mass counter term $\delta M^2_\mathrm{W} = \mathrm{Re}\,\Sigma^W_\mathrm{T}(M^2_\mathrm{W})$ (and the derived counter term for the weak mixing angle δc^2_W), yield a similar contribution with opposite sign. When adding these contributions, the real part of $\delta\mathcal{M}^{\text{unren.}}_{\mathcal{O}(s)}$ is exactly cancelled but the imaginary part survives. As a consequence the imaginary part of the one-loop matrix element for $\mathrm{W}^+_\mathrm{L}\mathrm{W}^-_\mathrm{L} \to \mathrm{W}^+_\mathrm{L}\mathrm{W}^-_\mathrm{L}$ grows with s and therefore violates unitarity. Because the lowest-order matrix element is real as long as no Higgs resonance needs to be included, this does not affect the $\mathcal{O}(\alpha^3)$ corrections to the cross-section. However, in higher orders or if the Higgs-boson width has to be included the imaginary part becomes relevant and the perturbative evaluation of corrections to $\mathrm{W}^+_\mathrm{L}\mathrm{W}^-_\mathrm{L} \to \mathrm{W}^+_\mathrm{L}\mathrm{W}^-_\mathrm{L}$ for on-shell external W bosons breaks down.

The reason for this breakdown becomes apparent by noting that the unitarity-violating term can be written as

$$\delta\mathcal{M}_{\mathcal{O}(s)} = \frac{4\pi\alpha}{s_{\mathrm{W}}^2}\cos^2\frac{\theta}{2}\frac{s}{M_{\mathrm{W}}^2}\frac{\mathrm{i}\,\mathrm{Im}\,\Sigma_{\mathrm{T}}^{W}(M_{\mathrm{W}}^2)}{M_{\mathrm{W}}^2} = \mathrm{i}\frac{4\pi\alpha}{s_{\mathrm{W}}^2}\cos^2\frac{\theta}{2}\frac{s}{M_{\mathrm{W}}^2}\frac{\Gamma_{\mathrm{W}}}{M_{\mathrm{W}}}\,, \tag{6.7}$$

i.e. it is proportional to the (lowest-order) decay width of the W boson. This shows that the problem is due to the instability of the W bosons.

From the previous considerations it is clear that the unitarity-violating terms would cancel if the W-boson-mass counter term were complex, i.e. if renormalization would also compensate the imaginary part of the W self-energy. Since the bare W-boson mass is real, this can only be achieved if the renormalized W-boson mass (and the renormalized weak mixing angle) become complex.

Let us consider the matrix element in this renormalization scheme. In the one-loop part and in the counter-term part, which are of order α, the renormalized parameters can be replaced by bare parameters and all unitarity-violating terms cancel out. In the tree-level matrix element, however, the complex renormalized parameters lead to unitarity-violating terms if it is calculated for $k_i^2 = M_{\mathrm{W}}^2$. This reflects the fact that a change in renormalization scheme in an $\mathcal{O}(\alpha^3)$ calculation cannot eliminate $\mathcal{O}(\alpha^3)$ corrections but only reshuffle them. However, if we evaluate the matrix element for complex external momenta squared, $k_i^2 = M_{\mathrm{W}}^2 - \mathrm{i}M_{\mathrm{W}}\Gamma_{\mathrm{W}}$, all unitarity-violating terms cancel in the tree-level part, and the loop and counter-term parts are not changed (up to terms of order α^4) with respect to the evaluation with real external momenta squared, $k_i^2 = M_{\mathrm{W}}^2$. As a result, the matrix element for $\mathrm{W}_{\mathrm{L}}^+\mathrm{W}_{\mathrm{L}}^- \to \mathrm{W}_{\mathrm{L}}^+\mathrm{W}_{\mathrm{L}}^-$ including $\mathcal{O}(\alpha)$ corrections respects unitarity, if the squares of the external momenta are equal to the physical complex masses, but violates unitarity for real on-shell external momenta.

The approach described above requires to consider matrix elements for complex external momenta squared. However, the momenta of physical particles are always real, even if these particles appear only as resonances in some process. Since it is not clear how to relate the physical real momenta to appropriate complex momenta this approach was not pursued any further.

The only fully consistent way to calculate corrections to longitudinal W-boson scattering beyond $\mathcal{O}(\alpha)^3$ seems to be the evaluation of a physical process, e.g. $\mathrm{e}^+\mathrm{e}^- \to \mathrm{W}^+\mathrm{W}^- \to \mathrm{W}^+\mathrm{W}^- \to 4$ fermions, or at least the resonant contributions to this process. This is beyond the scope of the present investigation.

Chapter 7

Conclusions

The electroweak Standard Model is the basis for today's understanding of high-energy physics. It is a spontaneously broken non-abelian gauge theory and is so far in agreement with many increasingly precise experiments. It is for this reason that the Standard Model, even though it lacks the simplicity and completeness a final theory of all fundamental forces would have to have, will almost inevitably constitute the low-energy limit of any larger theory.

Remarkably though, two of the pillars on which the Standard Model is built, namely the non-abelian gauge sector and the Higgs sector which is responsible for spontaneous symmetry breaking, are just at the beginning of undergoing decisive experimental tests. This is due in parts to the large masses of the W and Z gauge bosons which have come into experimental reach only in the last decade.

One of the most lucid methods to test both the non-abelian gauge sector and the symmetry-breaking sector is by the scattering of the non-abelian gauge bosons. These reactions involve to lowest order only interactions between gauge and scalar bosons and therefore depend very sensitively exactly on the as yet incompletely tested parts of the underlying theory. Unfortunately the neutral Z bosons have very small cross-sections, therefore from the experimental point of view the scattering of the charged W bosons, or $\mathrm{W^+W^-} \to \mathrm{W^+W^-}$ for short, is more promising. Still, one has to contend that these experiments are not possible with present-day machines and that data will not become available for perhaps the next decade.

In this thesis the amplitudes for $\mathrm{W^+W^-} \to \mathrm{W^+W^-}$ as predicted by the Standard Model are calculated in the Born (lowest-order) and one-loop approximations. The existing one-loop calculations in the literature have all either taken into account only leading corrections, or used approximations like the equivalence theorem; it is thus for the first time that the complete results are presented in this thesis.

The cross-sections are calculated with the aid of Feynman diagrams in perturbation theory. At Born level there are only 7 diagrams which makes it even possible to list the analytic results. This is not feasible at one-loop level, where some 1000 diagrams need to be calculated. Sect. 6.5 describes the computational methods which are based on computer algebra.

The cross-sections are peaked in forward direction which is expected from the electromagnetic interaction. The corrections are small near the threshold but become larger for larger energies, e.g. for energies $\gtrsim 1$ TeV the corrections are of the order of $\mathcal{O}(10\%)$.

Since the W bosons are very short lived, it is a problematic approximation to use stable particles in the calculation. Indeed, this haunts already the one-loop calculations (see Sect. 6.2). Taking into account the finite-width effects is as yet an unsolved problem of quantum field theory and was not undertaken in this thesis (see, however, Sect. 6.7 for a discussion).

The least-known part of the Standard Model is surely the Higgs sector. The Higgs particle is the remnant of a mass generation mechanism that gives the gauge bosons and the fermions their masses. The Higgs boson has not yet been discovered, but indirect measurements provide an allowed mass range which is presently $M_\mathrm{H} = 159^{+153}_{-86}$ GeV (1σ). In Sect. 4.2 it is shown that Higgs exchange is necessary to prevent the W–W scattering amplitudes from violating unitarity. In other words, it is not possible to put in mass terms by hand.

Furthermore, if the Higgs has a mass above the W–W threshold, i.e. $M_\mathrm{H} > 2M_\mathrm{W}$, it will be seen as a sizeable resonance peak in the W–W cross-sections (see Sect. 4.5).

The prediction of the equivalence theorem, which relates the scattering amplitudes of the longitudinal components of the gauge bosons with those of the unphysical Higgs fields, are compared to the full result in Sect. 6.3. For energies $\gtrsim 200$ GeV the deviations are below 10%, and above ~ 2 TeV they are less than 1%.

Bibliography

[AlMP87] G. Altarelli, B. Mele, and F. Pitolli, *Nucl. Phys.* **B287** (1987) 205.

[Am84] D. Amit, *Field Theory, the Renormalization Group, and Critical Phenomena*, World Scientific, Singapore (1984).

[BaBD93] D. Bardin, W. Beenakker, and A. Denner, *Phys. Lett.* **B317** (1993) 213;
V.S. Fadin, V.A. Khoze, and A.D. Martin, *Phys. Lett.* **B311** (1993) 311.

[BaBGH97] V. Barger, M.S. Berger, J.F. Gunion and T. Han, *Phys. Rev.* **D55** (1997) 142;
T. Han, preprint hep-ph/9704215.

[BlN37] F. Bloch and A. Nordsieck, *Phys. Rev.* **37** (1937) 54;
D.R. Yennie, S.C. Frautschi, and H. Suura, *Ann. Phys.* **13** (1955) 379.

[Bo90] R. Bouamrane, in: *Radiative Corrections: Results and Perspectives*, eds. N. Dombey and F. Boudjema, Plenum Press, New York (1990) 533;
D.A. Dicus and W.W. Repko, *Phys. Lett.* **B228** (1989) 503 and *Phys. Rev.* **D42** (1990) 3660;
S. Dawson and G. Valencia, *Nucl. Phys.* **B348** (1991) 23.

[BoRS95] V.I. Borodulin, R.N. Rogalyov, and S.R. Slabospitsky, preprint hep-ph/9507456.

[Ch93] M.S. Chanowitz, in: *Perspectives on Higgs Physics*, ed. G.L. Kane, World Scientific, Singapore (1993) 343;
M.S. Chanowitz and W.B. Kilgore, *Phys. Lett.* **B322** (1994) 147 and *Phys. Lett.* **B347** (1995) 387.

[CoLT74] J.M. Cornwall, D.N. Levin, and G. Tiktopoulos, *Phys. Rev.* **D10** (1974) 1145;

G.J. Gounaris, R. Kögerler and H. Neufeld, *Phys. Rev.* **D34** (1986) 3257;
M.S. Chanowitz and M.K. Gaillard, *Nucl. Phys.* **B261** (1985) 379.

[Da97] S. Dawson, preprint hep-ph/9703387.

[DaW89] S. Dawson and S. Willenbrock, *Phys. Rev. Lett.* **62** (1989) 1232 and *Phys. Rev.* **D40** (1989) 2880.

[De93] A. Denner, *Fortschr. Phys.* **41** (1993) 307.

[DeD93] A. Denner and S. Dittmaier, *Nucl. Phys.* **B398** (1993) 239.

[DeD96] A. Denner and S. Dittmaier, *Phys. Rev.* **D54** (1996) 4499.

[DeDS95] A. Denner, S. Dittmaier, and R. Schuster, *Nucl. Phys.* **B452** (1995) 80.

[DeDW95] A. Denner, S. Dittmaier, and G. Weiglein, *Nucl. Phys.* **B440** (1995) 95.

[DeDH97] A. Denner, S. Dittmaier, and T. Hahn, *Phys. Rev.* **D56** (1997) 117.

[dWS86] B. de Wit and J. Smith, *Field Theory in Particle Physics, Vol. 1*, North Holland, Amsterdam (1986).

[DiG96] S. Dittmaier and C. Grosse-Knetter, *Nucl. Phys.* **B459** (1996) 497.

[DiM73] D.A. Dicus and V.S. Mathur, *Phys. Rev.* **D7** (1973) 3111.

[DoGH96] J.F. Donoghue, E. Golowich, and B.R. Holstein, *Dynamics of the Standard Model*, Cambridge Univ. Press, Cambridge (1992, corr. ed. reprinted 1996).

[DuJM91] L. Durand, J.M. Johnson, and P.N. Maher, *Phys. Rev.* **D44** (1991) 127;
T.N. Truong, *Phys. Lett.* **B258** (1991) 402.

[EiJ95] S. Eidelman and F. Jegerlehner, *Z. Phys.* **C67** (1995) 585;
H. Burkhardt and B. Pietrzyk, *Phys. Lett.* **B356** (1995) 398.

[FaP67] L.D. Faddeev and V.N. Popov, *Phys. Lett.* **B25** (1967) 29

[Gl61] S.L. Glashow, *Nucl. Phys.* **22** (1961) 579;
S. Weinberg, *Phys. Rev. Lett.* **19** (1967) 1264;
A. Salam, in: *Elementary particle theory*, ed. N. Svartholm, Almqvist and Wiksell, Stockholm (1968) 367.

[GuHKD90] J.F. Gunion, H.E. Haber, G.L. Kane, and S. Dawson, *The Higgs Hunter's Guide*, Addison–Wesley, Redwood City (1990).

[GuJR93] S.N. Gupta, J.M. Johnson, and W.W. Repko, *Phys. Rev.* **D48** (1993) 2083.

[Hi66] P.W. Higgs, *Phys. Lett.* **B12** (1964) 132; *Phys. Rev. Lett.* **13** (1964) 508; *Phys. Rev.* **145** (1966) 1156;
R. Brout and F. Englert, *Phys. Rev. Lett.* **13** (1964) 321;
T.W.B. Kibble, *Phys. Rev.* **155** (1967) 1554.

[KüBD91] J. Küblbeck, M. Böhm, and A. Denner, *Comp. Phys. Commun.* **60** (1991) 165;
H. Eck and J. Küblbeck, *Guide to FeynArts 1.0*, Universität Würzburg (1992);
H. Eck, *FeynArts 2.0—A generic Feynman diagram generator*, Dissertation, Universität Würzburg (1995).

[Ku97] I. Kuss, *Phys. Rev.* **D55** (1997) 7165.

[KuS96] I. Kuss and H. Spiesberger, *Phys. Rev.* **D53** (1996) 6078.

[LEP96] LEP Electroweak Working Group, R. Clare et al., CERN-PPE/96-183;
A. Blondel, Proceedings of the XXVIII Intern. Conf. on High Energy Physics, Warsaw 1996.

[LeQT77] B.W. Lee, C. Quigg, and H.B. Thacker, *Phys. Rev.* **D16** (1977) 1519.

[LeSZ57] H. Lehmann, K. Symanzik, and W. Zimmermann, *Nuovo Cimento* **6** (1957) 319.

[MaVW89] W. Marciano, G. Valencia, and S. Willenbrock, *Phys. Rev.* **D40** (1989) 1725;
L. Durand, J.M. Johnson, and J.L. Lopez, *Phys. Rev. Lett.* **64** (1990) 1215 and *Phys. Rev.* **D45** (1992) 3112.

[MeBD91] R. Mertig, M. Böhm, and A. Denner, *Comp. Phys. Commun.* **64** (1991) 345;
R. Mertig, *Guide to FeynCalc 1.0*, Universität Würzburg (1992).

[Pa85] G. Passarino, *Phys. Lett.* **156B** (1985) 231 and *Nucl. Phys.* **B343** (1990) 31;
M. Veltman and F. Yndurain, *Nucl. Phys.* **B325** (1989) 1.

[PaV79] G. Passarino and M. Veltman, *Nucl. Phys.* **B160** (1979) 151.

[PDG] Review of particle properties, *Phys. Rev.* **D54** (1996) 1;
J.L. Rosner, preprint hep-ph/9704331 (for the W mass).

[PeS95] M. Peskin and D. Schroeder, *An Introduction to Quantum Field Theory*, Addison-Wesley, Redwood City (1995).

[RoT71] D.A. Ross and J.C. Taylor, *Nucl. Phys.* **B51** (1973) 125 and *Nucl. Phys.* **B58** (1973) 643;
A. Sirlin, *Phys. Rev.* **D22** (1980) 971.

[Ry85] L.H. Ryder, *Quantum Field Theory*, Cambridge Univ. Press, Cambridge (1985).

[SiSVZ80] P. Sikivie, L. Susskind, M. Voloshin, and V. Zakharov, *Nucl. Phys.* **B173** (1980) 189;
M.B. Einhorn and J. Wudka, *Phys. Rev.* **D39** (1989) 2758.

[tH71] G. 't Hooft, *Nucl. Phys.* **B33** (1971) 173 and *Nucl. Phys.* **B35** (1971) 167.

[tHV72] G. 't Hooft and M. Veltman, *Nucl. Phys.* **B44** (1972) 189;
C.G. Bollini and J.J. Giambiagi, *Nuovo Cimento* **12B** (1972) 20;
G. Leibrandt, *Rev. Mod. Phys.* **47** (1975) 849.

[tHV79] G. 't Hooft and M. Veltman, *Nucl. Phys.* **B153** (1979) 365;
A. Denner, U. Nierste, and R. Scharf, *Nucl. Phys.* **B367** (1991) 637;
W. Beenakker and A. Denner, *Nucl. Phys.* **B338** (1990) 349.

[Ve77] M. Veltman, *Acta Phys. Pol.* **B8** (1977) 475.

[Ve91] J.A.M. Vermaseren, *Symbolic Manipulation with FORM*, CAN, Amsterdam (1991).

[Ve93] M. Veltman, in: *Perspectives on Higgs Physics*, ed. G.L. Kane, World Scientific, Singapore (1993) 1.

[vOV90] G.J. van Oldenborgh and J.A.M. Vermaseren, *Z. Phys.* **C46** (1990) 425.

[We66] J. Werle, *Relativistic Theory of Reactions*, North Holland, Amsterdam (1966).

[We96] S. Weinberg, *The Quantum Theory of Fields, Vol. II: Modern Applications*, Cambridge Univ. Press, Cambridge (1996).

[Wo96] S. Wolfram, *The Mathematica Book*, Cambridge Univ. Press, Cambridge (1996).

[YaM54] C.N. Yang and R.L. Mills, *Phys. Rev.* **96** (1954) 191.

[YaY88] Y.-P. Yao and C.-P. Yuan, *Phys. Rev.* **D38** (1988) 2237;
J. Bagger and C. Schmidt, *Phys. Rev.* **D41** (1990) 264;
H.-J. He, Y.-P. Kuang, and X. Li, *Phys. Rev. Lett.* **69** (1992) 2619 and *Phys. Rev.* **D49** (1994) 4842.

[Yu93] C.P. Yuan, in: *Perspectives on Higgs Physics*, ed. G.L. Kane, World Scientific, Singapore (1993) 415;
W.B. Kilgore, preprint hep-ph/9610375.

[Ze92] P.M. Zerwas (ed.), $\mathrm{e^+e^-}$ *Collisions at 500 GeV: The Physics Potential, parts A–D*, DESY reports 92-123A, 92-123B, 93-123C, 96-123D;
F. Boudjema, preprint hep-ph/9701409;
W. Beenakker, preprint hep-ph/9704401.

Kapitel 8

Zusammenfassung

1961 formulierten Glashow, Salam und Weinberg das nach ihnen benannte GSW-Modell der elektroschwachen Wechselwirkung und hatten damit erstmals ein in sich konsistentes theoretisches Modell zur Beschreibung aller Phänomene der elektromagnetischen und schwachen fundamentalen Wechselwirkungen in Form einer spontan gebrochenen nichtabelschen Eichtheorie in der Hand. Im Laufe der Jahre wurde das GSW-Modell mit immer genaueren Messungen konfrontiert, die bislang alle in Übereinstimmung mit den theoretischen Vorhersagen waren. Aus diesem Grund wird das GSW-Modell auch als (elektroschwaches) Standardmodell bezeichnet und, obwohl es nicht die Einfachheit und Vollständigkeit besitzt, die man von einer abgeschlossenen Theorie aller fundamentalen Wechselwirkungen erwartet, wird es doch sicher den Niederenergie-Limes jeder umfassenderen Theorie darstellen müssen.

Bemerkenswerterweise ist aber über den nichtabelschen Eichsektor und den Higgs-Sektor, der für die spontane Symmetriebrechung verantwortlich ist, bislang nur wenig durch das Experiment bekannt. Das liegt zum Teil an den großen Massen der W- und Z-Eichbosonen, die erst seit etwa einem Jahrzehnt experimentell zugänglich sind.

Eine der transparentesten Methoden, sowohl den nichtabelschen wie auch den Higgs-Sektor zu testen, ist die Streuung schwerer Eichbosonen. In niedrigster Ordnung gehen bei diesen Reaktionen nur Wechselwirkungen zwischen skalaren Bosonen und Eichbosonen in den Streuquerschnitt ein, deshalb sind sie sehr empfindlich auf die genannten, bisher unzulänglich getesteten Bausteine der Theorie. Da die Streuung neutraler Z-Bosonen nur einen sehr kleinen Wirkungsquerschnitt hat, ist es aus experimenteller Sicht lohnender, W-Streuung zu betrachten, kurz $W^+W^- \to W^+W^-$. Es muß jedoch erwähnt werden, daß auch W-Streuung noch nicht mit den heutigen Beschleunigern möglich ist, und daß erste Daten frühestens in zehn Jahren zu erwarten sind.

In der vorliegenden Doktorarbeit wurden die Wirkungsquerschnitte für $W^+W^- \to W^+W^-$, wie sie das Standardmodell vorhersagt, in Bornscher und Ein-Schleifen-Näherung berechnet. Die bisher existierenden Ein-Schleifen-Rechnungen in der Literatur haben entweder nur führende Korrekturen berücksichtigt oder Näherungen wie das Äquivalenztheorem benutzt; diese Arbeit stellt also erstmals die vollständige Rechnung vor.

Die Bornsche Näherung wird in Kapitel 3 und die Ein-Schleifen-Näherung in Kapitel 5 beschrieben. Die Berechnung erfolgt störungstheoretisch mit Hilfe von Feynman-Diagrammen. Während es in Bornscher Näherung noch möglich ist, die Formeln der Wirkungsquerschnitte analytisch anzugeben (7 Feynman-Diagramme), ist dies auf Ein-Schleifen-Niveau nicht mehr praktikabel (ca. 1000 Diagramme). In Abschnitt 6.5 wird dargestellt, wie mit Hilfe der Computeralgebra diese Auswertung durchgeführt wurde.

Die Wirkungsquerschnitte sind stark in Vorwärtsrichtung gepeakt, was aufgrund der elektromagnetischen Wechselwirkung zu erwarten ist. Die Korrekturen sind klein in der Nähe der Schwelle, werden aber mit zunehmender Energie größer und liegen bei hohen Energien ($\gtrsim 1$ TeV) durchaus im Bereich von einigen 10%, sind also nicht vernachlässigbar.

Da die W-Bosonen eine sehr kurze Lebensdauer haben, ist es eine nicht unproblematische Näherung, sie in der Rechnung als stabile Teilchen anzunehmen. Einige Auswirkungen dieser Annahme werden auch schon in der Ein-Schleifen-Näherung offenkundig (s. Abschnitt 6.2). Die korrekte Berücksichtigung der endlichen Lebensdauer instabiler Teilchen ist jedoch ein ungelöstes Problem der Quantenfeldtheorie und wurde im Rahmen dieser Arbeit nicht behandelt (vgl. aber Abschnitt 6.7).

Der noch unbekannteste Teil des Standardmodells ist der Higgs-Sektor. Mit Hilfe des Higgs-Kibble-Mechanismus werden durch die Einführung von vier zusätzlichen Feldern die Massen der Fermionen und der Eichbosonen erzeugt. Drei dieser vier Felder werden durch eine Eichtransformation in die longitudinalen Komponenten der Eichbosonen absorbiert und es bleibt nur ein einziges skalares Teilchen, das Higgs-Boson, als Relikt der Massenerzeugung. Das Higgs-Boson wurde experimentell bislang nicht gefunden, jedoch können Grenzen an die Higgs-Masse aus indirekten Messungen angegeben werden, derzeit $M_{\mathrm{H}} = 159^{+153}_{-86}$ GeV (1σ).

In Abschnitt 4.2 wird gezeigt, daß die Existenz des Higgs-Bosons für die Konsistenz des Standardmodells zwingend erforderlich ist, d.h. daß es nicht möglich ist, Massenterme einfach „mit Hand" hinzuzufügen, da ansonsten die Unitarität bei W-Streuung verletzt ist.

Darüber hinaus hinterläßt das Higgs-Boson einen deutlichen Resonanz-Peak im W-Streuquerschnitt, wenn seine Masse über der Schwelle für W-Streuung liegt, d.h. $M_{\mathrm{H}} > 2M_{\mathrm{W}}$ (s. Abschnitt 4.5).

Es ist bekannt, daß das Standardmodell in Abhängigkeit von der Higgs-Masse für hohe Energien stark wechselwirkend wird, d.h. daß dann die Korrekturen mit zunehmender Ordnung der Störungstheorie wachsen. Auch wenn ein solches Verhalten noch nicht prinzipiell das Ende einer Theorie bedeutet, so heißt es doch, daß die störungstheoretische Auswertung nicht mehr sinnvoll ist. Es ist erstaunlich, daß sich die derzeitigen experimentellen Grenzen an die Higgs-Masse gerade in einem Bereich bewegen, in dem das Standardmodell bis zu sehr hohen Energien konsistent störungstheoretisch auswertbar bleibt.

Die Genauigkeit der Vorhersagen des Äquivalenztheorems, das die Streuamplituden longitudinaler Eichbosonen mit denen der korrespondierenden unphysikalischen Higgs-Felder verknüpft, werden in Abschnitt 6.3 untersucht. Für Energien $\gtrsim 200$ GeV liegen die Abweichungen unter 10% und oberhalb von ~ 2 TeV sogar unter 1%.

Vita

Persönliche Daten

Name	Thomas Hahn
Geburtsdatum	8. November 1970
Geburtsort	Würzburg
Eltern	Hans-Ludwig Hahn und Ingeborg Hahn, geb. Kern
Familienstand	ledig
Wohnort	Kopernikusstraße 4a, 97218 Gerbrunn
Staatsangehörigkeit	deutsch

Schulbildung

Sept. 1976–Juli 1980	Grundschule Estenfeld
Sept. 1980–Mai 1989	Riemenschneider-Gymnasium Würzburg
Mai 1989	Abitur

Wehr-/Zivildienst

Juni 1989–Juli 1989	Wehrdienst in Mellrichstadt
Aug. 1989–Sept. 1990	Zivildienst in der Med. Poliklinik Würzburg

Studium

Nov. 1990–Nov. 1995	Physikstudium an der Universität Würzburg
Okt. 1992	Diplom-Vorprüfung
Nov. 1995	Diplomprüfung
seit Jan. 1996	Doktorarbeit an der Universität Würzburg Betreuer: Prof. Dr. M. Böhm

Würzburg, den 11. Juni 1997

Thomas Hahn

Acknowledgements

This is the place to thank all the people who have helped me with this work. Foremost, I am deeply indepted to Prof. Dr. Manfred Böhm and PD Dr. Ansgar Denner whose constant support and proficient advice have been invaluable and can be felt while reading this thesis. I thank Stefan Bauberger for many discussions and for proofreading the manuscript and all my officemates for a friendly and scientific atmosphere.

Financial support by the Studienstiftung des Deutschen Volkes is gratefully acknowledged.

List of publications

A. Denner, S. Dittmaier, and T. Hahn, Radiative Corrections to $\mathrm{ZZ} \to \mathrm{ZZ}$ in the Electroweak Standard Model, preprint hep-ph/9612390, *Phys. Rev.* **D56** (1997) 117.